

Reducing Emissions of Volatile Organic Compounds (VOCs) From Agricultural Soil Fumigation

FINAL REPORT

California Air Resources Board, Contract No. 05-351
USDA-ARS, Project 5310-12130-008-00D

Prepared by:

Scott R. Yates
Principal Investigator
USDA-ARS, U.S. Salinity Laboratory
450 W. Big Springs Rd,
Riverside, CA 92507

and

Jay Gan
Principal Investigator
Department of Environmental Sciences
University of California
Riverside, CA 92521

May 12, 2010

Prepared for the California Air Resource Board and the California Environmental
Protection Agency

Preface

This report describes work carried out at the USDA-ARS, U.S. Salinity Laboratory and the University of California, Riverside under funding from the California Air Resources Board (CARB) through contract number 05-351 and the USDA-ARS CRIS Project 5310-12130-008-00D. The CARB contract and USDA-ARS CRIS project funded most of the experimental work described in this report.

Disclaimer

The statements and conclusions in this report are those of the contractors and not necessarily those of the California Air Resources Board. The mention of commercial products, their source, or their use in connection with material reported herein is not to be construed as actual or implied endorsement of such products.

Acknowledgments

The authors thank J. Knuteson, Q. Wang, W. Zheng, J. Lee, Q. Zhang, Y. Wang, F. Ernst, A. Khan and J. Jobes for their assistance in preparing and conducting the experiments. This Report was submitted in fulfillment of ARB Contract 05-351, Reducing Emissions of Volatile Organic Compounds (VOCs) From Agricultural Soil Fumigation, by the University of California, Riverside under the sponsorship of the California Air Resources Board. Work was completed as of December 30, 2009.

USDA Commercial Endorsement Disclaimer

The use of trade, firm, or corporation names in this document is for the information and convenience of the reader. Such use does not constitute an official endorsement or approval by the United States Department of Agriculture or the Agricultural Research Service of any product or service to the exclusion of others that may be suitable.

Table of Contents	Page
List of Figures.....	IV
List of Tables.....	IX
Abstract.....	X
Executive Summary	XI
1 Introduction	1
1.1 Problem Description	1
1.2 Objectives	2
1.3 Overall Approach	3
1.4 General Description of Field Experiments	5
2 Methodology	7
2.1 Methods for Calculating Emission Rates	7
2.2 General Field Experimental Procedures	12
2.3 General Laboratory Experimental Procedures	13
3 Results of Experiment #1 (2005): Telone II Fumigation	20
3.1 Experiment-Specific Methodology.....	20
3.2 Field #1: Broadcast-Shank Telone II Fumigation with Intermittent Water Seals.....	22
3.3 Field #2: Broadcast-Shank Telone II Fumigation with Organic Amendment.....	33
3.4 Summary	43
4 Results of Experiment #2 (2007): Telone C-35 Fumigation	44
4.1 Experiment-Specific Methodology.....	44
4.2 Ambient Weather Conditions During the Experiment.....	48
4.3 Field #3: Broadcast-Shank Telone C-35 Fumigation, Standard Fumigation Methodology (i.e., Control Field Site).....	51
4.4 Field #4: Broadcast-Shank Telone C-35 Fumigation, Deep Injection Treatment (South Field Site).....	63
4.5 Field #5: Broadcast-Shank Telone C-35 Fumigation, Ammonium Thiosulfate Treatment (i.e., North Field Site).....	77
5 Summary	87
References	89

List of Figures	Page
Figure 1.3.1. Schematic of the field experiments and location of air sampling and metrological sensors.	3
Figure 2.1.1. Using the trajectory simulation model (Wilson et al., 1982), a height in the atmosphere can be found that is relatively insensitive to atmospheric stability. For this example, roughness length was 0.22 cm and the instruments height was found to be approximately 2.5 m.	9
Figure 3.1.1. Diagram showing shank fumigation process (A) and a tool bar with 9 shanks (B). The shanks were oriented in a '<' shape with 4 shanks on each arm and a shank at the center point. In this picture, 5 shanks have lined up.	20
Figure 3.1.2. Schematic of the fields and positions of the air sampling equipment. A 10-m meteorological mast was used to collect wind speed and wind direction measurement for the back-calculation flux methods. The spatial position of a permanent benchmark was obtained to allow locating positions at a later date	21
Figure 3.2.1. Sprinkler irrigation to create a surface water seal.....	23
Figure 3.2.2. Schematic of irrigated field showing the positions of sensors and irrigation lines.	23
Figure 3.2.3. Incoming solar radiation ($W m^{-2}$) (A) and net solar radiation ($W m^{-2}$) (B) during the first 16 days of the experiment. Integer values occur at midnight.	24
Figure 3.2.4. Air temperature in $^{\circ}C$ at 0.4 m height above the soil surface (A), temperature difference between 0.8 and 0.4 m heights (B), and relative humidity measured at 0.8 m (C).	25
Figure 3.2.5. Gradient Richardson's Number, Ri	26
Figure 3.2.6. The variation in wind speed at 0.4 m above the soil surface during the experiment (A). A wind rose diagram (B) shows the wind direction, speed and probability the wind will occur in a specific direction.....	27
Figure 3.2.7. Measured 1,3-D concentration in the atmosphere at 0.4 and 0.8 m above the soil surface at the center of the irrigated field. Open circles are the period-averaged concentration collected with the on-field sampling mast.....	28

Figure 3.2.8. Volatilization rate ($\mu\text{g m}^{-2} \text{s}^{-1}$) as a function of time (day) after application for the aerodynamic (solid line, circles), integrated horizontal flux (solid line, triangles), theoretical profile shape (dashed line, squares). The inset shows cumulative 1,3-D emission as a function of time after application. The percentages on the right-most axis indicates percent of applied 1,3-D. All values are averages over the sampling period 29

Figure 3.2.9. Soil gas phase concentration (g cm^{-3}) with depth in soil. Each line represents the concentration distribution at a particular time after application. Error bars are provided on two curves ($t = 1 \text{ d}$ and $t = 4 \text{ d}$) to give a indication of the variability of the soil gas concentration across the 4 sampling locations. In B, Soil water content and bulk density with depth in the soil. Initial and final values of the water content are shown. 32

Figure 3.3.1. Setting up equipment in the organically amended field. 33

Figure 3.3.2. Schematic of organic-amended field showing the positions of sensors..... 34

Figure 3.3.3. Incoming solar radiation (W m^{-2}) and net solar radiation (W m^{-2}) in relation to time of day 35

Figure 3.3.4. The variation in temperature (A) and wind speed (B) at 0.4 m above the soil surface during the experiment. A wind rose diagram (C) shows the wind direction, speed and probability the wind will occur in a specific direction. 36

Figure 3.3.5. Variation in temperature gradient (A), Richardson’s number (B) and atmospheric stability parameter for momentum (C) during the experiment. 37

Figure 3.3.6. Measured 1,3-D concentration in the atmosphere at 0.4 and 0.8 m above the soil surface at the center of the field amended with composted green waste material. Open circles are the period-averaged concentration collected with the on-field sampling mast 38

Figure 3.3.7. Volatilization rate ($\mu\text{g m}^{-2} \text{s}^{-1}$) as a function of time (day) after application for the aerodynamic (solid line, circles), integrated horizontal flux (solid line, triangles), theoretical profile shape (dashed line, squares). The inset shows cumulative 1,3-D emission as a function of time after application. The percentages on the right-most axis of inset indicates percent of applied 1,3-D. All values are averages over the sampling period 40

Figure 3.3.8. Soil gas phase concentration ($\mu\text{g cm}^{-3}$) with depth in soil. Each line represents the concentration distribution at a particular time after application. Error bars are provided on two curves ($t = 1 \text{ d}$ and $t = 4 \text{ d}$) to give an indication of the variability of the soil gas concentration across the 4 sampling locations. In B, Soil water content and bulk density with depth in the soil. Initial and final values of the water content are shown. 42

Figure 4.1.1. Plot layout and wind-rose diagram for the 2007 experiment.....	45
Figure 4.1.2. Application of ammonium thiosulfate solution to the North Field site.....	46
Figure 4.2.1. Solar radiation ($W m^{-2}$) and net solar radiation ($W m^{-2}$) during Experiment #2.	49
Figure 4.2.2. Air temperature ($^{\circ}C$), Relative humidity (%) and barometric pressure (kPa) during Experiment #2.....	50
Figure 4.3.1. Field conditions during Experiment #2. This location is the control site.....	51
Figure 4.3.2. Field layout for the Control Field site. The letters indicate the positions of the off-field sampling equipment used for the back-calculation (i.e., ISCST3) method. The star, half-filled circle and half-filled square, respectively, are the locations of the gas-sampling mast (i.e., micrometeorological flux methods), the position of the soil gas sampling equipment, and the position of the soil temperature and heat flux sensors.....	52
Figure 4.3.3. Temperature gradient, wind speed gradient and Richardson's Number at the Control Field site. The values shown are averages over the flux sampling periods.	54
Figure 4.3.4. Concentration ($\mu g m^{-3}$) of Telone (cis + trans 1,3-D) and chloropicrin in the atmosphere during the experiment. The values shown are daily averages.	55
Figure 4.3.5. Emissions expressed as a flux density ($\mu g m^{-2} s^{-1}$) for Telone (cis + trans 1,3-D) and chloropicrin during the experiment for the Control field site. The values shown are daily averages.	56
Figure 4.3.6. Soil gas concentration ($\mu g cm^{-3}$) of 1,3-D (cis), 1,3-D (trans), and chloropicrin as a function of depth in the soil and time after fumigation. The injection depth is marked by the dashed grey line at 46 cm depth.	60
Figure 4.3.7. Effect of mass transfer coefficient on percent total emissions for chloropicrin $t_{1/2}$ of 29 h	62
Figure 4.4.1. Deep Injection (South) field site. Foreground shows the location of the soil temperature sensors. In the distance the micrometeorological sensors and gas sampling equipment is shown.....	63

Figure 4.4.2. Field layout for the Deep Injection (South Field) site. The letters indicate the positions of the off-field sampling equipment used for the back-calculation (i.e., ISCST3) method. The star, half-filled circle and half-filled square, respectively, are the locations of the gas-sampling mast (i.e., micrometeorological flux methods), the position of the soil gas sampling equipment, and the position of the soil temperature and heat flux sensors.....	64
Figure 4.4.3. Temperature gradient, wind speed gradient and Richardson's Number at the Deep Injection (South) field site. The values shown are averages over the flux sampling periods (see Section 4.1).....	65
Figure 4.4.4. Concentration ($\mu\text{g m}^{-3}$) of Telone (cis + trans 1,3-D) and chloropicrin in the atmosphere during the experiment. The values shown are daily averages.	67
Figure 4.4.5. Emissions expressed as a flux density ($\mu\text{g m}^{-2} \text{s}^{-1}$) for Telone (cis + trans 1,3-D) and chloropicrin during the experiment for the Deep Injection (South) field site. The values shown are daily averages.	68
Figure 4.4.6. Soil gas concentration ($\mu\text{g cm}^{-3}$) of 1,3-D (cis), 1,3-D (trans), and chloropicrin as a function of depth in the soil and time after fumigation. The injection depth is marked by the dashed grey line at 61 cm depth.	72
Figure 4.4.7. Trench showing position of shank fractures.	73
Figure 4.4.8. Trench showing position of shank fractures.	74
Figure 4.4.9. Pictures of the fracture openings.....	74
Figure 4.4.10. Simulation of point and shank sources at 1 hour and 1 day after fumigation. The depth of injection for a point source was 46 cm and 61 cm for a shank source. The shank extended from 30–61 cm depth.....	75
Figure 4.5.1. ATS (North) Field site. Shown are the anemometer mast, the in-field weather station, the gas sampling mast and the temperature gradient mast. In the distance the soil temperature and heat flux sensors are shown.....	77
Figure 4.5.2. Field layout for the ATS application (North Field) site. The letters indicate the positions of the off-field sampling equipment used for the back-calculation (i.e., ISCST3) method. The star, half-filled circle and half-filled square, respectively, are the locations of the gas-sampling mast (i.e., micrometeorological flux methods), the position of the soil gas sampling equipment, and the position of the soil temperature and heat flux sensors.....	78

Figure 4.5.3. Temperature gradient, wind speed gradient and Richardson's Number at the ATS (North) Field site. The values shown are averages over the flux sampling periods..... 79

Figure 4.5.4. Concentration ($\mu\text{g m}^{-3}$) of Telone (cis + trans 1,3-D) and chloropicrin in the atmosphere during the experiment. The values shown are daily averages. 80

Figure 4.5.5. Emissions expressed as a flux density ($\mu\text{g m}^{-2} \text{s}^{-1}$) for Telone (cis + trans 1,3-D) and chloropicrin during the experiment for the ATS (North) field site. The values shown are daily averages. 82

Figure 4.5.6. Soil gas concentration ($\mu\text{g cm}^{-3}$) of 1,3-D (cis), 1,3-D (trans), and chloropicrin as a function of depth in the soil and time after fumigation. The injection depth is marked by the dashed grey line at 61 cm depth. 86

List of Tables	Page
Table 1.3.1 Characteristics of 1,3-dichloropropene (1,3-D)	4
Table 1.3.2 Characteristics of chloropicrin	5
Table 4.1.1 Amount of fumigant applied to fields	46
Table 4.3.1. Summary of daily air temperature, wind speed, wind direction, atmospheric stability and Telone C-35 flux from the Control Plot.....	57
Table 4.3.2. Summary of the total flux estimates for Telone C-35 and component fumigants from the Control Field plot.....	58
Table 4.3.3. Parameters used in volatilization model (Yates, 2009)	62
Table 4.4.1. Summary of Telone C-35 flux from the South Field Plot (Deep Injection Treatment) using micrometeorological methods.	69
Table 4.4.2. Summary of daily air temperature, wind speed, wind direction, atmospheric stability and Telone C-35 flux from the South Field Site (Deep Injection Treatment).	70
Table 4.4.3. Summary of the total flux estimates for Telone C-35 and component fumigants from the Deep Injection (South) Field plot.....	71
Table 4.5.1. Summary of Telone C-35 flux from the ATS (North) Field Plot using micrometeorological methods.	83
Table 4.5.2. Summary of daily air temperature, wind speed, wind direction, atmospheric stability and Telone C-35 flux from the ATS (North) Field Plot.....	84
Table 4.5.3. Summary of the total flux estimates for Telone C-35 and component fumigants from the ATS (North) Field plot.	85

Abstract

Field experiments were conducted to measure subsurface movement and volatilization of the Telone® (1,3-dichloropropene, 1,3-D alone or with chloropicrin) after shank injection into agricultural soil.

The goal of this study was to evaluate the effectiveness of several emission-reduction methods, including: sprinkler irrigation, organic amendment, deep injection, and fertilizer amendment on the volatilization of 1,3-D, alone or with chloropicrin, to the atmosphere.

Several methods were used to estimate fumigant volatilization rates and total emission losses, including: aerodynamic, integrated horizontal flux, theoretical profile shape, and back-calculation methods. These methods provide estimates of the volatilization rate based on measurements of wind speed, temperature and 1,3-D concentration in the atmosphere.

During the 2005 experiment, the volatilization rate was measured continuously for 16 days and the daily peak volatilization rates ranged from 18–60 $\mu\text{g m}^{-2} \text{s}^{-1}$ (10–15% of applied Telone II) for the irrigated field and 4–23 $\mu\text{g m}^{-2} \text{s}^{-1}$ (3–8% of applied Telone II) for the field amended with organic matter.

During the 2007 experiment, the volatilization rates ranged from 12–30 $\mu\text{g m}^{-2} \text{s}^{-1}$ (11–23% of applied Telone C-35) for the standard fumigation; 13–34 $\mu\text{g m}^{-2} \text{s}^{-1}$ (10–17% of applied Telone C-35) for deep injection fumigation; and 7–20 $\mu\text{g m}^{-2} \text{s}^{-1}$ (9–18% of applied Telone C-35) for a field amended with ammonium thiosulfate. For all fields, very low (i.e. <2%) emissions of chloropicrin were observed.

Intermittent irrigation reduced total emissions by 45–70% and adding composted municipal green waste reduced total emissions by 80–85% compared to conventional fumigant applications. For deep injection and spraying the surface with ammonium thiosulfate (ATS) only a 20% reduction in emissions was observed.

Significant reduction in volatilization of 1,3-D was observed for the irrigation and organic matter treatments, but smaller reduction in emissions were observed for deep injection and ATS amendment in a surface spray (i.e., without surface irrigation).

Executive Summary

Background

Ozone is formed from the photochemical oxidation of nitrogen oxides and VOCs, such as pesticides and fumigants. This is leading to increased regulation of agricultural VOC sources. It has been estimated that 5% of the total VOC in the San Joaquin and Sacramento Valleys are from pesticides. This has led DPR to require reductions in pesticide-related VOC emissions from 1990 levels. Future regulations may require additional reductions to meet 1-hour and 8-hour SIP requirements.

Research was conducted to provide estimates of the cumulative and period-averaged emission rates for broadcast-shank fumigation for standard fumigation practices and four emission-reduction strategies: (i) intermittent irrigation water seal, (ii) addition of an organic surface amendment, (iii) deep injection, and (iv) addition of a fertilizer amendment (i.e., ammonium thiosulfate) applied as a spray (i.e., limited water).

Methods

This research was accomplished by conducting field experiments in 2005 and 2007. In each experiment, either two, or three, side-by-side emission experiments were conducted.

In the 2005 study, Telone II® was applied at a rate of 12–gal/acre and at a depth of 18 inches (46 cm) to two fields in an identical manner. One field was then subjected to intermittent water sealing in which water was sprayed onto the soil post-fumigation, and then again for the following four days. The other field had been applied with composted green waste the previous year.

In the 2007 study, Telone® C35 was applied to three fields in an identical manner at a target rate of 20 gal/acre and at a depth of either 18 inches (46 cm; control and ATS-applied fields) or 24 inches (60 cm; deep injection) One field served as a standard fumigation treatment and did not have any other agronomic operation performed that would affect emissions. For the thiosulfate treatment, ATS solution was sprayed on to the field immediately after fumigation. Since the effect of a surface water seal had already been shown to effectively reduce emissions (see 2005 field data), this test was to determine the effectiveness of thiosulfate, alone (i.e., without a water seal) in reducing emissions. For the deep injection treatment, only the depth of injection differed from the control.

Fumigant emissions were determined using two independent data sources. One set of emission estimates were obtained using aerodynamic (ADM), integrated horizontal flux (IHF) and theoretical profile shape (TPS) methods. These micrometeorological approaches require on-field measurement of the atmospheric fumigant concentration at one or more heights above the soil surface, wind speed measurements, and

temperature measurements. Another set of emission estimates were obtained using the so-called back calculation methods, where observed ambient concentrations in the atmosphere surrounding a fumigated field are used with the Industrial Source Complex Short Term (ISCST3) or the CalPuf (v.6) dispersion models to back-calculate the field-scale emission rates. These approaches utilize atmospheric fumigant concentration collected at a single height above the soil surface at numerous locations surrounding the field, along with weather data collected from a 10-m mast placed in the vicinity.

The results from this data set include: (a) period-averaged or daily emission rates, (b) total emissions, (c) atmospheric fumigant concentrations, (d) wind speed and directions, (e) air temperature and relative humidity, (f) atmospheric stability, (g) solar radiation, (h) barometric pressure information, (i) fumigant concentration in the soil pore space, (j) soil temperature, and (k) soil moisture content.

Results

Experiment #1 (2005)

The results of this study indicate that applying sprinkler irrigation water to the soil surface following soil fumigation leads to total 1,3-D (cis+trans) emissions between 10 to 15% of the applied material. Based on recent laboratory and field experiments conducted under similar soil and environmental conditions, it appears that atmospheric emissions of 1,3-D can be reduced by approximately 50% compared to conventional application methods.

The addition of composted municipal green waste material provides a means to reduce emissions of 1,3-D (cis+trans) after preplant soil fumigation. Application of green waste at a rate of 300 tons per acre the previous year and incorporated in the field soil reduced total of 1,3-D from approximately 28%-33% to approximately 5% of the applied fumigant. Based on recent laboratory and field experiments conducted under similar soil and environmental conditions, it appears that atmospheric emissions of 1,3-D can be reduced by approximately 80–85% compared to conventional application methods. This approach provides a simple, environmentally beneficial, effective and relatively low cost method to protect the environment from agricultural chemicals and to reduce VOC emissions to the atmosphere.

Experiment #2 (2007)

Very low levels of chloropicrin were lost from the three fields (i.e., < 2% total emissions). Two independent flux estimates both arrived at similar results and supported by soil gas measurements. It appears that soil-based processes were limiting chloropicrin movement to the soil surface and volatilization into the atmosphere. The most likely explanation is enhanced soil degradation in the near surface soil that rapidly degraded chloropicrin.

Due to the very low emission of chloropicrin, total emissions of Telone ® C-35 appear lower than expected. This is due to 1/3 of the Telone ® C-35 mass remaining in soil (i.e., the chloropicrin component).

Standard Fumigation Methodology. If the 1,3-D emissions are presented as a percentage of the applied 1,3-D (cis+trans); the total emission estimates from the ADM, ISCST and CalPuf methods, respectively, are 35.4%, 20.0%, and 27.2%. The average and standard deviation of the total emission from the 3 methods is, respectively, $27.5 \pm 7.7\%$.

Deep Injection Fumigation. The total emission estimates from the ADM, IHF, TPS, ISCST3 and CalPuf methods, respectively, are 26.7%, 18.8%, 15.1%, 15.8%, and 26.1% of the applied 1,3-D (cis+trans). The average and standard deviation of the total emission from the 5 methods is, respectively, $20.5 \pm 5.6\%$ and for the ADM, ISCST3, and CalPuf methods is, respectively, $22.9 \pm 6.1\%$.

By comparing the total emission estimates for the ADM, ISCST3 and CalPuf methods, deep injection reduces emissions of Telone (cis+trans) by approximately 16.9% compared to the standard fumigation methodology.

Soil Amendment with Ammonium Thiosulfate (ATS) as a Surface Spray. The total emission estimates from the ADM, IHF, TPS, ISCST3 and CalPuf methods, respectively, are 25.0%, 12.5%, 12.5%, 14.5%, and 26.7% of the applied 1,3-D (cis+trans). The average and standard deviation of the total emission from the 5 methods is, respectively, $18.2 \pm 7.0\%$ and for the ADM, ISCST3, and CalPuf methods is, respectively, $22.1 \pm 6.6\%$.

Using the total emission estimates for the ADM, ISCST3 and CalPuf methods, spraying the field with ATS reduces emissions of Telone (cis+trans) by approximately 19.9% compared to the standard fumigation methodology.

Conclusions

All methods reduced emissions of 1,3-D compared to standard fumigation practices. Emissions were reduced the most by applying composted municipal green waste to the upper 15 cm of the soil (approximately 80% emission reduction). Further research is needed to study the practicality of this method and the potential to reduce fumigant concentrations at the soil surface and compromise plant pest control.

Repeated surface irrigation appears to be a simple, relatively low cost, and effective method to reduce fumigant emissions (approximately 50% emission reduction). Incorporating this emission-reduction strategy into existing production systems should be relatively easy and straightforward. Recent laboratory and field research has also demonstrated similar results providing additional support for this methodology.

Application of fertilizer amendments as a low-water spray reduced emissions by approximately 20%. This represents a relatively simple approach to reduce emissions and could be readily incorporated into typical production systems. However, further research is needed to quantify the relationship between amounts of water added relative to applied thiosulfate. Previous research has shown that increasing the total applied water also increases the effectiveness of this emission reduction strategy. Furthermore, increasing the applied thiosulfate to produce a molar ratio exceeding (2 : 1) (thiosulfate to fumigant) significantly increases effectiveness. However, this exceeds the recommendations for application as a fertilizer and has the potential to cause plant injury, in some conditions. There is also a higher cost associated with combining application of thiosulfate and applying irrigation water compared to creating an irrigation water seal alone.

Deep injection reduced emissions by about 17% in a field-soil where the shank fractures remained. In a previous study involving methyl bromide, deep injection reduced emissions by about 67% (from about 64% to 21%; Yates et al., 1997). This study did not include an investigation of the shank fractures, but indicates that lower emissions may be possible. Further research is needed to determine if improved, low disturbance, shanks would increase the effectiveness of deep injection as an emission-reduction strategy.

This research project provides information that can be used to determine if proposed methods to control VOC emissions are adequate to achieve required reductions. This information may also be useful as a starting point in the development new cost-effective methods to further reduce emissions.

1 Introduction

1.1 Problem Description

Ground-level ozone is a primary ingredient of smog, which remains a severe pollution problem in California. Ozone is formed in the atmosphere by the reaction of VOCs and NO_x in the presence of heat and sunlight. Therefore, hot, dry weather is favorable to the formation of ozone. The highest concentration levels are typically found in suburban areas due to the transport of emissions from the urban center. Local topographic effects can exacerbate ozone levels.

From 1975 to 2003, summer emissions of nitrogen oxides (NO_x) decreased 35% from 900,000 to 600,000 tons statewide. In 2003, the principal sources of NO_x emissions were found to be on-road vehicles (46%), fuel combustion from industries (26%), and off-road sources (24%) (i.e., engines, aircraft, marine vessels, and railroads). VOC emissions decreased significantly from over 1.2 million tons in 1975 to less than 500,000 tons in 2003.

Ground level ozone is a public and environmental health concern. Ozone is a main component of smog and exposure to ozone for several hours has been identified as a potential factor that may reduce lung function and increase respiratory inflammation in humans. This has led to concern for active children who spend considerable time outdoors during summer months. For example in Fresno, the rate of childhood asthma is 16.4%, more than three times the national rate and may be due, in part, to high ozone levels. Ozone is also thought to contribute to higher rates of premature death, lost school days, increased health-care costs, and may lead to economic loss by damaging crops and reducing productivity, although further research is needed to substantiate these claims.

Recently, U.S. EPA has established a new federal 8-hour ozone standard that requires regulators to develop and submit State Implementation Plans (SIPs) to meet the 2007 deadline. Initial data from California Air Resources Board (ARB) and the California Department of Pesticide Regulation (DPR) indicate the need for reductions from many sources, including pesticides. Both agencies are working with stakeholders to determine the impact of pesticide emissions on ozone formation and the possible methods to reduce emissions.

In California, for example, pesticide VOC emissions are believed to be a significant contributor to the total VOC emissions statewide. In urban regions, pesticide VOC emissions are probably less significant compared to the more common industrial and automotive VOC sources. Even so, pesticide VOC emissions must be reduced by as much as 12–20% depending on the location.

Current non-fumigant pesticide VOC inventories are based on an estimated 100% loss of the VOC portion of the pesticide even though most pesticides are affected to some degree by irreversible sorption, and abiotic and biotic degradation. Since information is

available on typical field-scale emissions for fumigant applications, the VOC inventories are based on the median emission from the particular fumigation method (i.e., <100% loss), which is based on information available from recent field-scale experimentation. This provides much more accurate VOC inventories for fumigant use.

The results from the 2007 pesticide VOC inventory can be summarized as follows. Fumigants continue to contribute the most pesticide VOC emissions in the Southeast Desert and Ventura non attainment areas even using the improved estimation procedure. Pesticides formulated as emulsifiable concentrates are another major pesticide VOC contributor, particularly in the San Joaquin Valley non attainment area.

VOC emissions are below the SIP goal in Sacramento Metro and San Joaquin Valley NAA and non-fumigant VOCs were the primary source. VOC emissions are below the SIP goal in Southeast Desert and South Coast NAA and VOCs derived from fumigation were the primary source in the Southeast Desert NAA and a significant contributor in the South Coast NAA. VOC emissions are above the SIP goal in Ventura NAA and VOCs derived from soil fumigants were the primary sources.

As new stricter rules governing ambient ozone levels are implemented, regulations will be placed on activities that produce ozone. In regions with significant agricultural production, emissions of VOC from soil fumigation will likely be considered in an effort to be in compliance with regulation. Therefore, research is needed to accurately determine the true level of VOC emissions from fumigation and to develop methods to reduce emissions to low levels. Failure to do so may cause agricultural producers to face potentially restrictive control strategies, which may cause a reduction in profit or force farmers to cease food production.

1.2 Project Objectives

- a) Obtain accurate cumulative and instantaneous emission rates for 1,3-dichloropropene and/or chloropicrin.
- b) Determine cumulative and period (e.g., hourly) emission rates for four emission-reduction strategies and compare to standard fumigation practices: (i) broadcast-shank fumigation with the addition of intermittent water seals, (ii) broadcast-shank fumigation with the addition of a surface amendment (e.g., organic matter), (iii) broadcast-shank fumigation with the addition of a surface amendment (e.g., thiosulfate), and (iv) broadcast-shank fumigation with the fumigant applied at 24 inches (61 cm) deep in soil. Thus, a total of five experimental fields were used.
- c) Obtain soil fumigant gas concentrations with depth periodically after application.
- d) Collect a complete set of meteorological data to allow determination of the emission rate and to characterize the meteorological conditions during the experiments.

1.3 Overall Approach

The procedures for estimating field-scale emission rates and the overall experimental design followed that of Yates et al., (1996a,b, c; 1997) and Majewski et al., (1989; 1990; 1995). The five experimental fields were approximately 5-acres each, were located near one another and contained the same, or similar, soil type, soil moisture, and field preparation. Fields were fumigated with the same chemicals, at the same application rate, in the same manner, and at the same time when possible. Figure 1.3.1 gives a schematic of the typical design of the experiments

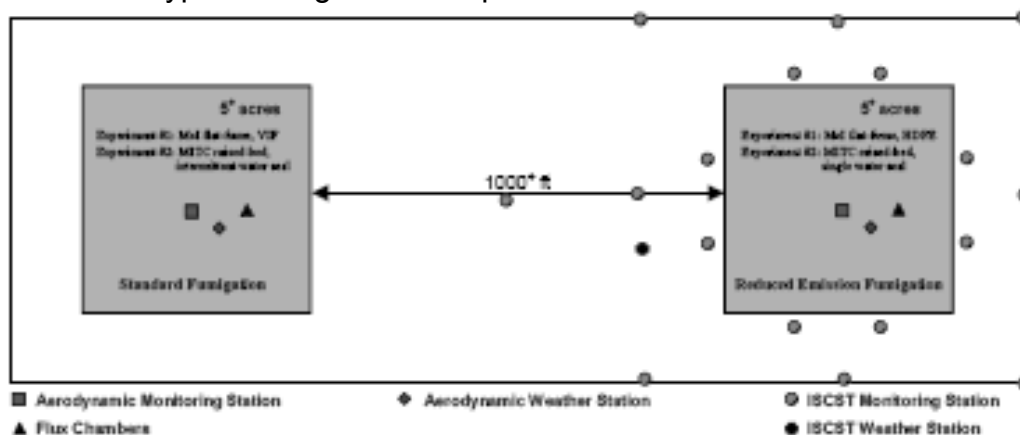


Figure 1.3.1. Schematic the field experiments and location of air sampling and metrological sensors.

1.3.1 Study Chemicals

1,3-Dichloropropene (1,3-D) is the active ingredient in two Dow AgroSciences LLC soil fumigants that are typically soil-injected, Telone[®] II Soil Fumigant (about 94 wt%) and Telone[®] C-35 Soil Fungicide and Nematicide (containing about 61 wt% 1,3-D and 35 wt% chloropicrin).

In southern San Joaquin Valley commercial crop production, Telone C-35 is primarily used as a broadcast treatment injected at the 45 – 46 cm (18 inch) depth. In general, the field is not covered or treated with any amendments. 1,3-D and chloropicrin are important methyl bromide alternative chemicals. Telone soil fumigants contain about a 50/50 mixture of *trans*-1,3-D and *cis*-1,3-D isomers. Characteristics of 1,3-D and chloropicrin are given in Tables 1.3.1 and 1.3.2. Degradation of 1,3-dichloropropene and chloropicrin begins immediately in the soil. The compounds degrade by hydrolysis and soil microbial metabolism. For 1,3-D, $t_{1/2}$ 20°C is 11 d for hydrolysis, and about 8 d for aerobic soil metabolism, respectively. For chloropicrin, values of 83 d for hydrolysis and 9.2 hours for aerobic soil metabolism have been reported (Zheng et al., 2004; Zheng et al., 2003). In Milham sandy loam, the degradation $t_{1/2}$ for 1,3-D is 90 hours and for chloropicrin is just 2.9 hours (Ashworth and Yates, 2009).

Previous air monitoring studies of soil injection application have shown that 1,3-dichloropropene and chloropicrin vapor concentrations above fields are low immediately following application, and reach a maximum between 1 to 5 days after application.

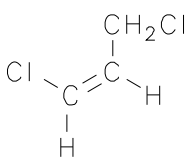
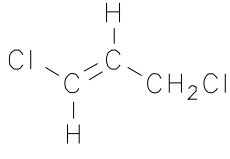
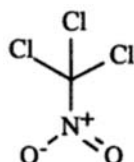
<i>Test Material #1</i>	
Chemical Name:	1,3-dichloropropene (CAS #542-75-6)
Common Name:	1,3-D
Empirical Formula:	C ₃ H ₄ Cl ₂
Synonyms:	DCP; Dichloro-1,3-propene; 1,3-dichloro-1-propene; <i>cis/trans</i> -1,3-dichloropropene; α-chloroallyl chloride; 1,3-dichloropropylene.
Isomers:	<i>cis</i> -1,3-dichloropropene (CAS #10061-01-5) <i>trans</i> -1,3-dichloropropene (CAS #10061-02-6)
Structures:	<div style="display: flex; justify-content: space-around; align-items: center;"> <div style="text-align: center;">  <p>cis-1,3-dichloropropene</p> </div> <div style="text-align: center;">  <p>trans-1,3-dichloropropene</p> </div> </div>
Properties:	
Molecular Weight	110.98
Appearance (25°C)	White to amber liquid
Odor	Sweet-penetrating
Boiling Point	104°C (<i>cis</i>); 112°C (<i>trans</i>)
Flash Point	about 28°C
Density (25°C)	1.217 g/mL
Vapor Pressure (25°C)	34.3 mmHg (<i>cis</i>); 23.0 mmHg (<i>trans</i>); Karris and Downey (1987a, 1987b)
Solubility in Water (25°C)	2180 ppm (<i>cis</i>); 2320 ppm (<i>trans</i>); Walbroehl (1987a, 1987b).
Log Octanol/Water Coefficient	2.04
Henry's Law Constant (25°C)	1.8 x 10 ⁻³ m ³ atm mole ⁻¹ (<i>cis</i>); 1.05 x 10 ⁻³ m ³ atm mole ⁻¹ (<i>trans</i>)

Table 1.3.1 Characteristics of 1,3-dichloropropene (1,3-D)

Test Material #2

Chemical Name:	chloropicrin (CAS #76-06-2)
Common Name:	chloropicrin
Chemical Formula:	CCl ₃ NO ₂
Synonyms:	Trichloronitromethane
Structure:	



Properties:	
Molecular Weight:	164.39
Appearance (25°C):	Colorless liquid
Odor:	Intensely irritating tear gas
Odor Threshold:	1.1 ppm
Boiling Point:	233.6°F, 112°C
Density:	1.66 g/mL
Vapor Pressure:	18.3 mmHg at 20°C
Solubility in Water:	2.3 g L ⁻¹ water
Log Octanol/Water Coefficient	2.09
Henry's Law Constant (25°C)	2.05 x 10 ⁻³ m ³ atm mole ⁻¹

Table 1.3.2 Characteristics of chloropicrin

1.4 General Description of the Field Experiments

Site Location and Description

The test site was located approximately 25 miles west of Bakersfield, CA and about 5 miles NNE of Buttonwillow, California, in the San Joaquin Valley (35° 26' 32"N, 119° 27' 25" W). The five experimental fields used were located north of Hwy 58, south of Burbank Street, east of Buttonwillow Drive and west of Tracey Avenue (i.e., Kern County, township 29 S, range 23 E, section 1). The elevation is approximately 270–300 feet above mean sea level. USDA NRCS Soil Survey indicates that the soil in four of the five field is classified as a *Milham sandy loam* soil with the exception of the treated portion of the northeast-most field site (i.e., 2007 study, ATS experiment), which is classified as a Kimberlina fine sandy loam. These soils are typical of vegetable production in the San Joaquin Valley. Representative soil series are Fine-Loamy,

Mixed, Superactive, Thermic Typic Haplargids (Milham) and Coarse-Loamy, Mixed, Superactive, Calcareous, Thermic Typic Torriorthents (Kimberlina) series soils.

The experimental fields were prepared and managed by the grower according to standard practice and included irrigation, cultivation, preparation, fertilization, weed, pathogen and insect control. Prior to the start of fumigation (approximately 1 week), the fields were prepared using a disk and ring roller or spiral packer. This was a necessary activity prior to soil fumigation. The fumigant was applied by a commercial applicator (Western Farm Services, Inc.), using a shank injector and according to the industry standard. The total amount of chemical was determined to the nearest gallon before and after application. The total mass applied to the field was calculated from these measurements. Following application of the fumigants, the soil was sealed with a single pass of a disk and a ring roller in the direction of the shanks.

In the 2005 study, Telone II was applied at a rate of 12-gal/acre and at a depth of 18 inches (46 cm) to two fields in an identical manner. One field was then subjected to intermittent water sealing in which water was sprayed onto the soil post-fumigation, and then again for the following four days. The other field had been applied with composted green waste the previous year.

In the 2007 study, Telone C35 was applied to three fields in an identical manner at a target rate of 20 gal/acre and at a depth of either 18 inches (46 cm; control and ATS-applied fields) or 24 inches (60 cm; deep injection) One field served as a control plot and did not have any other agronomic operation performed that would affect emissions. For the ammonium thiosulfate (ATS) treatment, ATS solution was sprayed on to the field immediately after fumigation. Since the effect of a surface water seal had already been shown to effectively reduce emissions (see 2005 field data), this test was to determine the effectiveness of thiosulfate, alone (i.e., without a water seal) in reducing emissions. For the deep injection treatment, only the injection depth differed from the control.

Thiosulfate fertilizers rapidly react with 1,3-D in soil and transforms the fumigant to non-volatile products. The reaction between thiosulfate and 1,3-D was found to be a nucleophilic substitution, in which a chlorine on 1,3-D was replaced by the thiosulfate ion. The rate of reaction was found to be proportional to the molar ratio of thiosulfate to fumigant (Gan et al., 2000b).

Applying thiosulfate (i.e., ATS, potassium thiosulfate, sodium thiosulfate, etc.) in water to the soil surface creates a reactive soil layer that rapidly degrades 1,3-D, which reduces the amount of 1,3-D available for emissions. Significant reductions of 1,3-D emissions were observed in laboratory experiments when ATS was applied to the soil surface in water (Gan et al., 2000a). This experiment also found that increasing the amount of water and/or amount of ATS decreased the emission rate.

There are several common methods for estimating the fumigant emissions from soils to the atmosphere. Three of these methods have been recently used to estimate MeBr

and 1,3-D emissions to the atmosphere. Available methods include: (a) estimating total emission by soil sampling, (b) enclosure-based methods, and (c) micrometeorological methods.

For Telone[®] II and C-35, determining the mass of fumigant degraded in soil is very difficult and expensive and is subject to high levels of uncertainty due to spatial and temporal variability. Without an easy to identify degradation product (e.g., Br ion), and one that is not generally present in soil, this approach is unsuitable for accurately estimating emissions. Furthermore, enclosure-based methods have been found to be accurate for cumulative emissions measurements, but not very accurate for short-term emission rates. Because of the limitation with these methodologies, several micro-meteorological methods were used to determine emission rates for in this project.

2 Methodology

2.1 Methods for Calculating Emission Rates

Aerodynamic Method. The aerodynamic method (ADM) is based on atmospheric gradients of wind speed, temperature and concentration and provides a measurement of the pesticide flux from the soil surface (Parmele et al. 1972; Brutsaert 1982; Majewski et al. 1989). The method requires a spatially uniform source and a relatively large upwind fetch so that the atmospheric gradients are fully developed. The fetch requirements are generally assumed to be from 50 to 100 times the height of the instruments, which is typically a height greater than or equal to 0.5 m. Chemical concentrations, wind speed, and temperature are determined at multiple heights at the sampling location to define the gradients. To characterize the temporal variability in flux, samples are collected over relatively short time intervals; typically 2–4 hr. Adsorbent tubes are often used to accumulate the volatilized mass throughout the sampling interval.

The aerodynamic method was originally developed for use under neutral atmospheric conditions. Using empirical relations, however, the method can be extended to stable and unstable atmospheric conditions, which commonly occur during the day. Numerous stability corrections have been proposed (Fleagle and Businger 1980; Brutsaert 1982; Rosenberg et al. 1983). The aerodynamic equation, suitable for general atmospheric stability conditions, is:

$$f_z(0, t) = k^2 \frac{[\bar{C}_1(t) - \bar{C}_2(t)] [\bar{u}_2(t) - \bar{u}_1(t)]}{\phi_m(t) \phi_c(t) \ln(z_2 / z_1)^2}$$

2.1.1

$$f_z(0, t) = \frac{-k^2 z^2}{\phi_m(t) \phi_c(t)} \left(\frac{\partial \bar{C}(t)}{\partial z} \right) \left(\frac{\partial \bar{u}(t)}{\partial z} \right)$$

where $f_z(0, t)$ is the interval-averaged vertical flux density at the soil surface [$\mu\text{g}/\text{m}^2\text{s}$], k is von Karman's constant (~ 0.4), t is the interval-averaged wind speed [m/s], z is height above the soil surface [m] and \bar{u}, \bar{c} are the interval-averaged wind speed [m/s] and concentration [$\mu\text{g}/\text{m}^3$] above the soil surface, and ϕ is a stability correction where the subscripts m and c indicate momentum and fumigant.

The gradient-based stability corrections, ϕ , for a particular time interval, t , can be written as (Rosenberg et al. 1983):

$$\begin{aligned} \phi_m &= (1 - 16R_i)^{-0.33} & \phi_c &= 0.885 (1 - 22R_i)^{-0.4} & R_i < 0 & \text{unstable} \\ \phi_m &= (1 + 16R_i)^{0.33} & \phi_c &= 0.885 (1 + 34R_i)^{0.4} & R_i > 0 & \text{stable} \end{aligned} \quad 2.1.2$$

where R_i is the Richardson's number, defined as:

$$R_i = \frac{g}{T} \frac{\partial T}{\partial z} \left[\frac{\partial u}{\partial z} \right]^{-2} \quad 2.1.3$$

where g is the gravitational acceleration (i.e., $9.8 \text{ m}/\text{s}^2$) and $T(t)$ is the absolute temperature [K]. The gradient Richardson's number is one means for characterizing the importance of buoyancy and mechanical mixing on the turbulence. In addition to Equation (2.1.2), several other stability corrections have been proposed (Fleagle and Businger 1980; Brutsaert 1982; Rosenberg et al. 1983).

A volatilization rate obtained using the aerodynamic method is based on gradients of wind speed, temperature and 1,3-D concentration (*Parmele et al., 1972*) collected over a relatively large and spatially-uniform source area. This is necessary to ensure that the atmospheric gradients are fully developed. The instruments are generally placed at a height that is 1–2% of the upwind fetch distance. For the tested field, 1% of minimum upwind fetch indicates that the instruments should be placed between the 0.0 and 0.9 m heights.

Theoretical Profile Shape Method. The theoretical profile shape (TPS) method (*Wilson et al., 1982*) is based on the trajectory simulation model Wilson et al. (1981a,b,c) and allows the 1,3-D volatilization rate to be obtained from a measurement of concentration and wind speed at a single height above the soil surface. The method does not require large fetch distances and is relatively insensitive to the atmospheric stability so temperature and wind gradients and stability corrections are unnecessary.

The theoretical profile shape method (Wilson et al., 1982), can be used to determine the volatilization rate from field experiments conducted on a circular plot. This method has advantages over the aerodynamic method in that (1) the large fetch requirement is not necessary, (2) measurements of the air concentration and wind speed are needed at only one height, and (3) the sensor is placed at a height that is relatively insensitive to the atmospheric stability so temperature and wind gradients and stability corrections are

unnecessary. This approach is based on the trajectory simulation model described by Wilson et al. (1981a–c). Wilson et al. (1983) and Majewski et al. (1990) have used this method, among others, to determine the rate of pesticide and ammonia volatilization from field experiments. Yates et al. (1996b, 1997) adapted the method so that MeBr volatilization from rectangular fields could be estimated. The flux density is estimated from

$$flux = \frac{\bar{u}(t)\bar{C}(t)}{\Omega} \Big|_{z_{inst}} \quad 2.1.4$$

where interval-average values of the wind speed, $\bar{u}(t)$, and air concentration, $\bar{c}(t)$, are obtained at the instrument height, Z_{inst} . Flux can be obtained by determining the ratio of the horizontal to vertical flux, Ω , using the trajectory simulation model discussed below. This ratio depends on surface roughness and upwind fetch distance (i.e., the radius of the circular plot) but does not depend on wind speed.

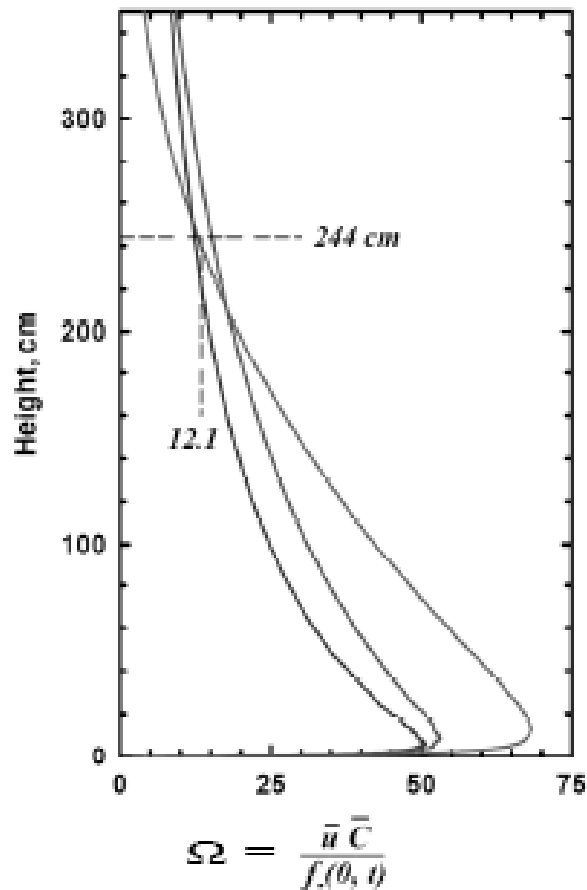


Figure 2.1.1 Using the trajectory simulation model (Wilson et al., 1982), a height in the atmosphere can be found that is relatively insensitive to atmospheric stability. For this example, roughness length was 0.22 cm and the instruments height was

To obtain Ω , simulations are conducted for strongly stable, strongly unstable and neutral atmospheric conditions. Plotting the results against height produces a curve similar to that shown in Figure 2.1.1. The height where the three curves more or less converge is the height where the sensor is positioned. At this location, the effects of atmospheric stability are minimized. One difficulty using this method is the determination of the instrument height before initiating the experiment; this involves estimating the surface roughness, which may not be known until after the experiment begins (i.e., when the plastic is placed on the field, at the time of application).

Another difficulty exists for rectangular fields, because the upwind source distance varies with the wind direction. For this situation, the trajectory simulation must be conducted for several upwind source distances ranging from the smallest to the largest distance between the sampling mast and edge of the field. Then, a relationship can be developed between wind direction, instrument height, and Ω , which may be used to estimate the flux using the average wind direction for the sampling interval (Yates et al. 1996b).

Integrated Horizontal Flux Method. The integrated horizontal flux (IHF) method (Denmead, et al., 1977) uses concentration and horizontal wind speeds measured at several heights. The flux is determined using principals of mass balance where the 1,3-D mass leaving the soil surface upwind from a sampling point is presumed equal to the mass that passes through a vertical plane located at the sampling point. Using a mass balance approach has an advantage in that no correction for atmospheric stability is needed.

The integrated horizontal flux method (Denmead et al. 1977; Wilson et al. 1982; Majewski et al. 1990) can be used to estimate the surface flux when the concentration, $\bar{c}(z)$ and horizontal wind speeds, $\bar{u}(z)$ in the atmosphere are known as a function of height. Measurements of chemical concentration and wind speed gradients are similar to those used for the aerodynamic method. Assuming a spatially uniform source (e.g., $flux(x)$ is constant), the $flux$ is estimated from:

$$flux = \frac{1}{L} \int_0^L f_z(x) dx = \frac{1}{L} \int_0^\infty \bar{u}(z) \bar{c}(z) dz \quad 2.1.5$$

From this equation, the cumulative mass emitted from the surface upwind from a sampling point is equal to the cumulative mass that passes through a vertical plane of infinite extent located at the sampling point. To use this method, the concentration profile at several heights must be determined, and the distance of the source area upwind from the sampling mast must be known. An advantage of this method over the aerodynamic method is that corrections for atmospheric stability are not needed because this approach is based on principals of mass balance.

Indirect Flux Method. Another method for determining the fumigant emission rate is the “indirect method”, where observed ambient concentrations in the atmosphere around the field are used with the Industrial Source Complex Short Term (ISCST3) or the CalPuf dispersion models to back-calculate the field emission rate.

The estimate of the emission rate is based on the relationship:

$$C_{meas} = b + E C_{ISC} \quad 2.1.6$$

where C_{meas} is the measured ambient concentration, E is the unknown emission rate, b is the background concentration that occurs when $E=0$, and C_{ISC} is a predicted concentration at the receptor. The model parameters are estimated by linear regression using observed ambient concentrations (C_{meas}) at many locations surrounding the treated field and the predicted concentrations (C_{ISC}) at each sampling location obtained using the ISCST3 model with a nominal emission rate (E_{nom}). The unknown emission rate, E , is estimated from

$$flux = E = mE_{nom} \quad 2.1.7$$

where the intercept, b , the slope, m , are obtained from linear regression.

In theory, subtracting out any background concentration observed during an experiment should result in $b \rightarrow 0$. However, due to a variety of factors, b is sometimes observed to be significantly different than 0. This may be due to periods where the meteorological parameters used in the ISCST3 model are not accurately representing the actual meteorological conditions; e.g. short intervals where the wind direction was outside the $\mu \pm \sigma$ wind direction. This would cause the ISCST3 model to predict zero concentration at receptors outside the plume, when in fact for a short period some of these receptors received fumigant gas. This circumstance would more likely occur during longer sampling intervals and could be identified if high-frequency wind direction measurements were retained.

When b is found to be significantly different from zero, the data are often processed by conducting linear regression after matching the rank order of the model predictions with the rank order of the observed data and the intercept forced to be zero. This may provide a more appropriate estimate of the slope and associated emission flux rate.

The data were analyzed following the methodology given by Johnson et al. (1999). The regression relationship between measured and ISCST concentrations were obtained using standard linear regression, with y-axis as measured values.

Total Emissions. The total mass lost from soil as a function of time since application can be found using

$$f_{total}(t) = \iiint_{x,y} f_z(x, y, 0, \tau) d\tau dy dx = A \int_0^t f_z(0, \tau) d\tau \quad 2.1.8$$

Where $f_z(x,y,0,t)$ is the volatilization flux density ($\mu\text{g m}^{-2} \text{s}^{-1}$), τ represents the time coordinate, and (x,y) is a horizontal coordinate in the treated region of the field. For a spatially uniform source, the right-hand equation can be used where A is the area (cm^2) of the treated field.

2.2 General Field Experimental Procedures

For each study, similar experimental procedures were employed. Specific information for a particular study is provided along with the results from each experiment; see experimental information.

Field Preparation

Prior to fumigation, the fields were prepared following industry standard practices and fumigant label directions. The positions of the sampling equipment were determined and a map of each experimental site developed.

Weather Station

A 10 m weather station was installed adjacent to one of the field and included a 10 m wind speed measurement. This information was used for the indirect flux method. The weather station measured air temperature, relative humidity, solar radiation, and wind speed and wind direction. Measurements were recorded at 2 min and hourly intervals.

This information also helps to identify prevailing wind directions and assists in the placement of air samplers.

Air Sampling

Prior to fumigant application to each field, background air samples were collected. The procedures for obtaining these samples were identical to the samples collected during the experiment and represent the background concentration at each location. During the fumigation period, and for approximately a week afterwards, no nearby fields were fumigated with Telone II or Telone C-35, so interferences were non-existent.

Air samples were collected for 12–16 days. Sample collection ceased when repeated non-detect values were evident. There were 6-8 sample heights at each aerodynamic monitoring station at the center of each field, and a minimum of 8 ISCST monitoring stations surrounding each field and located at a height of 1.5 m above the soil surface. The off-field samplers were installed prior to fumigation. The equipment used for on-field flux measurement was installed in the field as soon as practically possible i.e., as soon as the machinery has moved beyond the sampling position. The sampling intervals for offsite samples were similar to the on-field measurements. Specific information is included under “Experimental Information” for each experiment described below. For on-field measurements, the sampling began as soon as access to the field was available and equipment was setup and activated. For off-site air sampling, the measurements began prior the start of fumigant application.

Air monitoring of fumigant concentrations was conducted using personal air sampling pumps which pulled air through vapor collection tubes of either activated charcoal (2005 study where Telone II was used) or activated charcoal and XAD-4 (2007 study where Telone C-35 was used). In both studies, sorbent tubes had an 'A' section a 'B' section to allow for determination of breakthrough. Once samples were collected, the sample tubes were tightly capped, sealed in plastic bags, and placed on ice, or in a freezer, until transported to the laboratory. Samples remained frozen until analysis and were stored at -75°C, once in the laboratory.

Soil Sampling

A series of soil-gas samples were taken periodically during each experiment at up to 8 depths. Stainless steel sampling probes were installed in the soil shortly after fumigant application. Charcoal (2005 study) or XAD (2007 study) sorbent tubes were used to sample 50–500 cm³ of the soil air phase.

Soil water content, soil temperature and soil heat flux measurements were collected periodically during each experiment. At the end of the experiment, soil samples were taken to a depth of 1 m to obtain final water content.

Direct Flux Measurement

Direct volatilization flux measurements were obtained using standard micro-meteorological methods. Meteorological equipment was set up in the treated area to measure local wind speed gradients, near-surface wind direction, and ambient air temperature gradients. Auxiliary information, including the relative humidity over the field, incoming solar radiation, and net radiation were also measured. Measurements were recorded at 2–5 minute intervals.

To obtain flux measurements, pesticide vapor concentrations were measured using the charcoal or XAD sampling tubes which sampled air at 6–8 heights above the surface near the center of each field. Wind speed measurements were obtained using a mast with either six Thornthwaite Anemometers at 10, 20, 40, 80, 160, and 320 cm above the field surface, or 5 Windsonic anemometers placed at 20, 40, 80, 160 and 400 cm. Replicated air temperatures were measured at 3 heights (e.g., 20, 40 and 80 cm) above the field.

Indirect Flux Measurement

Indirect volatilization flux measurements were obtained using the charcoal or XAD sampling tubes which sampled air around the field at a height of 1.5 m above the soil surface.

2.3 General Laboratory Experimental Procedures

Fumigant Extraction From Sorbent Tubes, General Methodology

For the sorbent tubes, solvent extraction using hexane (XAD tubes) or acetone (charcoal tubes) was used to remove the 1,3-D (cis), 1,3-D (trans) and chloropicrin. For

some samples, the 'A' and 'B' sections were analyzed separately by dispensing each section into an individual glass vial and adding 3–4 mL of solvent. Sufficient solvent was added to ensure complete coverage of the sorbent material. When both sections were analyzed together, the entire contents of a sorbent tube was dispensed into a glass vial and 3–8 mL of solvent was added, again ensuring complete coverage of the sorbent material. The vials were then immediately capped and shaken for 30 mins. After settling, approximately 1 mL of supernatant was transferred to a GC vial for analysis.

Analysis of Telone (1,3-D) and Chloropicrin (CP) in Solvent Extracts

The concentrations of 1,3-D and CP in solvent extracts were determined by gas chromatography (GC) using an HP 6890 GC (Agilent Technologies, Palo Alto, CA) equipped with an electron capture detector (ECD). The GC conditions were: use of a 30 m x 0.25mm x 1.4 µm DB-VRX capillary column (J & W Scientific, Folsom, CA) with 230°C inlet temperature, 280°C detector temperature and 1.3 mL/min column flow rate (He). The initial oven temperature were 50°C and the temperature were increased to 80°C at 2.5°C/min, then increased to 110°C at 30°C/min and held for 4 min. Under these conditions, the retention times for *cis*-1,3-D, *trans*-1,3-D, and CP are 11.3, 12.5, and 13.4 min, respectively.

The limit of detection (LOD) and the limit of quantification (LOQ) of this method were determined to be, 0.015 µg/tube and 0.05 µg/tube, respectively. Tests were conducted to determine the extraction efficiency of 1,3-D vapors trapped by charcoal sampling tubes at a airflow rate of 0.15 L/min. The extraction efficiency was found to be 84 ± 7% (1,3-D *cis*) and 86 ± 7% (1,3-D *trans*). Further, connecting 4 sampling tubes in series and sampling for 8 hours it was found that more than 99.99% of the total mass was contained in the first tube.

Experiment #1 (2005)

Analysis of Air Sampling Tube Breakthrough. During the 2005 study, a total of 2762 charcoal sampling tubes were collected, 900 at the center of the two field plots and 1862 from locations surrounding the fields. Due to the large number of samples that were collected, and to keep analytical costs within budget, only a portion of the samples were split into A & B sections and analyzed separately. Tubes from sampling periods: 1-15, 29-32, 35-37, 49-52, 62-64, 70-73, 90-92 were analyzed for the concentration in the A and B sections. For all other tubes, A and B sections were combine and analyzed together. The following is a summary of the number of number of sampling tubes and percent that had A and B sections analyzed.

Number of tubes collected at center of fields =	900
Number of tubes collected surrounding the fields =	1862
Total number of tubes =	2762
Number of sampling tubes tested for A & B =	707
Percent analyzed for A & B =	
	25.6%

For both the irrigation and organic matter treatments, an analysis of the A & B sections for 1,3-D (cis+trans), leads to the following results. A total of 707 samples tubes were analyzed and 26 had measurable mass in the B section (i.e., 3.7% of the total). The total mass on all tubes collected at, and surrounding, the fields was 892 ng/μL. The total mass on the B sections was 0.63 ng/μL or 0.07% of the total collected mass. The following summarizes this information and provides a breakdown based on the length of the sampling interval.

Number of tubes analyzed (both treatments) =	707
Total 1,3-D (cis+trans) mass in sampling tubes =	892.1 ng/μL
Total 1,3-D (cis+trans) mass in B section only =	0.63 ng/μL
Percent of 1,3-D (cis+trans) mass in B section =	0.07 %
Number of tubes with measurable concentration in B section =	26
Percent of tubes with measurable concentration in B section =	3.7%

Sampling Interval Duration, h	Number of Tubes	Number of Tubes with Concentration	
		in B Section > 0	Frequency
2	402	6	0.8%
3	58	3	0.4%
5	80	3	0.4%
6	107	8	1.1%
10	10	6	0.8%
12	50	0	0.0%
Totals	707	26	3.7%

Summary of recovery from travel spikes. Four sets of triplicate sampling tubes were fortified at three 1,3-D (cis+trans) concentrations several days prior to the day of application. Three sets were sent to the field frozen and then stored, shipped back to the laboratory, and analyzed along with the field samples. This procedure documents the amount of 1,3-D lost during field storage, transit, and laboratory storage prior to analysis. The following summarizes the results of the travel spikes. In general, no loss of sample was observed.

Sample Concentration	Lab %	Set 1 (9-2-2005)		Diff from Average %	Set 2 (9-8-2005)		Set 3 (end) Travel %	Set 2 Diff from Average %	Set 3 Diff from Average %
		Travel %	Average %		Lab %	Travel %			
10 μg/tube	85.3	86.2	-0.010		74.0	74.8	73.1	-0.010	0.013
100 μg/tube	75.4	76.7	-0.016		68.0	67.9	68.2	0.002	-0.004
2000 μg/tube	74.8	74.5	0.004		73.3	73.8	73.2	-0.007	0.001
Average Recovery =		78.8	%			71.9	71.6	%	
Avg % Travel Loss =		-0.007	%			-0.005	0.003	%	
Stdev % Travel Loss =		0.010	%			0.006	0.009	%	

Experiment #2 (2007)

Analysis of Air Sampling Tube Breakthrough. Charcoal sampling tubes were used to collect 1,3-D (cis+trans) concentration from locations surrounding each field. A total of 1800 charcoal sampling tubes were collected with 586 tested for 'A' and 'B' concentrations. For all other tubes, the A and B sections were combined and analyzed together. The following is a summary of the number of sampling tubes and percent that had A and B sections analyzed.

Number of tubes collected surrounding the fields =	1800
Number of sampling tubes tested for A & B =	586
Percent analyzed for A & B =	32.6%

For this experiment, more than half of the samples had measurable concentrations in the 'B' section. Even so, the total mass found in the 'B' section was approximately 0.2% of the total mass collected on the 586 tubes. The following summarizes this information and also provides a breakdown based on the length of the sampling interval.

Number of tubes analyzed (all treatments) =	586
Total 1,3-D (cis+trans) mass in sampling tubes =	1886.3 ng/ μ L
Total 1,3-D (cis+trans) mass in B section only =	3.796 ng/ μ L
Percent of 1,3-D (cis+trans) mass in B section =	0.20 %
Number of tubes with measurable concentration in B section =	374
Percent of tubes with measurable concentration in B section =	63.8%

Sampling Interval Duration, h	Number of Tubes	Number of Tubes with Concentration in B Section > 0	Frequency
3	262	159	27.1%
6	72	43	7.3%
12	252	172	29.4%
Totals	586	374	63.8%

XAD-4 Sampling Tubes. A total of 1258 XAD-4 sampling tubes were collected from locations surrounding the field to capture chloropicrin. A total of 216 were tested for concentration in the 'A' and 'B' sections, which represents about 17% of the tubes collected. For all other tubes, the A and B sections were combine and analyzed together. The following is a summary of the number of number of sampling tubes and percent that had A and B sections analyzed.

Number of tubes collected surrounding the fields =	1258
Number of sampling tubes tested for A & B =	216
Percent analyzed for A & B =	17.2%

Nearly three quarters of the samples had measurable concentrations in the 'B' section. For chloropicrin, the total mass found on the 'B' section was a significant fraction of the total mass collected from all tubes, 18%. Therefore, the possibility of breakthrough cannot be eliminated.

Number of XAD-4 tubes analyzed (all treatments) =	216
Total chloropicrin mass in sampling tubes =	1.2 ng/ μ L
Total chloropicrin mass in B section only =	0.228 ng/ μ L
Percent of chloropicrin mass in B section =	18.31 %
Number of tubes with measurable concentration in B section =	154
Percent of tubes with measurable concentration in B section =	71.3%

Sampling Interval Duration, h	Number of Tubes	Number of Tubes with Concentration in B Section > 0	Frequency
3	144	91	42.1%
12	72	63	29.2%
Totals	216	154	71.3%

It is possible that this outcome reflects the very low chloropicrin air concentrations measured during this experiment. The total chloropicrin mass collected on the tubes is about 300 times lower than the mass collected for 1,3-D (cis) (based on total isomer mass divided by number of tubes collected). This is very low considering the proportions of 1,3-D (cis) : 1,3-D (trans) : chloropicrin applied to the fields were nearly the same. Therefore, this may be a reflection of the difficulty sampling very low fumigant concentrations.

Mast XAD-4 Samples. The 'A' and 'B' sections for all of the XAD-4 sampling tubes collected at the center-of-field sampling masts were analyzed for 1,3-D and chloropicrin. A total of 1458 samples were collected from all three treatments. The following provides a summary.

	1,3-D (cis+trans)	chloropicrin
Number of tubes collected surrounding the fields =	1458	1458
Number of sampling tubes tested for A & B =	1458	1458
Percent analyzed for A & B =	100	100 %

For 1,3-D (cis+trans), less than 2% of the mass was found in the 'B' section. This suggests that breakthrough was not significant for these samples, even though about 25% of the samples had measurable mass in the 'B' section. For chloropicrin, about 17% of the samples had measurable mass and about 6% of the total mass collected was found in the 'B' sections. The total chloropicrin mass collected was about 40 times less than for 1,3-D (cis).

	1,3-D (cis+trans)	chloropicrin
Number of XAD-4 tubes analyzed (all treatments) =	1458	1458
Total mass in sampling tubes =	1659.6	21.3 ng/μL
Total mass in B section only =	28.882	1.383 ng/μL
Percent of mass in B section =	1.74	6.48 %
Number of tubes with measurable concentration in B section =	345	254
Percent of tubes with measurable concentration in B section =	23.7	17.4 %

Sampling Interval Duration, h	Number of Tubes	Number of Tubes with 1,3-D in B Section > 0	Frequency	Number of Tubes with chloropicrin in B Section > 0	Frequency
2	522	117	8.0%	88	6.0%
3	342	52	3.6%	43	2.9%
4	162	14	1.0%	10	0.7%
5	36	5	0.3%	4	0.3%
6	90	22	1.5%	21	1.4%
7	18	0	0.0%	0	0.0%
10	72	56	3.8%	23	1.6%
12	162	49	3.4%	43	2.9%
13	54	30	2.1%	22	1.5%
Totals	1458	345	23.7%	254	17.4%

Summary of recovery from travel spikes. Four sets of triplicate sampling tubes were fortified at three 1,3-D (cis+trans) and two chloropicrin concentrations several days prior to the day of application. Three sets were sent to the field frozen and then stored, shipped back to the laboratory, and analyzed along with the field samples. This procedure documents the amount of 1,3-D and chloropicrin lost during field storage, transit, and laboratory storage prior to analysis. The following summarizes the results of the travel spikes. In general, no loss of sample was observed.

1,3-D (cis+trans) Spike	Lab	Set 1 (9-5-07) Travel	Set 2 (9-12-07) Travel	Set 3 (9-23-07) Travel	Set 1 Diff from Average	Set 2 Diff from Average	Set 3 Diff from Average
	%	%	%	%	(%)	(%)	(%)
10 ug/tube	83.8	83.2	96.0	89.2	0.007	-0.135	-0.062
100 ug/tube	88.0	84.2	95.4	87.4	0.044	-0.081	0.007
2000 ug/tube	87.6	82.7	88.8	85.2	0.058	-0.013	0.028
Average Recovery =					87.6%		
average % Loss Due To Travel =					-0.016%		
stdev % Loss Due To Travel =					2.730%		

chloropicrin		Set 1	Set 2	Set 3	Set 1	Set 2	Set 3
Spike		(9-5-07)	(9-12-07)	(9-23-07)	Diff from	Diff from	Diff from
	Lab	Travel	Travel	Travel	Average	Average	Average
	%	%	%	%	(%)	(%)	(%)
10 ug/tube	87.0	84.6	92.5	87.2	0.027	-0.062	-0.003
100 ug/tube	93.6	90.4	95.3	89.1	0.035	-0.018	0.049

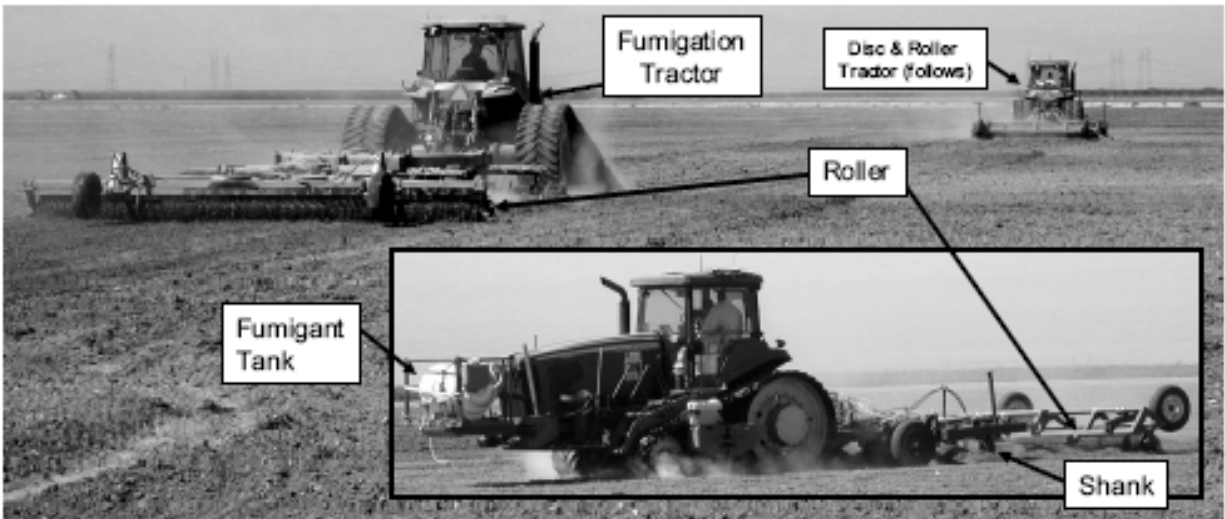
Average Recovery = 90.0%
 average % Loss Due To Travel = 0.005%
 stdev % Loss Due To Travel = 3.446%

3 Results of Experiment #1: (2005): Telone II Fumigation

Since this experiment had an irrigation treatment, existing on-field sampling equipment (i.e., gradient mast, weather station) was modified to allow sample collection during irrigation. This allowed measurement of volatilization losses during irrigations.

3.1 Experiment-Specific Methodology

Since the primary method to obtain the volatilization rate involved the use of micro-meteorological methods, the field site was located in a production area with large vacant field areas that provided a large up-wind fetch. The field experiment began on August 31, 2005 and was concluded September 16, 2005. About two weeks before conducting the field experiment, the each field was plowed followed by multiple discing operations to break up large soil aggregates. In addition, the field was irrigated and allowed to drain so that the initial soil water content was approximately 0.2 ($\text{cm}^3 \text{cm}^{-3}$). At the time of application, 1,3-D was applied to the field by a commercial applicator using a tractor containing 9 shanks mounted on a 4.5 m tool bar at 0.5 m spacing increments. The target depth of application was 0.46 m (i.e., 18 inches). Telone II® (CAS: 542-75-6) was applied to the field as 97.5% mixture of 1,3-dichloropropene cis (CAS: 10061-01-5) and trans (CAS: 10061-02-6) isomers and 2.5% inert components.



A



Figure 3.1.1. Diagram showing shank fumigation process (A) and a tool bar with 9 shanks (B). The shanks were oriented in a 'V' shape with 4 shanks on each arm and a shank at the center point. In this picture, 5 shanks have lined up.

B

In Milham sandy loam, 1,3-D has a reported soil degradation half-life of approximately 5 d (Ashworth and Yates, 2007). 1,3-D has a dimensionless Henry's Law constant, $K_h = 0.04-0.06$ (Leistra, 1970); and an organic carbon distribution coefficient, $K_{oc} = 32 \text{ mL g}^{-1}$ (Wauchope et al., 1992).

Sampling Mast at Center of Field. The concentration of 1,3-D in atmosphere was obtained by passing air through 8 x 110 mm charcoal sampling tubes (SKC 226-09, SKC, Incorporated, Fullerton, CA). The charcoal tubes contained two beds, 400 and 200 mg, of coconut charcoal. A vacuum system was used to draw air through the charcoal sampling tube at a nominal flow rate of 0.15 L/min using battery-powered personal air samplers (SKC, Inc. MODEL 224-44XR). Flow meters were (McMillan, Inc. Model 100-4) connected to a data logger and used to monitor the flow rate. Chemical breakthrough tests were conducted in the laboratory prior to the field experiment to verify that the second charcoal bed was free of 1,3-D. The position of the sampling mast is shown in Figure 3.1.2.

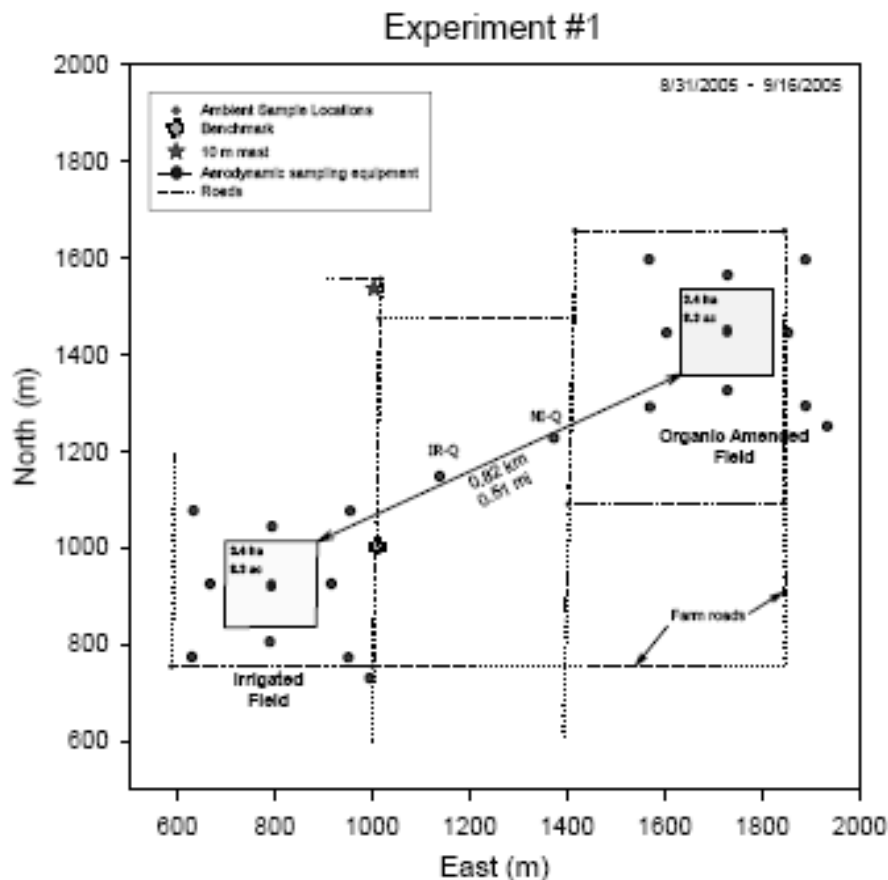


Figure 3.1.2. Schematic of the fields and positions of the air sampling equipment. A 10-m meteorological mast was used to collect wind speed and wind direction measurement for the back-calculation flux methods. The spatial position of a permanent benchmark was obtained to allow locating positions at a later date.

Off-site Sampling Mast. The concentration of 1,3-D in atmosphere surrounding the field was obtained by passing air through charcoal sampling tubes contained two beds, 800 and 200 mg, of coconut charcoal (SKC 226-16, SKC, Incorporated, Fullerton, CA). The flow rate was monitored at the start and end of each sampling period. A vacuum system was created using battery-powered personal air samplers (SKC, Inc. 224-44XR) to draw air through the charcoal sampling tube at a nominal flow rate of 1.5 L/min. A total of 9 offsite samplers were positioned around each field and 2 samplers were placed between the fields. Chemical breakthrough tests were conducted in the laboratory prior to the field experiment to verify that the second charcoal bed was free of 1,3-D. The position of the air sampling equipment is shown in Figure 3.1.2.

After each sampling interval, the tubes were removed from the sampling mast, capped, stored on ice, and transported to a freezer for temporary storage. Several times during the experiment, the samples were removed from the portable freezer, placed in an ice chest, transported to the laboratory and stored in a -70°C freezer until analysis of the 1,3-D concentration. Chemical breakthrough tests were conducted in the laboratory prior to the field experiment to verify that the second charcoal bed was free of 1,3-D.

Meteorological Measurements. Gradients of wind speed and temperature are necessary to obtain emission rates using the aerodynamic method. Wind speed measurements were obtained using five Thornthwaite anemometers (CWT-1806, C.W. Thornthwaite Assoc.) positioned at 0.2, 0.4, 0.8, 1.6, and 2.4 m above the field surface. In addition, a MetOne (014A or 034B, Campbell Scientific Inc.) wind speed sensor was placed at 3.44 m. The air temperature gradient was obtained by placing pairs of fine-wire thermocouples (FW3, Campbell Scientific, Inc.) at 0.4 and 0.8 m heights and connecting them to a data logger (10X, Campbell Scientific, Inc.) in a configuration that allows the gradient to be measured directly. Other meteorological information was also obtained including relative humidity and temperature (HMP35C, Campbell Scientific, Inc.), incoming solar radiation (LI-200S, LI-COR, Inc.[§]), net solar radiation (Q-6, Radiation and Energy Balance Systems, Inc), and barometric pressure (Vaisala PTA-427, Campbell Scientific, Inc.).

3.2 Field #1: Broadcast-Shank Telone II Fumigation with Intermittent Water Seals

3.2.1 Field Specific Information

The experiment was conducted in Field-23W which is comprised of a Milham sandy loam soil. Fumigation began on August 31, 2005 at 10:45 am and ended at 3:00 pm. The target application rate was 132 kg/ha (i.e., 12 gal/ac) and was applied to a nearly square area (178.3 m x 188.5 m) of 3.41 ha (i.e., 8.4 acres). This results in a total applied mass of 446.7 kg. A picture showing the sprinkler irrigation is shown in Figure 3.2.1.



Figure 3.2.1 Sprinkler irrigation to create a surface water seal.

The irrigated-field layout showing position of the sensors, the treated area and sprinkler irrigation lines is shown in Figure 3.2.2.

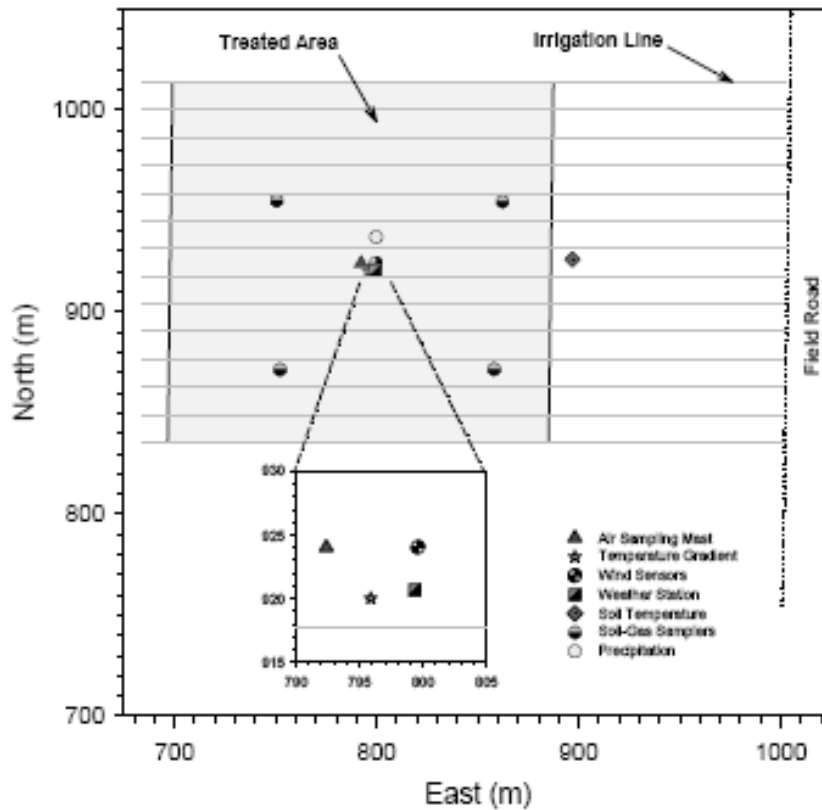


Figure 3.2.2. Schematic of irrigated field showing the positions of sensors and irrigation lines.

The soil surface was irrigated with a total of 7.48 cm of water. The irrigation schedule was 1.88 cm of water applied immediately after fumigant application and 1.4 ± 0.13 cm of water applied each day for the following 4 days; at approximately 11:00 am. After the fifth irrigation, the soil was allowed to dry.

On-site, the concentration of 1,3-D in the atmosphere was collected at 10, 40, 80, 159, 236, and 360cm above the soil surface. During the first 6 days of the experiment, the measurement periods consisted of 2-hour samples from 0700–2100 hours and a 10-hour nighttime sample. Beginning on the 7th day, there were 3-hour sample intervals from 0700–1900 and a 12-hour nighttime sample. Beginning on the 10th day, two 6-hour daytime and a 12-hour nighttime sample were collected. Beginning on day 13, two 12-hour samples were collected each day.

Measurements of the 1,3-D concentration at the several locations surrounding the field and 1.5 m above the land surface (off-site) were also collected using this sampling schedule. Longer sampling periods were used later in the experiment to ensure sufficient mass was collected in the sampling tubes, since volatility losses for 1,3-D typically decrease over time.

3.2.2 Results and Discussion

Ambient Conditions. The incoming (Q_{in}) and net (Q_{net}) solar radiation are shown in Figure 3.2.3 as flux densities. Solar radiation is important since it is a measure of the energy available at the surface to heat the soil, heat the atmosphere and induce evaporation; all of which affect volatilization from the surface. The regular behavior presented in the graphs is a result of sunny, clear-sky conditions. The maximum and average of the solar radiation measurements, respectively, were 870 and 245 W/m^2 .

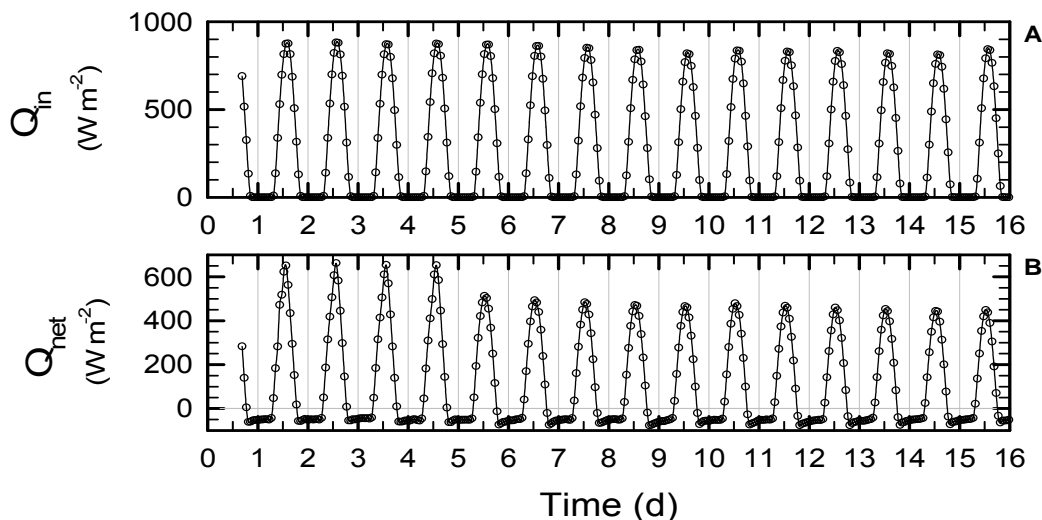


Figure 3.2.3. Incoming solar radiation ($W m^{-2}$) (A) and net solar radiation ($W m^{-2}$) (B) during the first 16 days of the experiment. Integer values occur at midnight

The net radiation (Figure 3.2.3 B) appears to be slightly higher during the first 4 days of the experiment and is due to the application of irrigation water to the surface soil during this time. The higher Q_{net} is due to a combination of factors including changes in albedo causing a reduction in short-wave radiation reflected from the surface, a reduction in long-wave radiation as a result of lower surface temperatures and an increase in absorbance due to presence of the irrigation water. During the first 4 days, the maximum Q_{net} was 662, the minimum was -63 W m^{-2} , and the 4-day average was 139 W m^{-2} . For the remainder of the experiment (days 5-16), the Q_{net} was lower with maximum, minimum and average values, respectively, of 513, -77 , and 103 W m^{-2} .

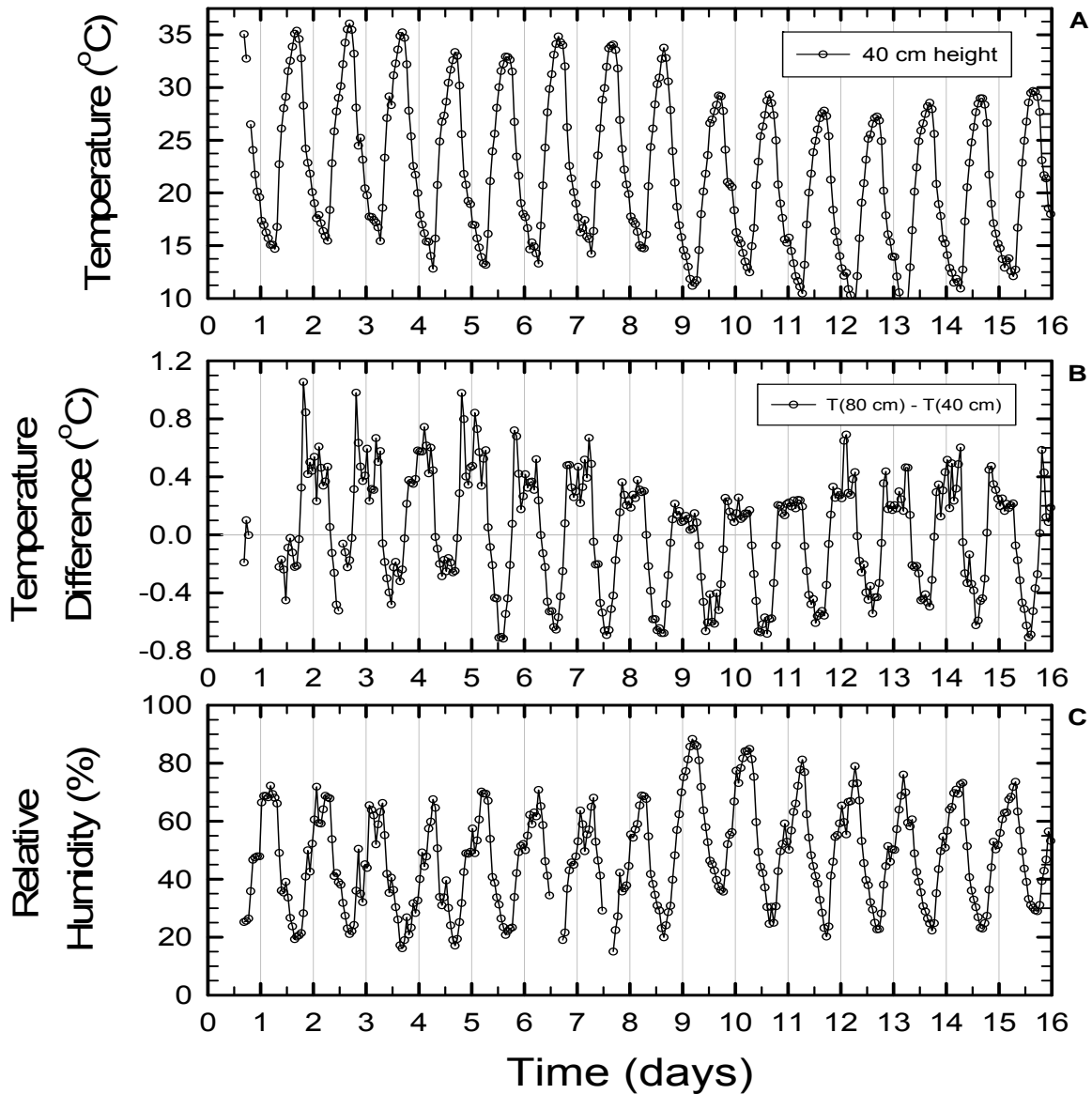


Figure 3.2.4. Air temperature in °C at 0.4 m height above the soil surface (A), temperature difference between 0.8 and 0.4 m heights (B), and relative humidity measured at 0.8 m (C)

Figure 3.2.4 B is a graph of the temperature gradient during the experiment. The gradient was obtained from measurements taken at 80 and 40 cm above the soil surface. Negative values indicate that the temperature near the surface is greater than the temperature at positions higher in the atmosphere. In general, the temperature gradient varied ± 1 °C throughout the experiment and negative gradients, i.e., unstable conditions, generally occurred during the middle of the day. Unstable conditions generally leads to increased volatilization since the air over the soil surface is buoyant compared to the air above, and rises. This moves the fumigant away from the soil surface and increases the concentration gradients across the soil-atmosphere boundary, which is an important driving force in the volatilization process.

Gradient Richardson Number. The gradient Richardson number (Figure 3.2.5) is a dimensionless parameter describing the relative importance of buoyancy and convective forces and approaches zero for neutral stability conditions. By definition, the sign of the Richardson number is determined by the temperature gradient.

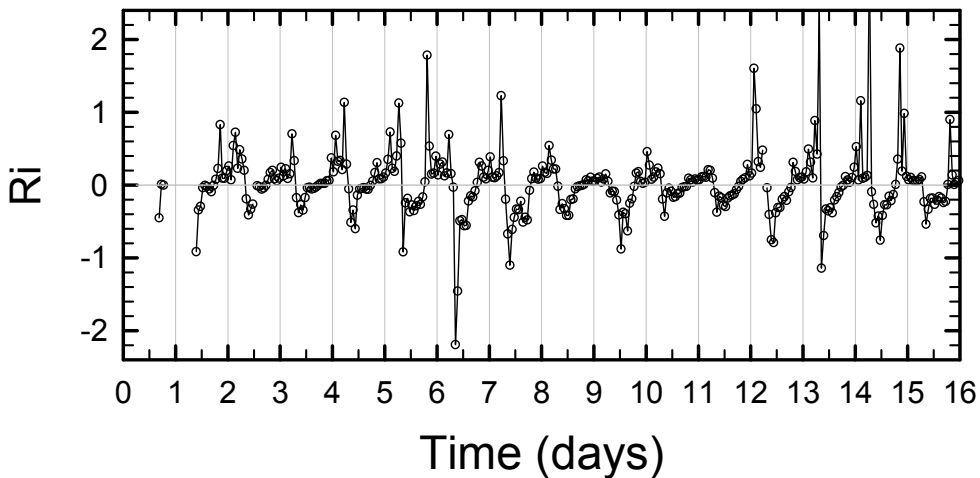


Figure 3.2.5. Gradient Richardson's Number, Ri.

In general, the Richardson number varied by ± 2 throughout the experiment and negative values, indicating unstable conditions, generally occurred during the middle of the day. Unstable conditions generally leads to increased volatilization since the air over the soil surface is buoyant compared to the air above, and rises. Buoyancy driven convection can transport the fumigant away from the soil surface and increases the concentration gradients across the soil-atmosphere boundary, which is an important driving force in the volatilization process.

The presence of the irrigation water at the beginning of the experiment led to reduced daytime temperature differences as shown by smaller midday negative values (Figure 3.2.4 B). During the irrigation period, the average temperature difference between the hours of 1100 and 1300 was -0.24 °C. Later in the experiment the average temperature difference between 1100 and 1300 was -0.54 °C.

Wind Speed and Direction. The wind speed at a height 40 cm and wind direction at 10 m are shown in Figure 3.2.6. The winds are predominately out of the north as shown in the wind rose diagram (Figure 3.2.6B). The maximum wind speed was 4.2 m/s but daily maxima were generally between 2 m/s to a high of about 3 m/s. During the middle of the night, wind speeds were commonly from 0.2 to 0.4 m/s.

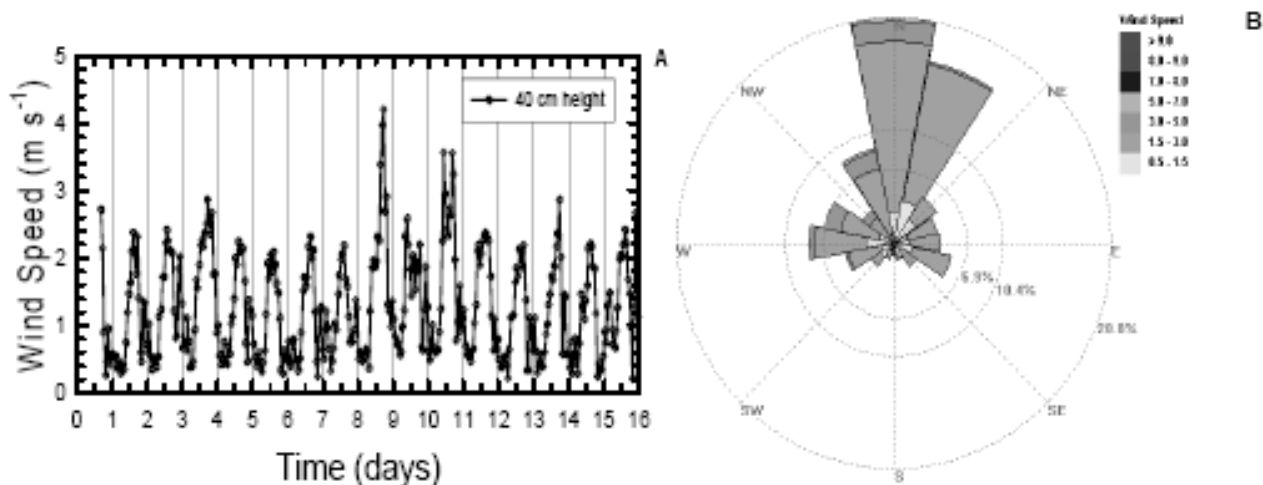


Figure 3.2.6. The variation in wind speed at 0.4 m above the soil surface during the experiment (A). A wind rose diagram (B) shows the wind direction, speed and probability the wind will occur in a specific direction.

Air Concentrations. Concentrations of 1,3-D were collected at several heights in the center of the field. The concentrations at 40 and 80 cm above the surface are shown in Figure 3.2.7. The levels were relatively high during the first 4 days of the experiment and were very low from 8–16 days. Near the soil surface, observed concentrations exceeded 1000 $\mu\text{g m}^{-3}$, while at a height of 80 m the concentration remained below 500 $\mu\text{g m}^{-3}$. These levels are significantly higher than the concentrations measured at the offsite locations surrounding the field (data not shown). For example, the peak concentration measured at the field center at a height of 160 cm was 137 $\mu\text{g m}^{-3}$, and occurred during the 24th sample period (i.e., at 3.58 d). At the same time, the peak measured concentration 30 m outside the field boundary, at a height of 150 cm, was 6.12 $\mu\text{g m}^{-3}$.

The relatively large concentrations at the beginning of the experiment were due primarily to the larger soil fumigant mass present in the soil shortly after application and the rapid soil diffusion caused by the presence of soil disturbances resulting from the fumigation shanks (Yates, 2009). As the fumigant volatilizes and degrades, atmospheric concentrations are reduced. The presence of the irrigation water also plays a role in the 1,3-D concentration in the atmosphere. While increased water content at the soil surface tends to reduce gas phase diffusion to the atmosphere by reducing the air phase porosity (Jin and Jury, 1995), higher water contents at the surface increase evaporative cooling which tends to create more stable atmospheric conditions when compared to the presence of a hot and dry surface. For a similar volatilization rate, this will lead to higher atmospheric concentrations. The cooling effect

of applying irrigation water to the soil surface is readily seen in Figure 3.2.4B with smaller temperature differences shortly after irrigation.

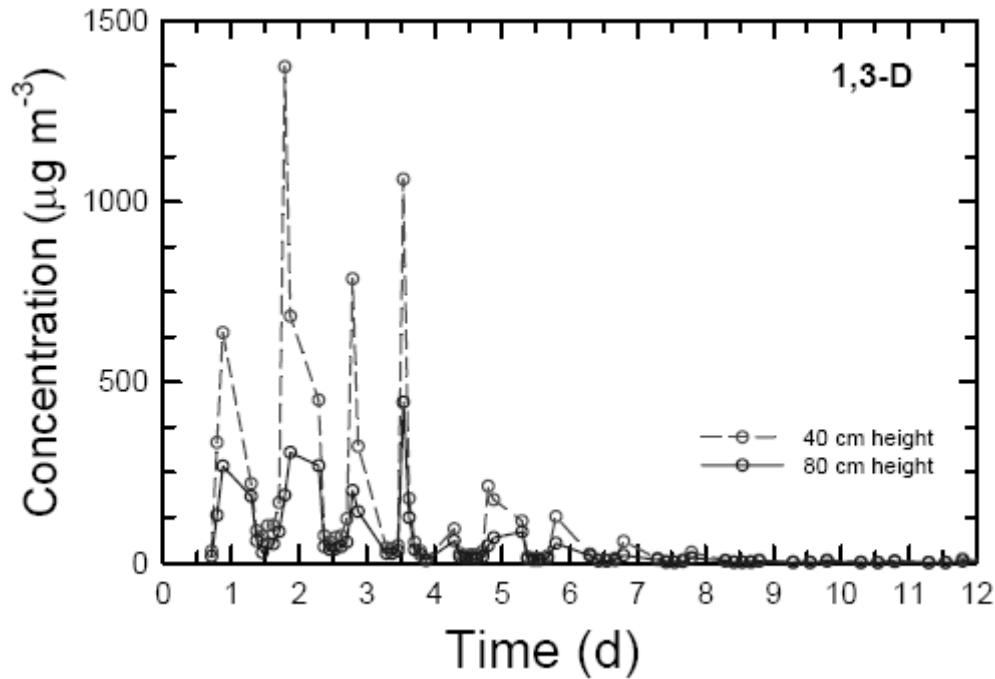


Figure 3.2.7 Measured 1,3-D concentration in the atmosphere at 0.4 and 0.8 m above the soil surface at the center of the irrigated field. Open circles are the period-averaged concentration collected with the on-field sampling mast.

This effect is also apparent in the values of the gradient R_i , which tend toward zero shortly after irrigation and this pattern continues until the soil is allowed to dry, after day 5. Under stable conditions (e.g., positive Richardson number), the air mass over the field experiences less vertical mixing which leads to increased concentrations. The increased concentration in the atmosphere also reduces the concentration gradients across the soil-atmospheric boundary. This can lead to a reduction in volatilization relative to more unstable conditions.

1,3-D Volatilization. Shown in Figure 3.2.8 are time series of the volatilization rate (i.e., flux density) and the timing and amounts of irrigation water applied to the field.

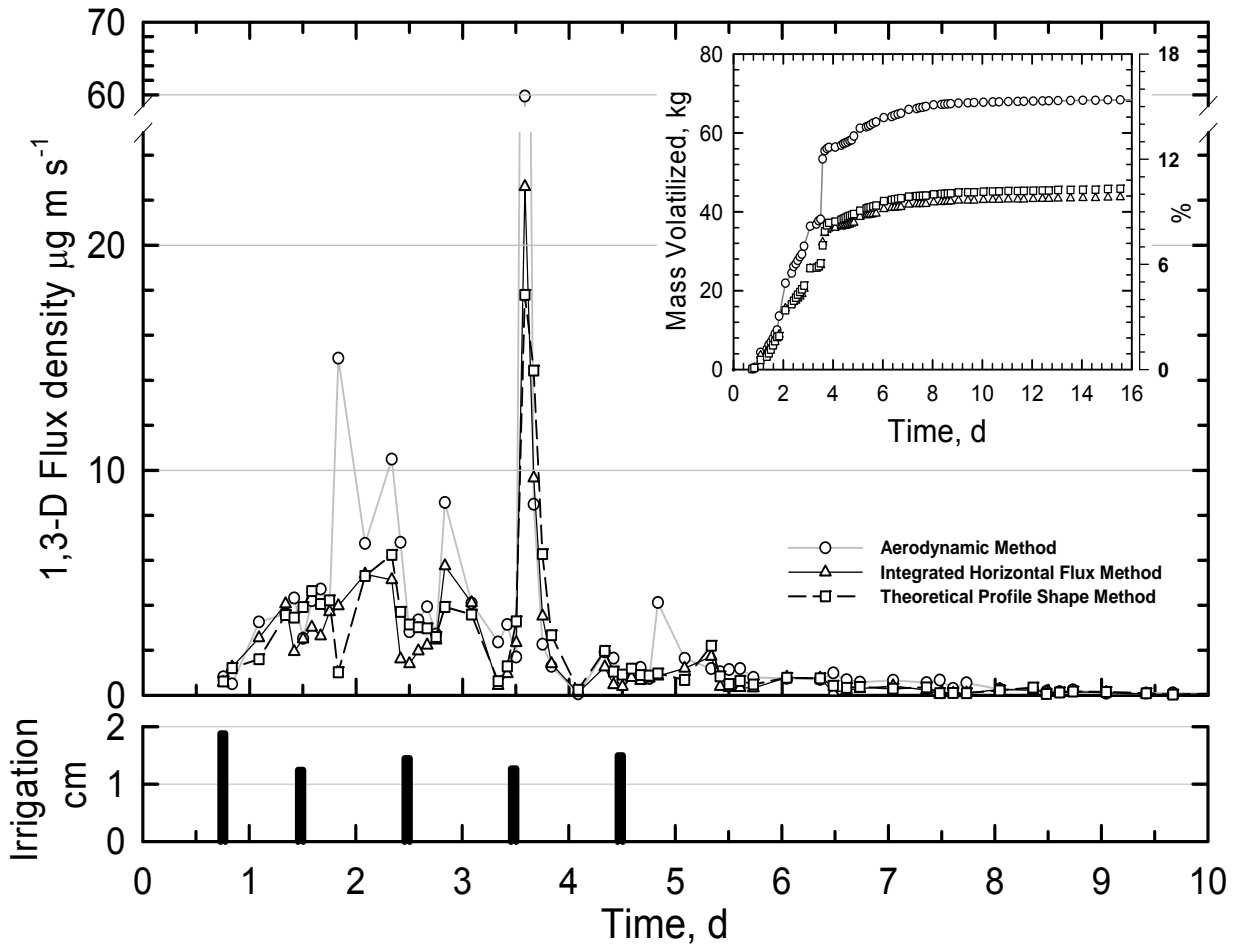


Figure 3.2.8. Volatilization rate ($\mu\text{g m}^{-2} \text{s}^{-1}$) as a function of time (day) after application for the aerodynamic (solid line, circles), integrated horizontal flux (solid line, triangles), theoretical profile shape (dashed line, squares). The inset shows cumulative 1,3-D emission as a function of time after application. The percentages on the right-most axis indicates percent of applied 1,3-D. All values are averages over the sampling period.

The three methods demonstrate a similar temporal pattern throughout the experiment. Under non-irrigated conditions, peak fumigant volatilization rates commonly occur during the midday (Yates *et al.*, 1996b, 1997; Majewski 1997). However, application of surface irrigation causes the midday peak volatilization rates to be damped by the apparent formation of a surface water seal. The surface water seal inhibits fumigant transport to the soil surface by reducing, or eliminating, the gas-phase diffusion process by filling the soil pore space with water or by 1,3-D partitioning into the water phase. For this soil, the porosity was approximately $0.5 \text{ cm}^3 \text{ cm}^{-3}$, soil liquid-phase diffusion coefficient $0.0078 \text{ cm}^2 \text{ d}^{-1}$, and the soil gas-phase diffusion coefficient is $1100 \text{ cm}^2 \text{ d}^{-1}$. Fumigant diffusion through a soil saturated with water is approximately 5-orders of magnitude less than diffusion through the same soil at 25% of saturation; clearly soil gas diffusion dominates when the soil pores are devoid of water.

The maximum daily volatilization rate for each method occurred on the 3rd day ($t = 3.54$ d) and ranged from approximately 18 to 60 $\mu\text{g m}^{-2} \text{s}^{-1}$. Viewing Figure 3.2.8 it is clear that, for several measurement periods, the ADM estimates higher volatilization rates compared to the IHF and TPS methods and that the IHF and TPS methods agreed more closely throughout the experiment.

The inset shown in Figure 3.2.8 provides an illustration of the total 1,3-D mass lost to the atmosphere with time after application. This information was obtained by integrating the volatilization rate over time and multiplying by the total field area. It is clear that the IHF and TPS methods provide estimated volatilization rates that were very similar. After 16 d, the total emission estimates from the IHF and TPS methods were between 9.8 and 10.3% of the applied material. The cumulative emission estimate from the ADM, however, is larger, and after 16 d was determined to be 15.3%. Based on the amount of 1,3-D applied to the field, the ADM estimate is 5.2% greater mass loss than the IHF and TPS methods. The average total mass lost for the three methods was $11.8 \pm 3\%$. These results are consistent with estimates of the experimental uncertainty for emissions of methyl bromide obtained using the ADM, as reported by Majewski (1997), which was based on a regression analysis of the log-linear wind speeds and concentrations with respect to height. This analysis should also apply to other fumigants that have log-linear concentration profiles. In a report by Wilson and Shum (1992), the theoretical accuracy of the IHF method was determined using a Lagrangian stochastic model and found to be within approximately 20% for appropriately large field sites and surface roughness lengths below 10 cm. This study also provides guidelines that can be used to design IHF experiments with suitable experimental accuracy.

It is clear from Figure 3.2.8 that, for most of the experiment, the measured ADM flux rates were similar in magnitude to the IHF and TPS methods. However, for a few time periods the ADM flux is considerably larger than the IHF and TPS methods. To investigate the relative effect of these values, their contribution to the total emissions was determined. The single largest value occurred at $t = 3.54$ d and the difference between the ADM and IHF-TPS methods represents 2.3% of the cumulative emissions and explains 43% of the difference between methods on a percent-difference basis. The effect of the 5 points with the largest differences was found to contribute 3.5% to the cumulative emissions and explains 66% of the percent difference between the methodologies. Although this analysis suggests that the ADM overestimated the cumulative emissions, no quantitative information is available on an absolute scale to determine if one or more method overestimated or underestimated the flux rates.

A laboratory study quantifying 1,3-D flux loss was conducted using soil collected from this same field site for comparative purposes (Ashworth and Yates, 2007). The study was conducted with temperatures cycles that closely matched field observations. This study reported that the total emissions of *cis*-1,3-D after 14 days were 33.1% for a non-irrigated treatment and 17.1% for an irrigation treatment that duplicated the amounts and timing of water applied to the field. The laboratory results compared very well with the estimated total *cis*-1,3-D emission using the aerodynamic method (i.e., 17.5%) but is

larger than the total *cis*-1,3-D field emissions estimates from the TPS and IHF methods (i.e., 11.5-12.1%). A similar field study (see Section 4.3, below) conducted under standard fumigation conditions, total 1,3-D (*cis* and *trans*) emissions was approximately 28% of the applied material.

Another study of 1,3-D volatilization from a large field in the Salinas Valley of California reported that 25% of the applied material was lost to the atmosphere (*Chen et al., 1995, 1996; Cryer et al., 2003*) over a 14-day sampling period. The ADM was used to estimate the volatilization rate and the total emissions. During this experiment, irrigation water was not applied to the field, and therefore, also suggests that repeated surface irrigation could reduce emissions by as much as 30–40%.

Gao et al. (2008) conducted a field plot experiment to investigate several methods to reduce emissions of 1,3-D after shank injection. The experiment was conducted in a Hanford sandy loam and included a 46 cm injection depth. Emissions were periodically measured using passive flux chambers and total emissions from a bare-soil, non-irrigated control were 36% of the applied 1,3-D; which is similar to the value obtained in the laboratory experiment of Ashworth and Yates (2007). While this study did not include a post-fumigation sequential irrigation treatment, they studied the effect of applying water prior to soil fumigation and found that this could reduce emissions by nearly 50%.

1,3-D Concentration in Soil Profile. Shown in Figure 3.2.9 is the soil gas-phase concentration at various times after application of 1,3-D. After 24 hours, the soil gas phase concentration for 1,3-D at the injection depth exceeded 25 g m^{-3} , and the treated zone had extended from about 30 to 70 cm depth. Each day, the concentrations in soil were reduced as diffusion moved 1,3-D throughout the soil. By day 4, a fairly constant concentration was observed from 20 cm to 80 cm depth. By day 11, soil concentrations were low along with the volatilization rate (see Figure 3.2.8).

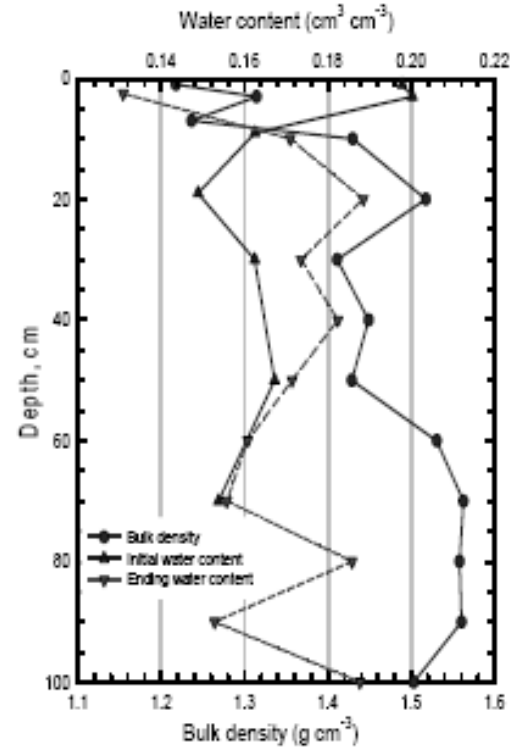
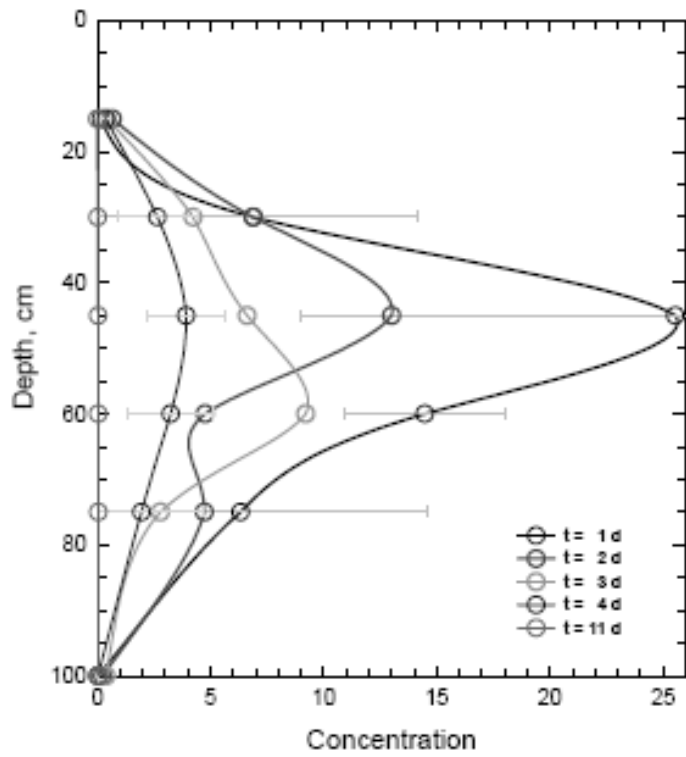


Figure 3.2.9 Soil gas phase concentration (g cm^{-3}) with depth in soil. Each line represents the concentration distribution at a particular time after application. Error bars are provided on two curves ($t = 1\text{ d}$ and $t = 4\text{ d}$) to give a indication of the variability of the soil gas concentration across the 4 sampling locations. In B, Soil water content and bulk density with depth in the soil. Initial and final values of the water content are shown.

3.3 Field #2: Broadcast-Shank Telone II Fumigation with Organic Amendment.

3.3.1 Field Specific Information.

The experiment was conducted near Buttonwillow, CA, in Field-24NW which is comprised of a Milham sandy loam soil (see Figure 3.3.1). To improve soil fertility, the grower added 300 tons/acre of composted municipal green waste to the field the previous year. The material was spread over the top of the field, debris was removed, a moldboard plow was used to incorporate the green waste, and this was followed by several disking operations.



Figure 3.3.1 Setting up equipment in the organically amended field.

Fumigation began on August 31, 2005 at 10:15 am and ended at 2:00 pm. The target application rate was 132 kg/ha (i.e., 12 gal/ac) and was applied to a nearly square area (178.4 m x 188.5 m) of 3.36 ha (i.e., 8.3 acres). The total 1,3-D mass applied was 446.7 kg. The chemical was applied as 97.5% mixture of the cis (CAS: 10061-01-5) and trans (CAS: 10061-02-6) isomers, the remainder were inert components. During this time, no irrigation water or precipitation was added to the field.

The 1,3-D concentration in the atmosphere was collected 12, 40, 80, 160, 236 and 359 cm above the soil surface. For the first 6 days of the experiment the measurement periods were 2 hours long during the daytime (0700-2100) and included a single nighttime sample. Starting on days 7, 10 and 13, respectively, the daytime sampling intervals were increased to 3, 6 and 12 hours. As the experiment progressed, the sampling period were lengthened to ensure that sufficient mass was collected in the sampling tubes for residue analysis. The field layout is shown in Figure 3.3.2.

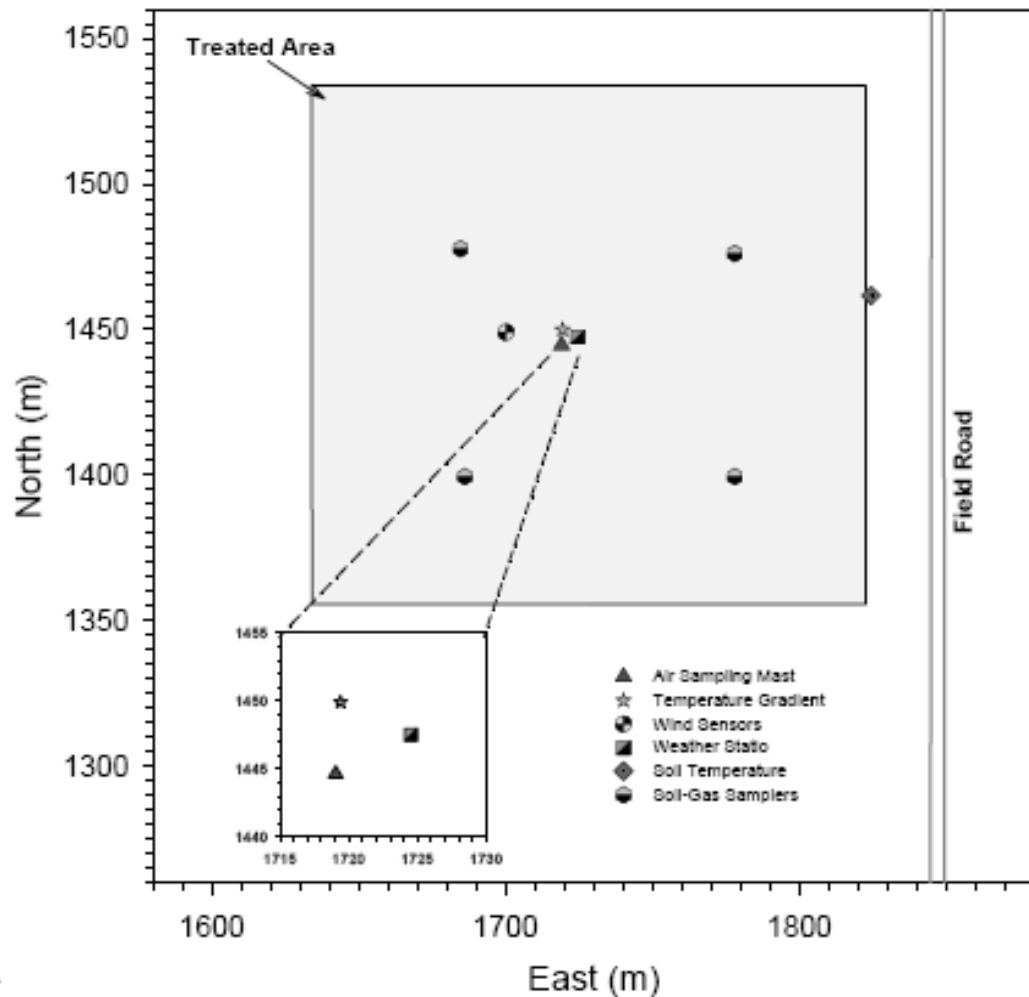


Figure 3.3.2 Schematic of organic-amended field showing the positions of sensors

Solar and net radiations were collected as hourly averages of instrument measurements taken every 5 seconds. This yielded a nominal time series of 360 values (i.e., 24 hours x 15 daily values). Then, using the 15 daily values occurring at a particular hour, an average and standard deviation was calculated to represent a typical hour of the day. This resulted in 24 average solar and net radiations and their standard deviations.

3.3.2 Results and Discussion

Ambient Conditions. The typical summer weather in the Buttonwillow region includes warm temperatures and cloudless conditions and nearly constant wind directions. At times, windblown dust may reduce incident solar radiation, but this did not occur during the experiment. Figure 3.3.3 contains hourly mean and standard deviation of the solar irradiance (Q_{in}) and net solar radiation (Q_{net}) during the experiment. For a particular hour of the day, the measurement values were found to be nearly the same throughout the experiment. Noting the small standard deviation for Q_{in} , it is clear that the incident

radiation was relatively uniform and cyclic during the experiment, which is indicative of continuously clear sky conditions. The maximum and average of the solar radiation measurements, respectively, were 881 and 264 W m^{-2} . Like the solar irradiance, the net radiation was also found to be a smoothly varying throughout the day and the daily patterns were highly uniform during this experiment. The maximum, minimum and average values, respectively, were 478 W m^{-2} , -79 W m^{-2} , and 97 W m^{-2} .

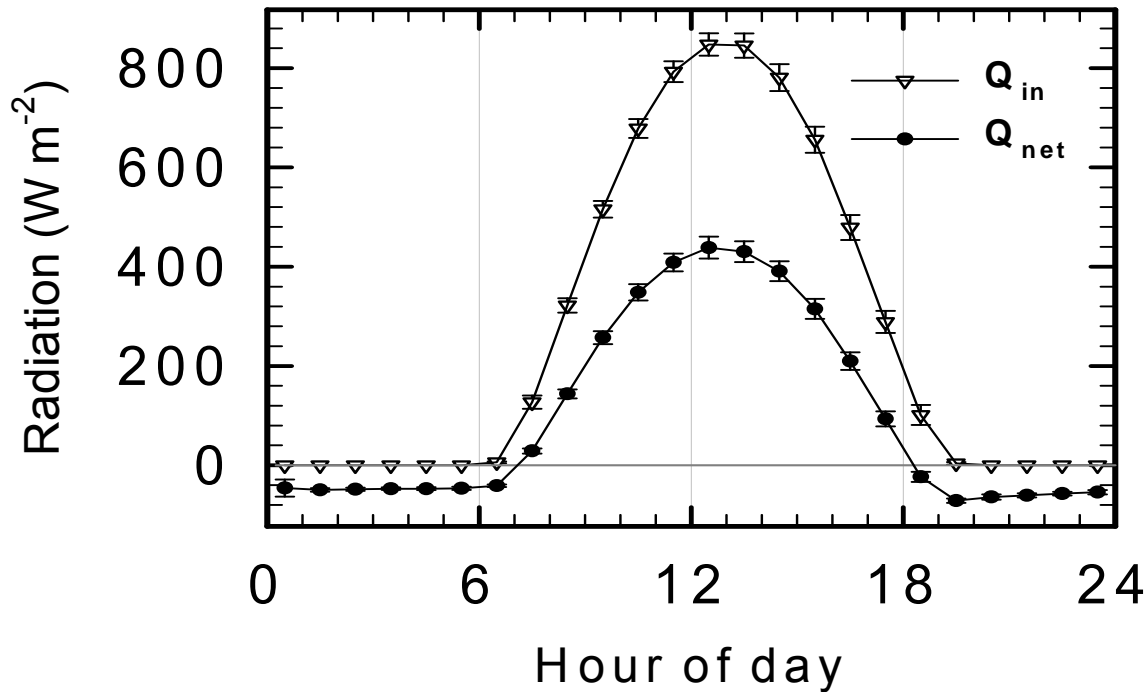


Figure 3.3.3 Incoming solar radiation (W m^{-2}) and net solar radiation (W m^{-2}) in relation to time of day

Figure 3.3.4 (A) shows the ambient air temperature at a 40 cm height above the soil surface during the experiment. During the first 8 days of the experiment, the maximum temperature was approximately 37.3 $^{\circ}\text{C}$, daily minimum temperature was 11.6 $^{\circ}\text{C}$ and the averaged temperature was 24.0 $^{\circ}\text{C}$. Starting day 9, a slight cooling trend appeared with temperatures increasing gradually for the next several days (max, min, mean 30.7, 8.3, 18.7 $^{\circ}\text{C}$).

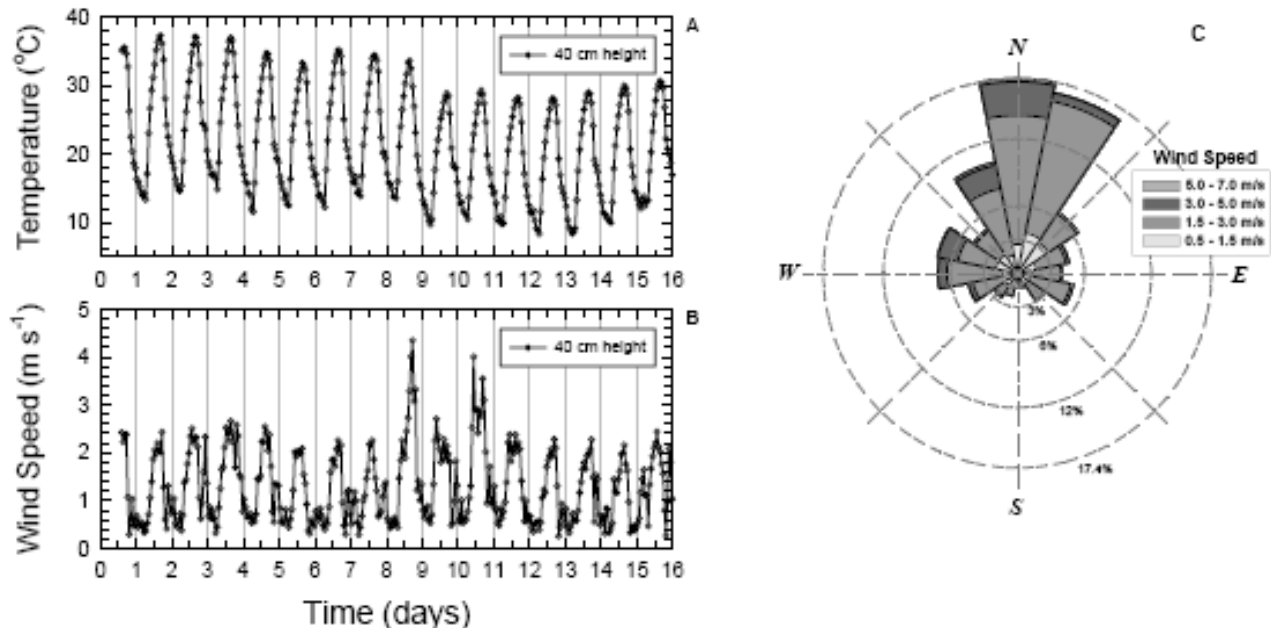


Figure 3.3.4 The variation in temperature (A) and wind speed (B) at 0.4 m above the soil surface during the experiment. A wind rose diagram (C) shows the wind direction, speed and probability the wind will occur in a specific direction.

Shown in Figure 3.3.4 is the wind speed at 40 cm above the surface (B) during the experiment and a wind-rose diagram (C), which provides information about the frequency that the winds occur in a particular direction. The winds moved predominately from the north to the south as shown in the diagram (Figure 3C) and the dashed circles indicate that 17.4% of the time the wind direction is ± 11.25 degrees from due north and that the wind speeds are usually from 1.5 to 3.0 m s⁻¹. This wind rose diagram was created using 2 min wind speed and wind direction data and indicates that occasionally winds in excess of 5 m s⁻¹ were observed. On an hourly-averaged basis, the maximum wind speed was 4.3 m s⁻¹, but daily maxima were generally between 2 – 3 m s⁻¹. During the middle of the night, wind speeds were commonly from 0.2 to 0.6 m s⁻¹.

Figure 3.3.5 is a graph of the temperature gradient, Richardson's number and atmospheric stability parameter for momentum. The temperature gradient was obtained from measurements collected at 80 and 40 cm above the soil surface, where negative values indicate higher temperatures near the soil surface. During the sampling period, the observed temperature gradient varied by approximately ± 1 °C with an occasional value approaching +2 °C. Also, negative gradients occurred during the day which is indicative of unstable atmospheric conditions. During the daylight hours, the temperature gradient increases from approximately zero an hour after sun rise, to a maximum negative value at solar noon and then decreases to zero an hour before sunset. During the nighttime, the temperature gradient has positive values, but the gradient is much more erratic compared to daytime values.

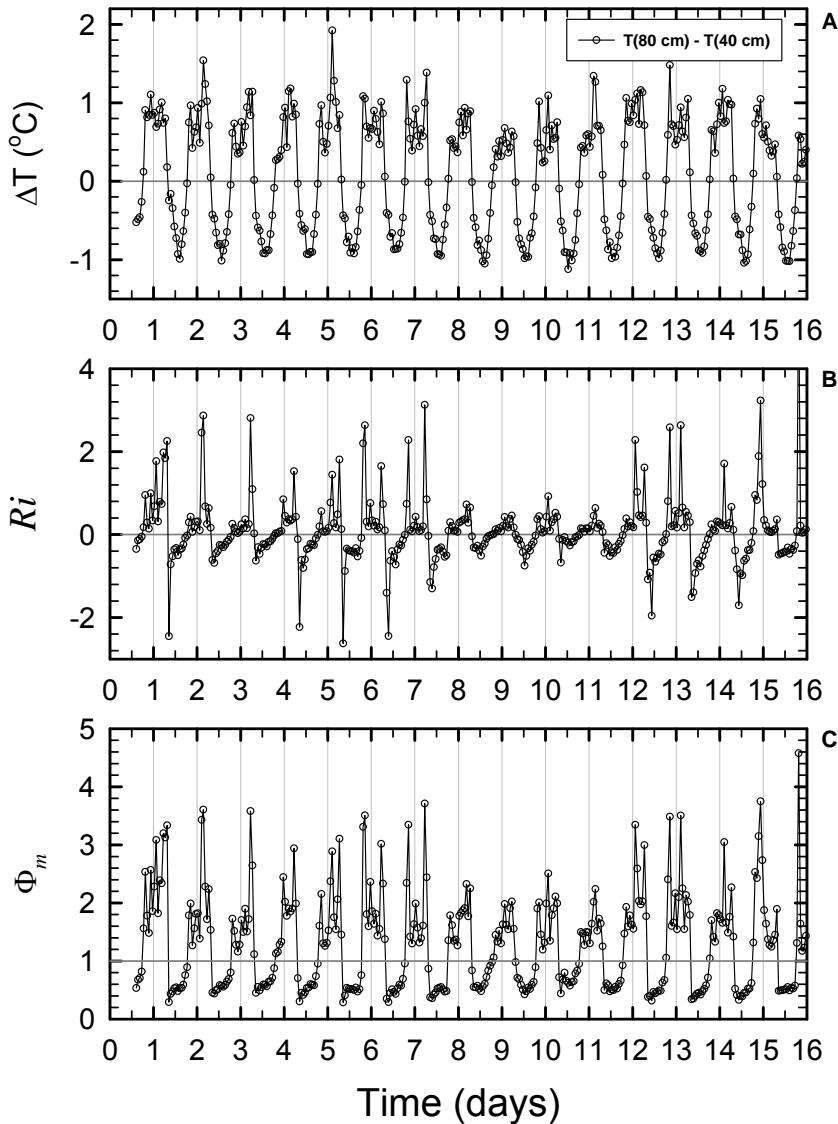


Figure 3.3.5 Variation in temperature gradient (A), Richardson's number (B) and atmospheric stability parameter for momentum (C) during the experiment.

The gradient Richardson number provides a means to determine the effect of thermal stability on the shape of the wind speed profile and on turbulent exchange. The Ri provides information on the relative importance of buoyancy and mechanical forces on fumigant movement in the atmosphere. Ri near zero indicates near neutral conditions, negative values indicate unstable conditions, and positive values occur for stable atmospheric conditions.

Figure 3.3.5 (C) shows the stability parameter for momentum, Φ_m . Since Φ_m is in the denominator of Equation 2.1.1, this parameter tends to increase the emission rate when it has values less than unity. In general, $\Phi_m < 1$ when the Richardson's number is less than zero. For these time periods, unstable conditions generally lead to increased volatilization since the air over the soil surface is warmer, and therefore buoyant, compared to the air above and rises. This causes the fumigant to move away from the

soil surface and tends to increase the concentration gradient at the soil-atmosphere boundary. This can be an important factor driving the volatilization process. At night, when the stability parameter is greater than zero, the stable atmosphere tends to produce higher concentrations near the soil surface, which reduces volatilization.

Air Concentrations

The effect of atmospheric stability, Φ_m , and turbulence on 1,3-D concentration in the atmosphere can be seen in Figure 3.3.6 at two heights, 40 and 80 cm, above the soil surface. Nighttime concentrations tend to be much higher than midday values. Also, the concentration levels were relatively high during the first 4 days of the experiment and were found to be much lower after about 6 days. At 40 cm above the soil surface observed concentrations exceeded $400 \mu\text{g m}^{-3}$, and had a peak value of nearly $500 \mu\text{g m}^{-3}$. At a height of 80 cm above the soil surface, the concentration remained below $130 \mu\text{g m}^{-3}$.

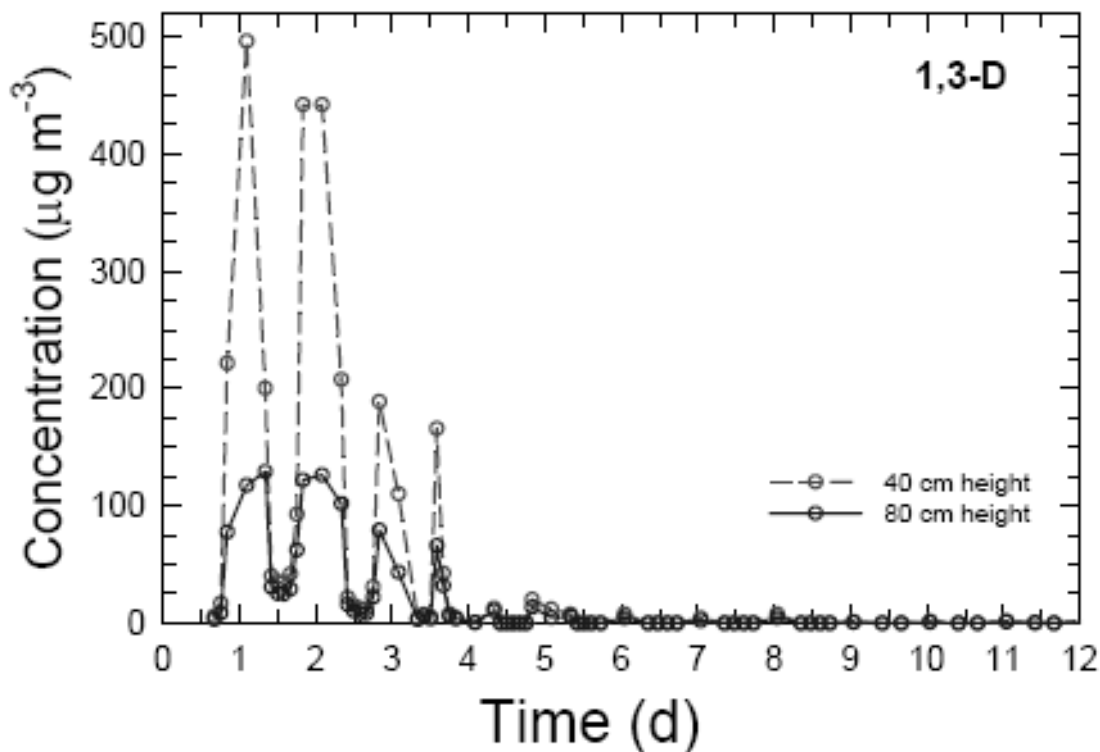


Figure 3.3.6 Measured 1,3-D concentration in the atmosphere at 0.4 and 0.8 m above the soil surface at the center of the field amended with composted green waste material. Open circles are the period-averaged concentration collected with the on-field sampling mast.

The large concentrations at the beginning of the experiment are due to a combination of factors including a larger source of chemical present in the soil, larger concentration gradients directed toward the soil surface, and rapid upward diffusion caused by the presence of soil fracture zones caused by the fumigation shanks (see Figure 3.1.1). The shanks have been shown to create a more uniform soil

concentration and higher concentrations near the soil surface compared to injection methods that do not produce a soil fracture (Yates, 2009). As time advances, the fumigant volatilizes and degrades in soil so atmospheric concentrations lessen.

1,3-D Volatilization

Knowledge of fumigant emissions is of importance to state and federal regulators since atmospheric loadings are used to determine various environmental risk endpoints. For issues related to bystander exposure and public health, the short-term emission rate is needed to determine risk associated with transient high-level emission events. These events may lead to unacceptable exposure to pesticide vapors. To determine the effect of VOC emissions on near surface ozone, the total atmospheric loading is a useful indicator of soil fumigation's contribution to regional VOC which may participate in ozone formation.

Figure 3.3.7 shows time series for the three methods used to calculate the volatilization rate (flux density), which includes the aerodynamic (ADM), integrated horizontal flux (IHF) and the theoretical profile shape (TPS) methods. The three methods demonstrate a similar overall pattern of high rates early in the experiment and low rates after about 5–6 days post application. At a particular time point, the three methods produce a range of volatilization rates and the, and occasionally the ADM method is 3–5 times higher than the IHF and TPS methods. Under typical shank injection, the volatilization rates commonly are highest during midday (Yates *et al.*, 1996b, 1997; Majewski 1997). In general, higher fluxes occur during the daytime, but the peak values occur at different times of day. Also, all three methods have low flux values at midday compared to other field-scale measurements. This could be due to a dry soil surface and increased vapor phase adsorption to the organic material present in the upper layer of soil. Vapor phase adsorption has been shown to strongly bind volatile pesticides to soil particles in a highly nonlinear process as water contents decreases (Chen *et al.*, 2000). Research has also shown that the water content of the surface soil layer fluctuates due to heating and cooling of the soil. This can be interpreted to be a result of evaporation and the movement of water vapor due to changes in the thermal regime in soil. Visually, the soil was very dry and powdery during midday, so vapor adsorption would be highest during this time.

The aerodynamic method produced the maximum period-averaged volatilization rate of $23 \mu\text{g m}^{-2} \text{s}^{-1}$ which occurred at 3.58 d (2.9 d after application). Prior to this, two other large volatilization rates were measured at 1.3 d ($12 \mu\text{g m}^{-2} \text{s}^{-1}$) and 2.3 d ($13 \mu\text{g m}^{-2} \text{s}^{-1}$). For the IHF method, the peak volatilization rate also occurred at 3.58 d ($4.1 \mu\text{g m}^{-2} \text{s}^{-1}$) and for the TPS method the peak flux occurred at 1.75 d ($4.4 \mu\text{g m}^{-2} \text{s}^{-1}$). Generally, the three methods provide similar volatilization rates except at 4 time points, where the ADM method estimates higher rates compared to the IHF and TPS methods.

Also shown in Figure 3.3.7 (inset) is the total 1,3-D emission from soil as a function of time after application. It is clear from the proximity of the curves that the IHF and TPS methods provide estimated volatilization rates that are very similar; with estimated values of 3.3 and 3.4 %. The estimate of the cumulative emission from the ADM, 8.2 %, is larger compared to the other methods. The discrepancy between

methodologies is approximately 5% based on the amount of 1,3-D applied to the field. This is similar the results of *Yates et al. (2008)* for different field experiment conducted at the same time and in the vicinity of this study described herein.

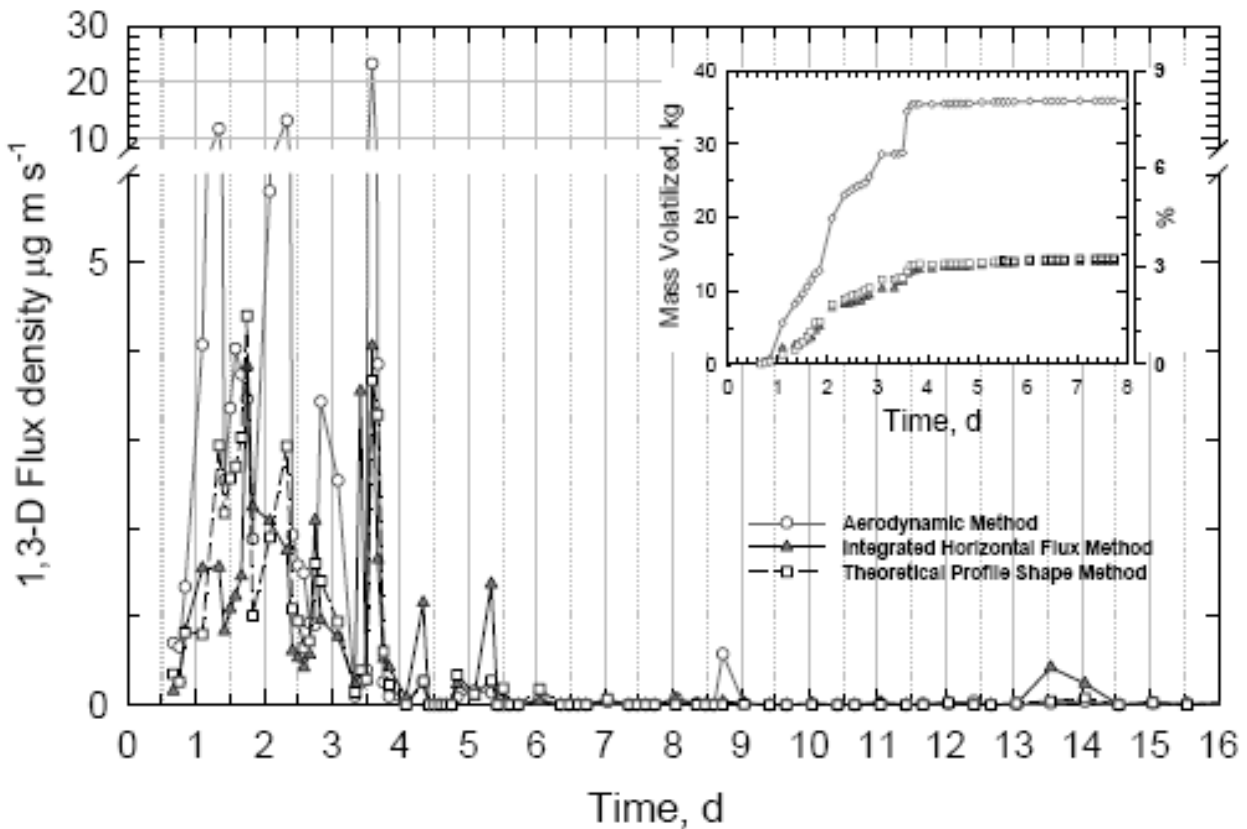


Figure 3.3.7 Volatilization rate ($\mu\text{g m}^{-2} \text{s}^{-1}$) as a function of time (day) after application for the aerodynamic (solid line, circles), integrated horizontal flux (solid line, triangles), theoretical profile shape (dashed line, squares). The inset shows cumulative 1,3-D emission as a function of time after application. The percentages on the right-most axis of inset indicates percent of applied 1,3-D. All values are averages over the sampling period.

The deviation between methodologies are consistent with studies of the experimental uncertainty for emissions estimation methods (*Majewski, 1997; Wilson and Shum, 1992*). These studies investigated the experimental and theoretical accuracy of the methods to estimate emissions and found that accuracy was in the range $\pm 20\text{--}50\%$. The approach taken by *Majewski (1997)* was based on a regression analysis of the log-linear wind speeds and concentrations with respect to height and found the accuracy for methyl bromide emissions was approximately $\pm 50\%$. This analysis should also apply to other fumigants that have log-linear concentration profiles. In a study of the theoretical accuracy of the IHF method, *Wilson and Shum (1992)* found that appropriately large field sites with surface roughness lengths below 10 cm would have experimental accuracy within approximately 20%. This result was obtained using a Lagrangian stochastic model and provides guidelines that can be used in the design of field experiments.

For purposes of verification, soil was collected from the field site for use in a laboratory study (Ashworth and Yates, 2007). The experiment was conducted using 1.5 m stainless steel soil columns that were placed in a controlled temperature so that the observed temperature conditions at the field site could be closely simulated. This study reported that the total emissions of *cis*-1,3-D after 14 days were 33.1% for soil collected in a nearby field that did not receive any municipal green waste and 5.7% for soil collected from the field described herein. This estimate is smaller compared with the estimated total *cis*-1,3-D emission (Table 1) using the aerodynamic method (i.e., 9.7%; *cis*-1,3-D) and is larger than the total *cis*-1,3-D emissions estimates from the TPS and IHF methods (i.e., 3.8–3.9%). The average of the three field-scale flux methods compares very well with the laboratory value (i.e., 5.8%). Further, when compared to the total emission estimate from the laboratory treatment that did not contain organic material (33.1 %), the total emission estimates for both the field-scale and laboratory experiments demonstrate that significant reduction in emission is possible using composted municipal green waste.

Several other field-plot and laboratory studies have been reported that found addition of organic material to surface soil reduces emissions of 1,3-D. Dungan *et al.* (2001, 2005) conducted a field plot experiment on raised beds (5 m x 1 m x 0.15 m) and found that steer manure or chicken manure, respectively, incorporated into the top 5 cm of the bed would result in emissions of 1,3-D that were 48 and 28 % less than the unamended control plot. They also found that the measured reduction in emissions did not change after increasing the rate at which organic material was applied from 5% to 10%. Gan *et al.*, (1998) found that total emissions of 1,3-D were reduced from 30% to 16% by the addition of 5% organic matter to the top 5 cm of a soil column. In a laboratory column study, McDonald *et al.* (2008) found that the addition of 5% organic material (steer manure) to the upper 5 cm of the soil reduced emission from 51% to 29%.

All of the current literature investigating the effect of adding organic material to the surface prior to soil fumigation demonstrates that emissions can be reduced by 40% or more. The type of organic material plays a factor in how effective this methodology will be in reducing emissions.

Soil Gas Phase 1,3-D Concentration

Figure 3.3.8 is a graph of the soil gas-phase concentration at various times after application of 1,3-D. At the first sampling, the concentration of the soil gas phase at 0.45 m depth was approximately 29 mg cm⁻³, and the soil zone that had significant 1,3-D concentration was between 0.3 to 0.6 cm. On consecutive days, the peak concentration decreased and the treatment zone increased to approximately 0.8 m.

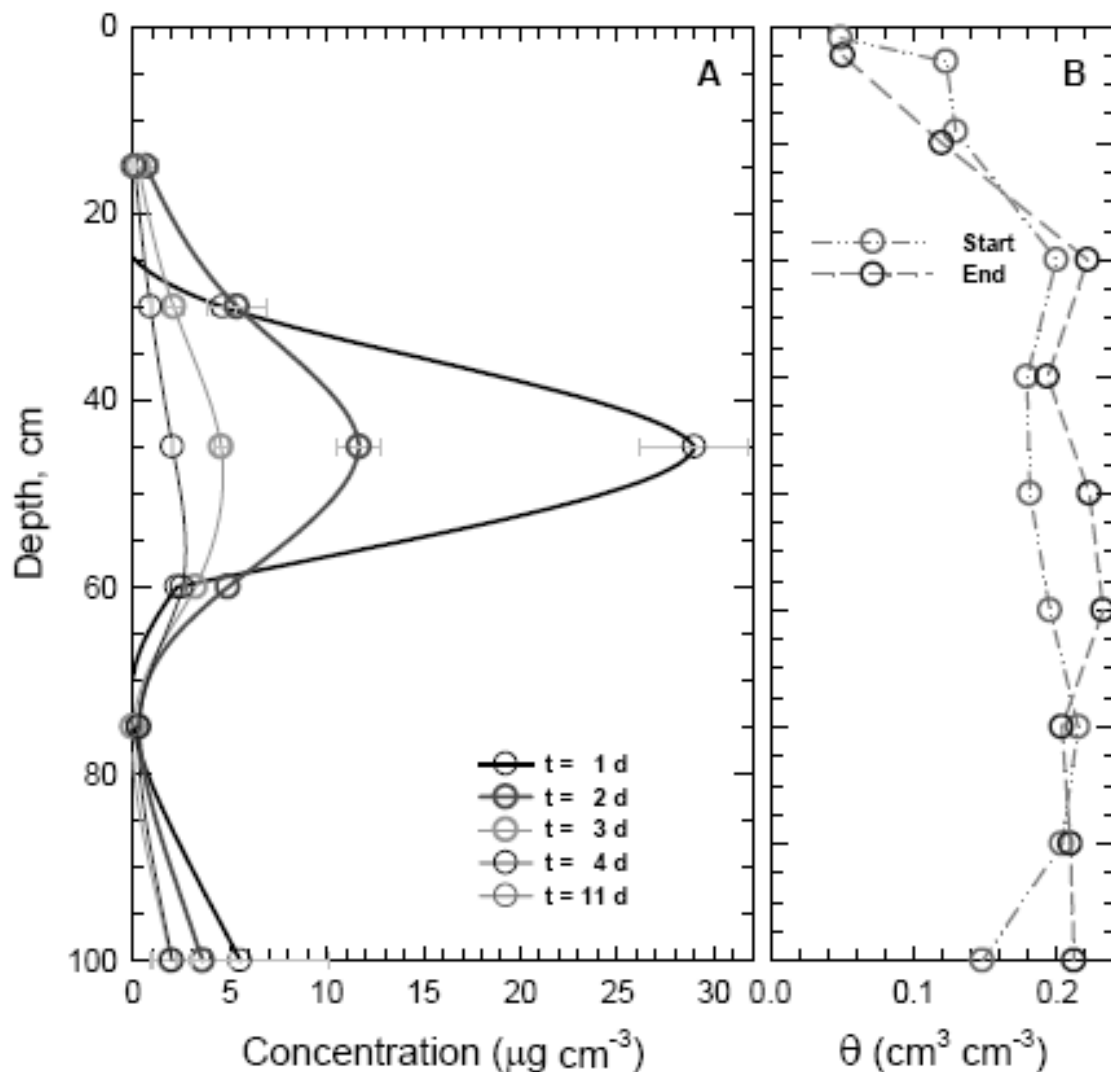


Figure 3.3.8 Soil gas phase concentration ($\mu\text{g cm}^{-3}$) with depth in soil. Each line represents the concentration distribution at a particular time after application. Error bars are provided on each curve to give an indication of the variability of the soil gas concentration across the 4 sampling locations. In B, Soil water content and bulk density with depth in the soil. Initial and final values of the water content are shown

The experiment of *Yates et al. (2008)* conducted at the same time and in an adjacent field that did not receive composted green waste observed similar soil gas concentrations. For example, a comparison of the concentrations at 0.45 cm depth on days 1, 2, 3, 4 and 11, respectively were 25.5, 13.0, 6.6, 3.93, 0.038 $\mu\text{g cm}^{-3}$ (*Yates et al., 2008*). In Figure 3.3.8, the soil gas concentrations at 0.45 m for days 1, 2, 3 and 4, respectively, were 29.0, 11.7, 4.57 and 2.05 $\mu\text{g cm}^{-3}$. The organic material was incorporated into the surface layer, thus degradation was limited to the near surface soil. This can be seen in Figure 3.3.8 by the near zero concentrations at 15 cm depth. However, it appears that a surface application of organic material doesn't markedly affect soil gas concentration at deeper depths, so fumigant efficacy would not be compromised below the organic-material incorporation zone.

The incorporation of composted organic green waste into the upper soil layer also resulted in fumigant emissions that were significantly reduced, so this approach could be beneficial in reducing atmospheric loading of VOCs, providing material to crop land that improves soil tilth and nutrient levels, and providing an outlet for municipalities to dispose of large quantities of green waste material that are often otherwise destined for disposal in land fills. Further research is needed to demonstrate the plant pest control is sufficient in the upper soil layer and that crop production wouldn't be compromised.

3.4 Summary

The results of this study indicate that applying sprinkler irrigation water to the soil surface following soil fumigation leads to total 1,3-D emissions between 10 to 15% of the applied material. Based on recent laboratory and field experiments conducted under similar soil and environmental conditions which found total emissions of 1,3-D to be approximately 28-33% (Section 4.3, below; *Ashworth and Yates 2007*), it appears that atmospheric emissions of 1,3-D can be reduced by 45–70% compared to conventional application methods. This provides a simple, effective and low cost method to protect the environment from agricultural chemicals and to reduce VOC emissions to the atmosphere. This study also demonstrates that 1,3-D, and hence, VOC emissions from field soil is significantly less than current regulatory estimates.

This OM study demonstrates the benefit of amending soil with composted municipal green waste as a means to reduce emissions of 1,3-D after preplant soil fumigation. Application of green waste at a rate of 300 tons per acre reduced total of 1,3-D from approximately 28% (section 4.3, below) to 33% (*Ashworth and Yates 2007*) to approximately 5% of the applied fumigant. Based on recent laboratory and field experiments conducted under similar soil and environmental conditions, it appears that atmospheric emissions of 1,3-D can be reduced by approximately 80–85% compared to conventional application methods. This provides a simple, environmentally beneficial, effective and relatively low cost method to protect the environment from agricultural chemicals and to reduce VOC emissions to the atmosphere. This study also demonstrates VOC emissions from 1,3-D fumigation is significantly less than current regulatory estimates based on 100% emission losses.

4 Results of Experiment #2: (2007): Telone C-35 Fumigation

4.1 Experiment-Specific Methodology

Test Plots

Three fields, each enclosing about 2.9 ha (i.e., 7 acres) and separated by a minimum of 1000 m (i.e., 0.6 miles), were treated with the test material. Two of these fields were injected at approximately 18" deep and one of these fields served as the control for comparing period-average emission rates and emission fractions. The second field included an emission-reduction method and received a surface application of thiosulfate amendment applied by a spray tractor. This treatment had minimal water application and tested the effectiveness of ATS alone. Therefore, this treatment did *not* test the combined effect of ATS and a surface water seal. The third field was a deep-injection (i.e., 24" depth) emission-reduction treatment.

The field experiment began on September 5, 2007 and was concluded September 21, 2007. Field preparation followed the same sequences as described in 3.1. The initial soil water content was approximately 0.15 (cm³ cm⁻³). Telone C-35® was applied to the field as a mixture containing 63% 1,3-dichloropropene (CAS: 542-75-6) and 33% chloropicrin (CAS: 76-06-2).

The plot layout for this experiment is shown in Figure 4.1.1 Also shown in this figure is a wind rose diagram. The winds are predominately out of the northwest and wind speeds were predominately between 1.5 and 5.0 m/s. Approximately 45% of the time, the winds were from the north and northwest, about 10% of the time the winds were out of the west. The other directions had very low frequency. This indicates that interferences between fields would have occurred less than 5% of the time.

Telone C35 Application Rate and Method

Commercial end-use product Telone C-35 was used for this study. The test material was delivered to the site in bulk 110-gallon containers, which were part of a fleet of re-useable containers. The application methodology followed standard industry practices and followed produce label requirements.

Telone C-35 applications was made using commercial application units (Western Farm Services, Inc., 9355 Copus Rd. Bakersfield CA 93313). Two fields (control and deep injection treatments) were fumigated at approximately the same time. A third field (ATS treatment) was fumigated approximately 6 hours later. Off-plot airborne concentrations of 1,3-dichloropropene and chloropicrin were measured at each field during fumigation.

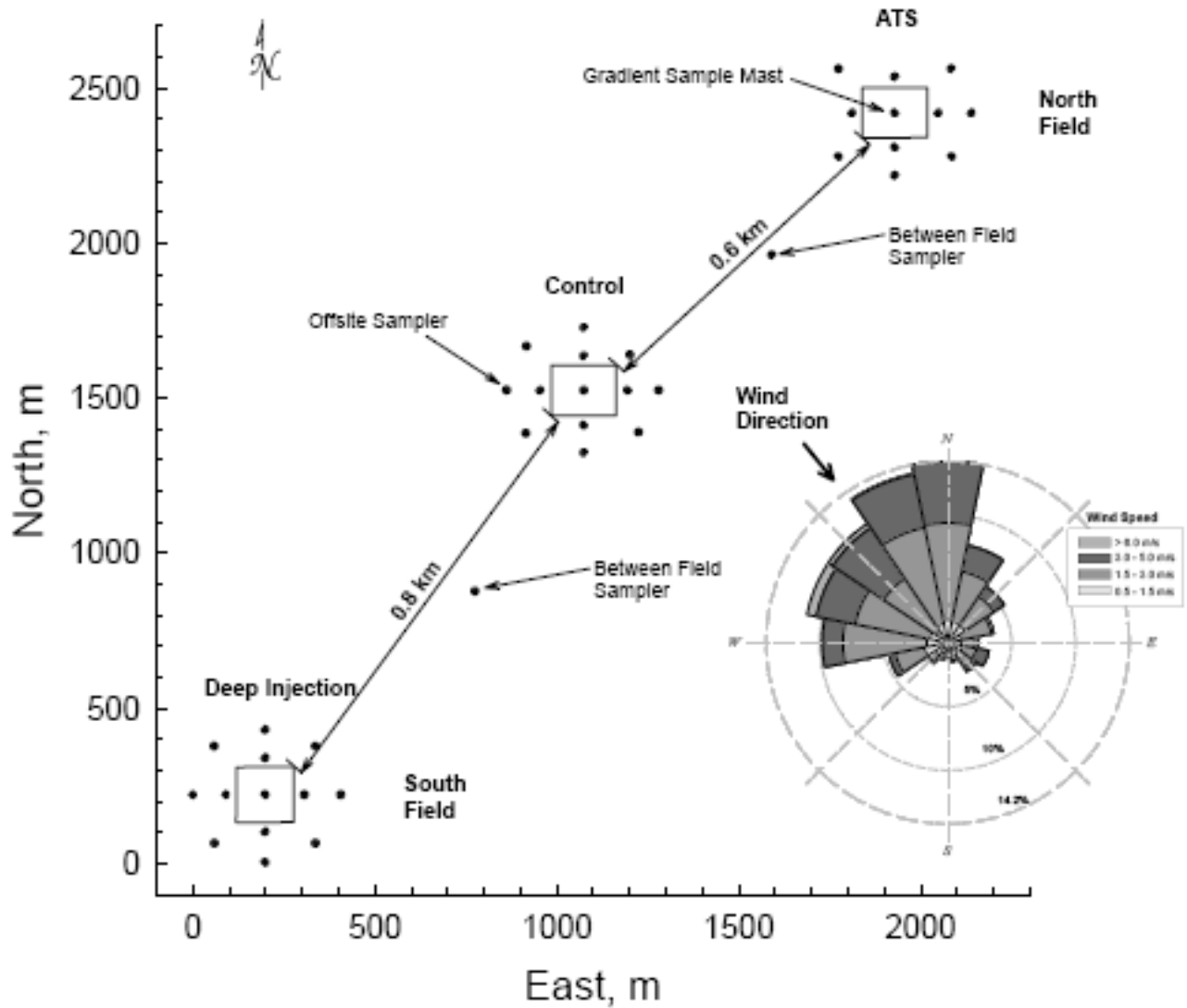


Figure 4.1.1 Plot layout and wind-rose diagram for the 2007 experiment.

In two fields (i.e., control and ATS treatments), Telone C-35 was injected under pressure at approximately the 45-46 cm (18 inch) depth. In the third field (i.e., deep-injection treatment), Telone C-35 was injected under pressure at approximately 60-62 cm (24 inch) depth. The target application rate was 20 gallons per acre of Telone C-35; the actual application rates are shown in Table 4.1.1. The application was broadcast injected with a chisel applicator. The fumigant was applied to the field by a commercial applicator using a tractor containing 9 shanks mounted on a 4.5 m tool bar at 0.5 m spacing increments.

Table 4.1.1 Amount of fumigant applied to fields

Experimental Treatment	Field Designation	Total Weight Applied, lb	Total 1,3-D Applied, lb	Total Chloropicrin Applied, lb	% Active Ingredient
Deep Injection	25NW/South	1553.0	947.2	533.3	95.5
Control Plot	22SW	1596.0	1046.0	490.1	96.2
ATS Plot	12SE/North	1648.5	1035.2	549.0	96.2

Ammonium Thiosulfate Application Rate and Method

Immediately prior to fumigation of the North field, a liquid “floater” (see Figure 4.1.2) with an attached spray boom delivered a thiosulfate-water solution to the soil surface. This was followed by discing the surface to mix the upper 5-10 cm of soil. The *target spray* rate was 150 gal/acre of solution containing 471 kg/ha (i.e., 420 lbs/ac) thiosulfate at a 1.66 : 1 molar ratio (thiosulfate:fumigant).



Figure 4.1.2. Application of ammonium thiosulfate solution to the North Field site.

A total of 40 sampling plates were placed onto the field to intercept the spray along three transects; one on the east, middle and west side of the fields. Computing the average of the 40 sprayer samples provides in an estimate of 537.8 kg/ha for the actual ATS application rate with a standard deviation of 97.1 kg/ha. The actual molar ratio of ATS to Telone C-35 was 1.8 : 1; which is close to the target value.

Instrumentation and Layout

Meteorological and air sampling equipment were located on or near each test plot. This equipment was placed to gather the necessary information for flux calculations and

ancillary information. The horizontal spatial position of each instrument was obtained using a Sokkia RTK GPS system capable of 1–2 cm of positional accuracy.

Meteorological Measurements

- solar radiation (pyranometer and net radiation),
- precipitation
- ambient air temperature and relative humidity (probe with radiation shield),
- soil temperature (surface and with depth),
- near-surface temperature gradients in the atmosphere,
- wind speed and direction: near-surface gradients and at 3 m and/or 10 m,
- barometric pressure.

A 10 m meteorological station was installed near a test plot. This station collected 10–m wind speed and direction as the primary information for the back calculation methods. Air temperature, relative humidity, barometric pressure, and solar radiation were also collected.

An on-site meteorological mast was located near the center of each plot. These masts were placed from within a few meters from the air sampling mast. At the center of the Control and Deep Injection field plots, the mast held five sonic anemometers at 20, 40, 80, 160 and 400 cm above the soil surface. At the center of the ATS field plot, a mast held two sonic anemometers at 20 and 160 cm and six ultra-sensitive Thornwaithe¹ rotating-cup anemometers at 20, 40, 80, 160, 240 and 360 cm above the soil surface. Each field had replicated fine-wire (0.003" dia. Type E thermocouples) ambient air temperature sensors located at 20, 40, 80 and 150 cm heights.

Measurements of 1,3-D and Chloropicrin in Air

Chloropicrin and 1,3-D vapors were collected on XAD4 adsorption tubes (PN:226-175) and 1,3-D vapors were collected on activated charcoal adsorption tubes (ca. off-site samples: 800 mg front section, 200 mg back section, on-field samples: PN: 226-09; 400 mg/200mg). For all sampling, either XAD4 and charcoal tubes were used side-by-side, or an XAD4 tube was used with a charcoal tube as a backup.

Air was drawn through the sampling tubes using battery-operated vacuum pumps at a target airflow rate. For off-site samples, the flow rate was 1.5 L/min for 1,3-D (charcoal), and 100 mL/min for chloropicrin (XAD4). For on-field samples, the target flow rate was 100 mL/min for both charcoal and XAD4 tubes. For off-site samples the airflow rates were checked and recorded before and after each sample with a flow meter to ensure consistent operation. For on-site sampling, the flow rate was continuously monitored using calibrated electronic flow meters (McMillan, Inc Model 100-4).

An on-site air-sampling mast was placed at the center of the treated plot. This mast allowed sampling the air at approximately 10, 40, 80, 150, 250 and 400 cm above the soil surface.

¹ Thornwaithe model CWT-1806, C.W. Thornthwaite Assoc.

There were twelve off-plot sample locations at the Deep Injection (South) and Control Fields, ten off-plot sample locations for the ATS (North) field and two air monitoring locations between the fields were used to check for interferences. At the midpoint along each side of the field, four samplers were positioned approximately 30 m (100 ft) outside the field boundary and four samplers were located approximately 60 m (200 ft) outside the field boundary. An additional four samplers were located 60 m (200 ft) from each corner of the treated area along a line that bisects the field center (See Figure 4.1.1).

The distances between fields were approximately 1340 m (0.8 mile) from the Deep injection site to the Control site and 1000 m (0.6 mile) between the control and the ATS field. Furthermore, the wind direction and orientation of the field sites result in minimal interferences between fields.

Soil Sampling

Soil Water. On the day before application and at the end of the experiment, samples for gravimetric soil water content were collected. Gravimetric soil water content (oven-dry basis) was determined by a standard laboratory convection-oven procedure.

Soil Gas Sampling. Soil gas was sampled at least once per day during the first 4 days of the study, and periodically thereafter. Soil gas measurements were taken using dedicated soil gas probes at 2 locations within each field at depths of approximately 5, 10, 25, 50, 75 and 100 cm below the soil surface. A vacuum was applied using a gas-tight syringe to draw soil air through XAD4 sorbent tubes.

4.2 Ambient Weather Conditions during the Experiment

The global solar radiance (Q_{in}) and net solar radiation (Q_{net}) are shown in Figure 4.2.1 as flux densities. Due to clear skies during the experiment, the solar radiation has a relatively constant diurnal pattern with peak values shortly after noon. The maximum and average of the solar radiation measurements, respectively, were 917 and 415 W/m^2 . The net radiation (Figure 4.2.1B) was fairly constant during the experiment. The maximum Q_{net} was 423, the minimum was $-67 (W m^{-2})$, and the average was 169 W/m^2 . Slightly lower values appear to have occurred during day 8.

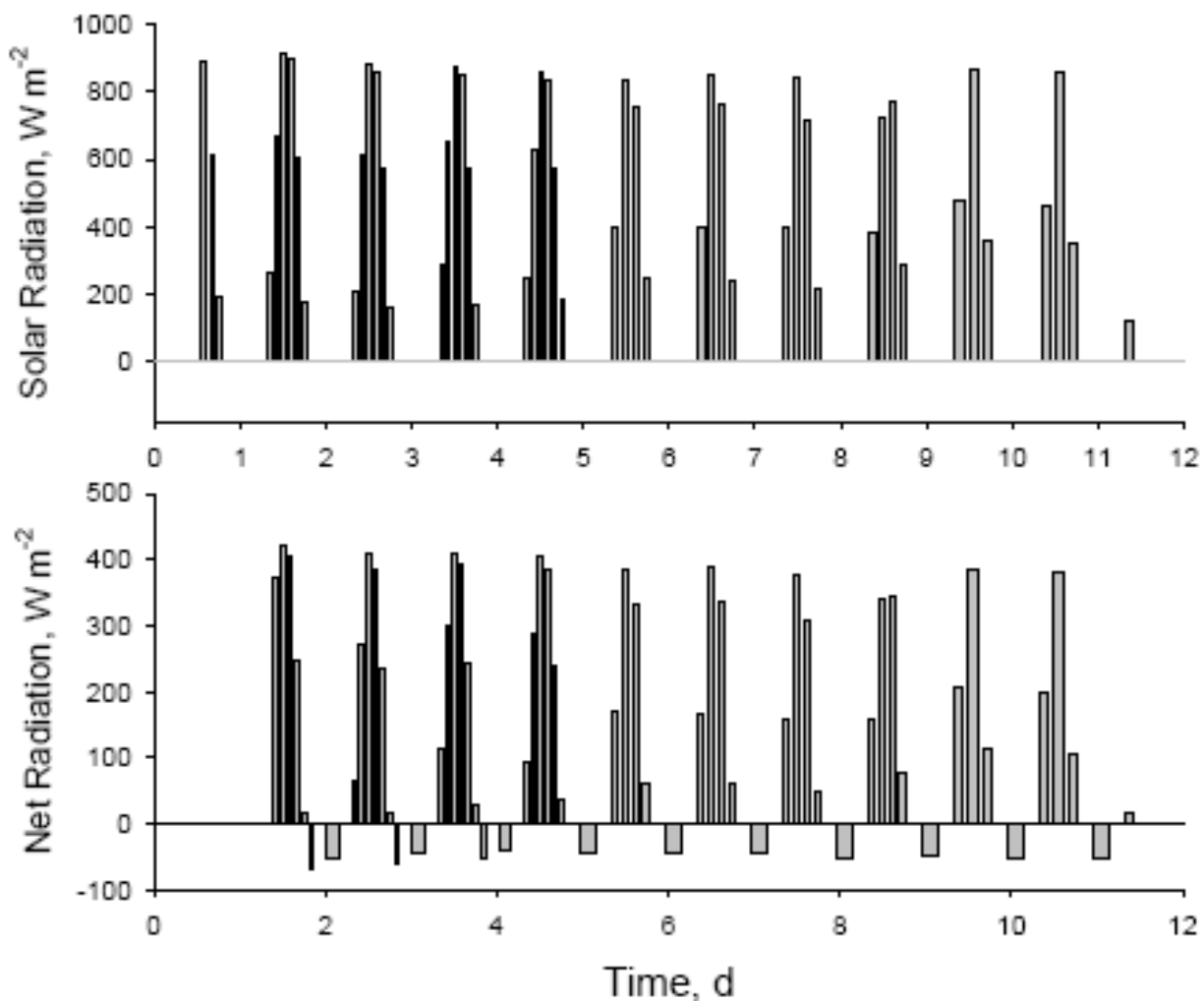


Figure 4.2.1. Solar radiation ($W m^{-2}$) and net solar radiation ($W m^{-2}$) during Experiment #2.

This information is useful since it provides a measure of the energy available at the soil surface that heats soil, which has an effect on the fate and transport of fumigant chemicals in the subsurface. Typically, the volatilization rate often has a similar diurnal behavior with high fluxes at midday.

Figure 4.2.2 shows the ambient temperature and relative humidity during the first 12 days of the experiment. The integer values on the time axis indicate midnight. During the first 12 days of the experiment, the maximum temperature was approximately 35.6 °C, daily minimum temperature was 14.6 °C and the averaged temperature was 25.6 °C. There appears to be a slight reduction in air temperature during day 8.

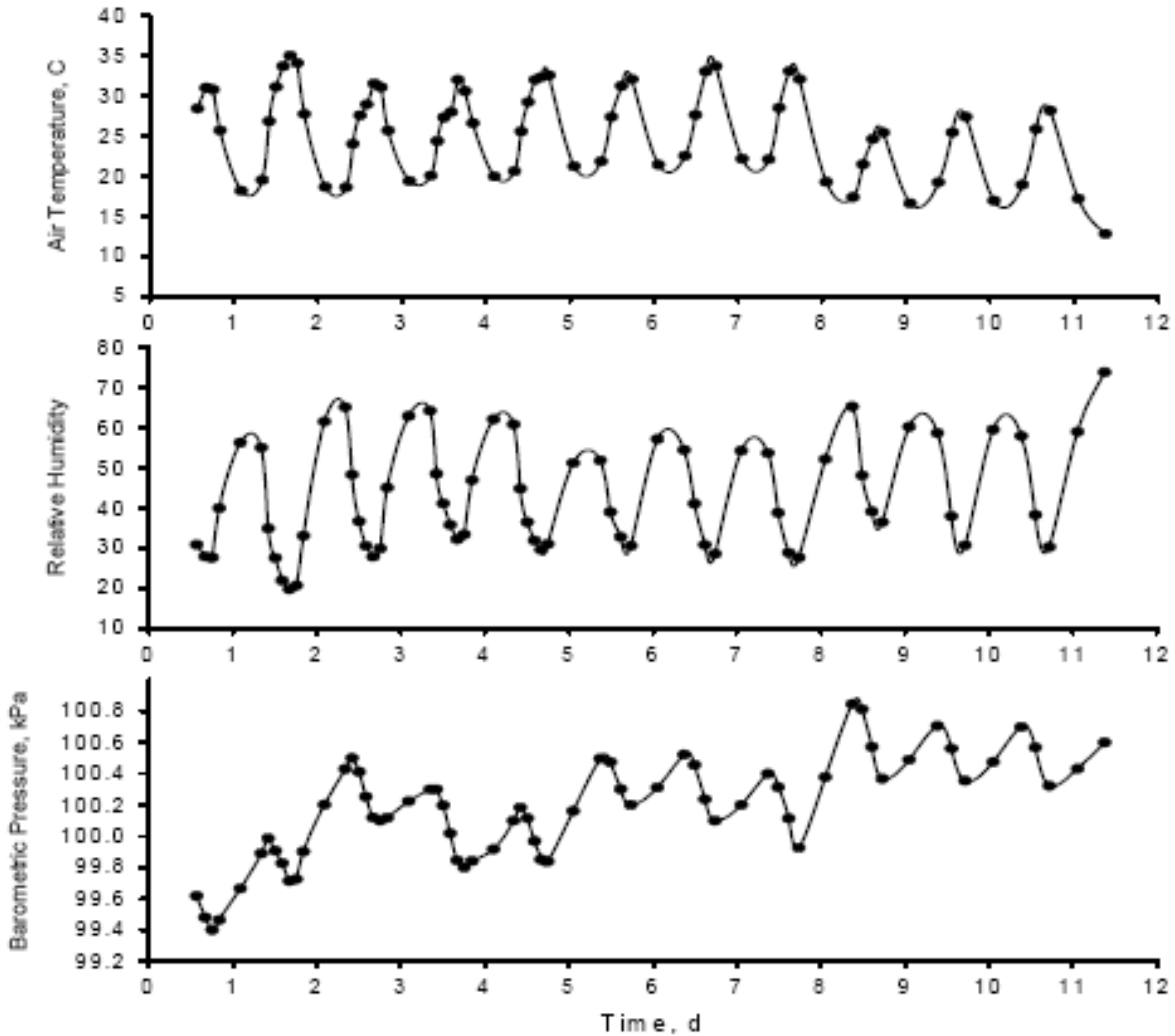


Figure 4.2.2. Air temperature (°C), Relative humidity (%) and barometric pressure (kPa) during Experiment #2.

The relative humidity follows a daily cyclic pattern with high levels occurring at low air temperatures. The observed maximum, minimum and mean relative humidity, respectively, were 80, 18 and 40 %.

Figure 4.2.2c is a graph of the barometric pressure during the experiment. The maximum, mean and minimum values, respectively, were 100.85, 99.40, and 100.18 kPa. There was an increase in the barometric pressure during days 0 to 3, and another slight increase after day 8.

4.3 Field #3: Broadcast-Shank Telone C-35 Fumigation, Standard Fumigation Methodology (i.e., Control Field Site).

4.3.1 Field Specific Information

The control field was located in between the two emission-reduction field sites. The fields were oriented perpendicular to the dominant wind direction; limiting interferences between fields. The nearest corner-to-corner distance to the Deep Injection Field site was 1340 m (i.e., 0.8 mi) and the nearest distance to the ATS Field site was 1000 m (i.e., 0.6 mi). The treated area was 2.89 ha (i.e., 7.15 ac). A total of 474.5 kg of (i.e., 1046 lbs) of 1,3-D (cis + trans), and 76.8 kg chloropicrin (i.e., 490.1 lbs) was applied at a depth of 0.46 m (i.e., 18 in). The soil type for this field was Milham sandy loam. Figure 4.3.1 shows a picture taken during the experiment and gives a sense of the experimental conditions. Figure 4.3.2 shows a schematic of the field site and the positioning of instruments and sampling equipment.



Figure 4.3.1 Field conditions during Experiment #2. This location is the control site.

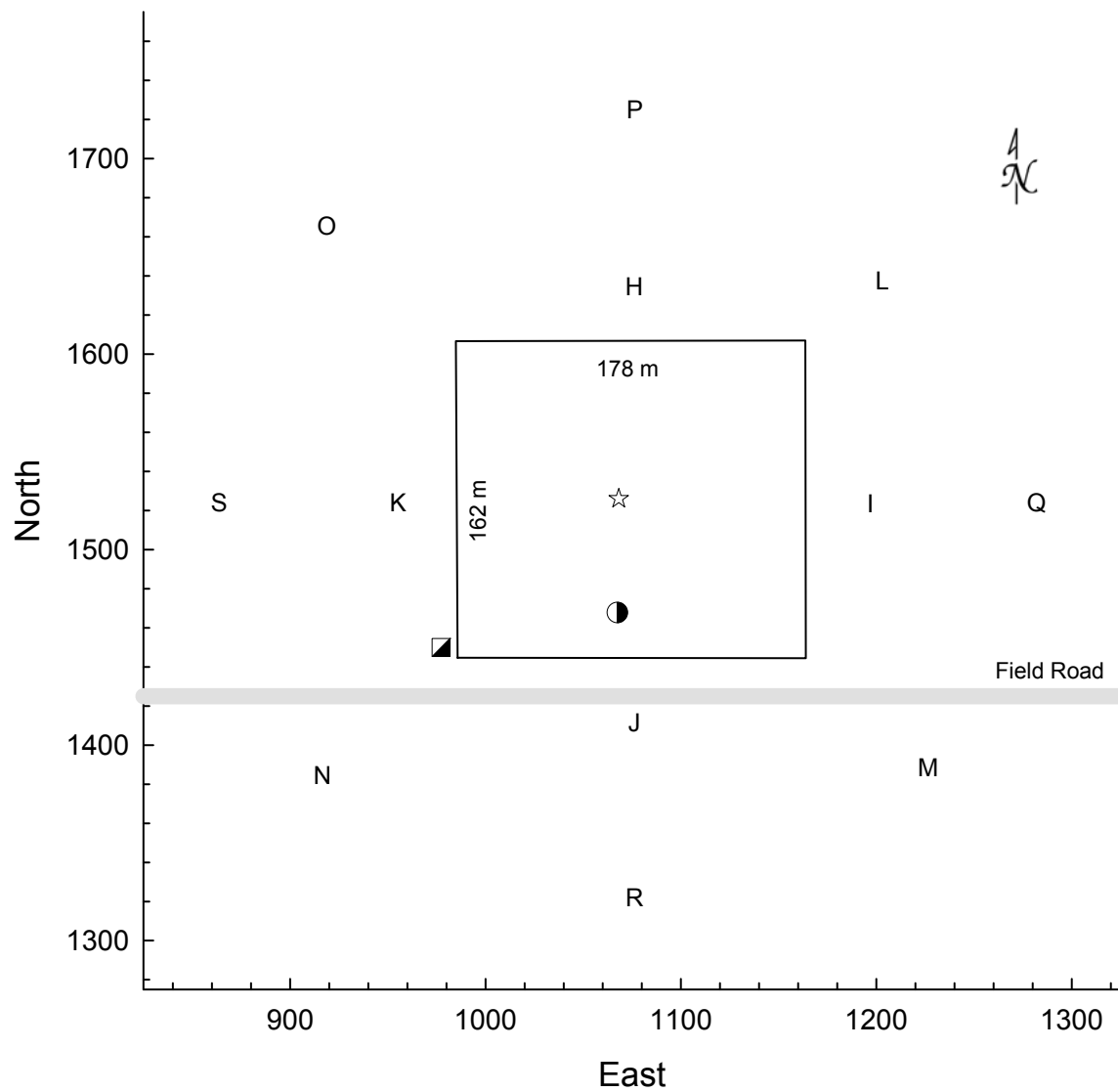


Figure 4.3.2 Field layout for the Control Field site. The letters indicate the positions of the off-field sampling equipment used for the back-calculation (i.e., ISCST3) method. The star, half-filled circle and half-filled square, respectively, are the locations of the gas-sampling mast (i.e., micrometeorological flux methods), the position of the soil gas sampling equipment, and the position of the soil temperature and heat flux sensors.

4.3.2 Results and Discussion

Several methods were used to obtain estimates of the emission flux density, including the aerodynamic and two back calculation methods. Due to an equipment malfunction, estimates of the integrated horizontal flux and theoretical profile shape methods were not possible since upper level concentration samples were unavailable.

Since the aerodynamic and back-calculation flux estimates use different sets of atmospheric concentration data and weather information, they represent completely independent flux estimates. However, the two estimates using the back-calculation approach (i.e., ISCST3 and CalPuf v6) are based on the same concentration and weather information; so are not completely independent.

Estimates using the aerodynamic method require gradients of temperature, wind speed and concentration. Using the weather information, collected at the field site, estimates of the atmospheric stability are obtained. Figure 4.3.3 shows the temperature gradient, wind speed gradient and the gradient Richardson's number for the first 12-days of the experiment as a bar graph. These values were obtained over the air concentration measurement period to yield a period-averaged estimate that coincides with the air concentration measurements.

The temperature gradient (Figure 4.3.3A) and wind speed gradient (Figure 4.3.3.B) are used to calculate the gradient Richardson's number (Ri). These gradients were obtained by using temperature and wind speed values at 40 and 80 cm heights.

The gradient Richardson number (Ri) is shown in Figure 4.3.3C and is a dimensionless parameter describing the relative importance of buoyancy and convective forces. While many soil and environmental condition affect the measured flux density, a negative Ri indicates unstable or buoyant conditions and tends to promote the emission process.

In general, Ri varied from about +0.3 during the nighttime to -0.5 during the mid-day.

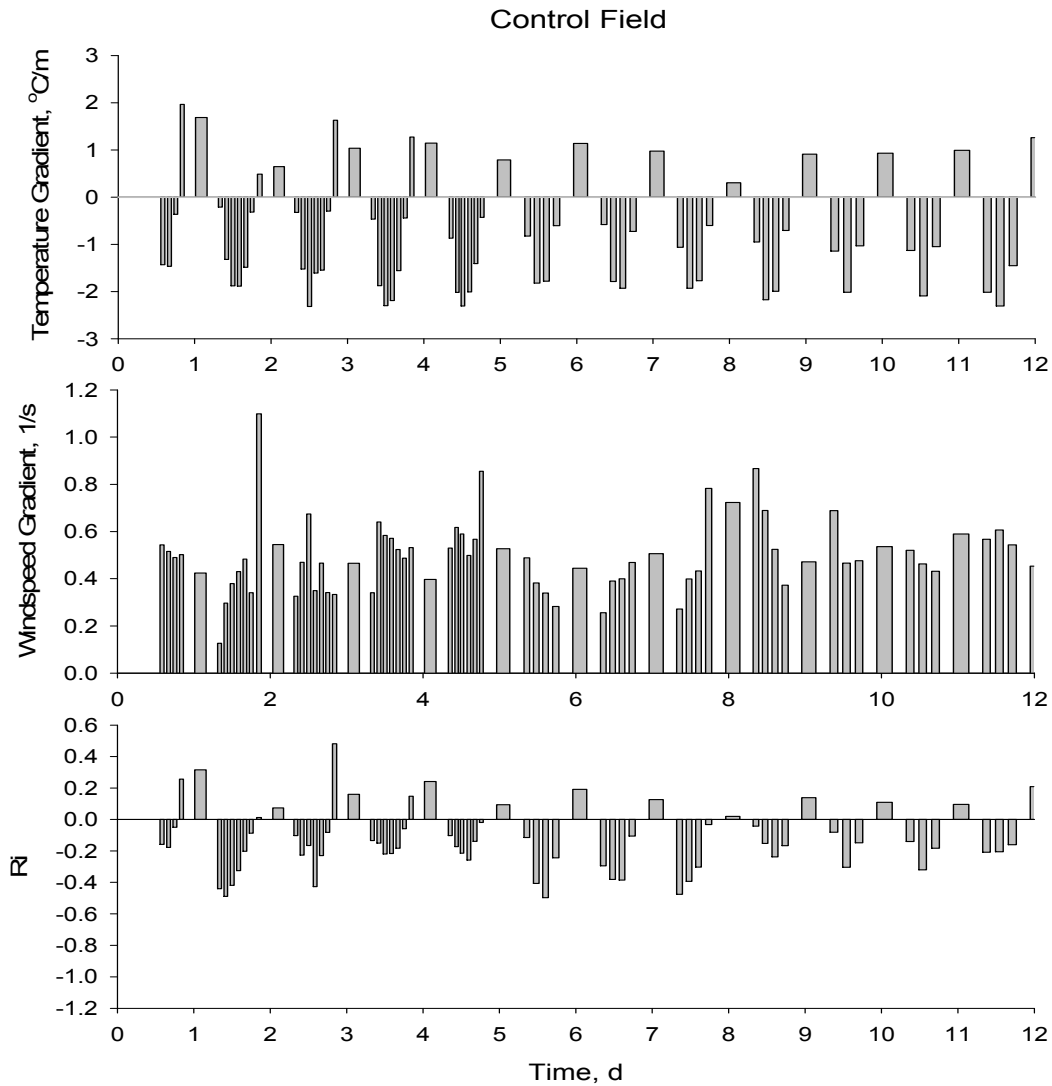


Figure 4.3.3 Temperature gradient, wind speed gradient and Richardson's Number at the Control Field site. The values shown are averages over the flux sampling periods.

Fumigant Concentrations in Air

After liquid Telone C35 is applied to the soil, the distribution in the soil can be perceived as narrow horizontal cylinders of concentrated liquid. Shortly afterwards, the liquid absorbs sufficient heat from the surrounding environment and rapidly vaporizes, with the vapor partitioning to the soil, water and gas phases. Driven by large concentration gradients, the fumigant diffuses outward from the injection point and begins to disperse throughout the soil profile and eventually to the atmosphere.

Air concentrations of 1,3-D and chloropicrin were collected at several heights in the center of the field. The daily concentrations at 40 cm above the surface are shown in

Figure 4.3.4. The concentration levels were relatively high during the first 4 days of the experiment and were very low by the end of the experiment. The peak concentrations near the soil surface exceeded 1000 $\mu\text{g m}^{-3}$.

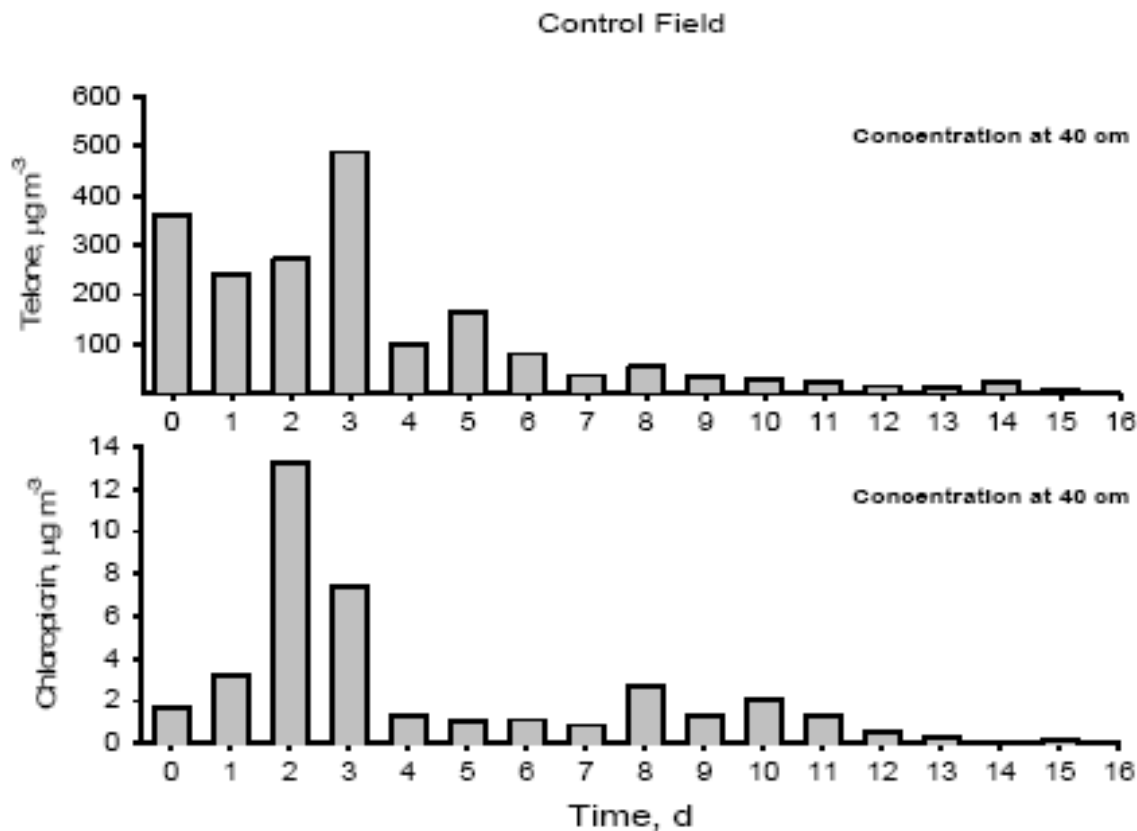


Figure 4.3.4 Concentration ($\mu\text{g m}^{-3}$) of Telone (cis + trans 1,3-D) and chloropicrin in the atmosphere during the experiment. The values shown are daily averages.

The relatively large concentrations at the beginning of the experiment were due to the higher fumigant mass in the soil immediately after application. Furthermore, soil disturbances caused by the fumigation shanks promote rapid soil diffusion from the injection depth to the bottom of the disked layer. Each day, some of the fumigant volatilizes and degrades which leads to a reduction in fumigant material available to escapes to the atmosphere.

Telone C-35 Volatilization

Shown in Table 4.3.1 is a time series of the daily volatilization rate (i.e., flux density). Due to equipment malfunctions, only the flux estimates from the ISCST, CalPuf v. 6 and aerodynamic methods are available.

The three methods demonstrate a similar temporal pattern throughout the experiment. Under these conditions, the peak fumigant flux occurred between 1.8 and 2.3 days. The maximum sampling-period flux values for the ADM, ISC and CalPuf methods, respectively, were 26.2, 11.7, and 29.9 $\mu\text{g m}^{-2} \text{s}^{-1}$. The maximum daily-average flux

values were considerably lower since they include lower nighttime flux rates (respectively, the values were 19.50, 6.77 and 11.70 $\mu\text{g m}^{-2} \text{s}^{-1}$).

Shown in Figure 4.3.5 is a graph of the daily-average flux density estimates for 1,3-D (cis+trans) and chloropicrin using the aerodynamic method. The high flux rates early in the experiment are readily apparent. Furthermore, by day 16, the flux rates are very low.

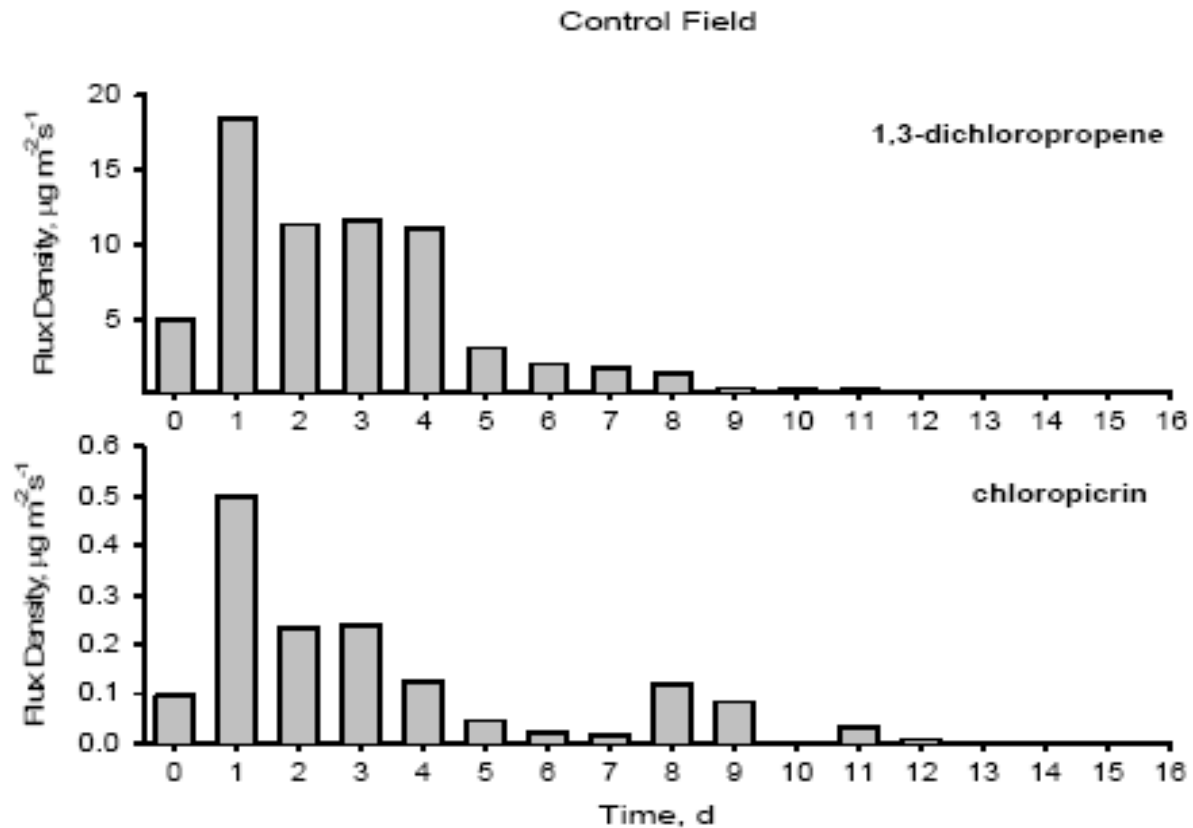


Figure 4.3.5. Emissions expressed as a flux density ($\mu\text{g m}^{-2} \text{s}^{-1}$) for Telone (cis + trans 1,3-D) and chloropicrin during the experiment for the Control field site. The values shown are daily averages.

Table 4.3.1 Summary of daily air temperature, wind speed, wind direction, atmospheric stability and Telone C-35 flux from the Control Plot.

Day Number	Calendar Date	Min Air Temperature	Max Air Temperature	Min Wind Speed	Max Wind Speed	Richardson's Number Ri	Average Wind Speed	Max Wind Speed	Average Wind Direction	Aerodynamic Method		ISCST3 Back Calculation Method		CalPuf v6 Back Calculation Method			
		@ 80 cm (°C)	@ 80 cm (°C)	@ 80 cm (m/s)	@ 80 cm (m/s)		@ 10 m (m/s)	@ 10 m (m/s)	@ 10 m (deg)	Mass Lost (kg)	Flux Density Rate ($\mu\text{g}/\text{m}^2 \text{ s}$)	Mass Lost (kg)	Flux Density Rate ($\mu\text{g}/\text{m}^2 \text{ s}$)	Mass Lost (kg)	Flux Density Rate ($\mu\text{g}/\text{m}^2 \text{ s}$)		
0	5-Sep-07	18.1	31.4	0.71	2.64	0.016	2.14	3.62	4.0	12.84	5.30	8.86	4.58	15.09	6.04		
1	6-Sep-07	18.9	35.4	0.65	3.03	-0.395	2.10	5.20	335.3	47.22	19.50	16.70	6.68	24.47	9.79		
2	7-Sep-07	19.0	32.1	0.52	2.69	-0.078	2.25	3.43	352.7	28.92	11.94	14.50	5.80	29.26	11.70		
3	8-Sep-07	20.1	31.9	0.62	2.26	-0.140	2.09	3.53	333.5	29.72	12.27	12.51	5.00	19.32	7.73		
4	9-Sep-07	21.1	33.9	1.15	2.60	-0.175	2.38	4.89	340.9	28.05	11.59	6.23	2.49	11.40	4.56		
5	10-Sep-07	21.5	32.3	0.84	1.72	-0.315	1.80	2.68	311.2	7.88	3.25	7.12	2.85	12.30	4.92		
6	11-Sep-07	22.2	34.0	1.13	2.09	-0.265	2.29	3.44	340.9	5.11	2.11	4.44	1.78	6.98	2.79		
7	12-Sep-07	19.5	33.5	1.23	2.45	-0.349	2.62	5.62	328.3	4.24	1.75	1.59	0.64	3.00	1.20		
8	13-Sep-07	16.7	25.8	0.75	2.86	-0.102	2.38	4.10	320.5	3.74	1.54	1.75	0.70	2.74	1.09		
9	14-Sep-07	16.9	27.7	0.93	2.25	-0.163	2.25	3.51	313.5	1.16	0.48	1.39	0.56	2.22	0.89		
10	15-Sep-07	17.2	28.5	1.02	1.83	-0.239	2.20	3.38	316.5	0.52	0.21	0.71	0.28	0.99	0.39		
11	16-Sep-07	13.3	28.0	0.46	2.43	-0.053	2.68	3.41	318.5	0.74	0.30	0.54	0.21	0.96	0.38		
12	17-Sep-07	16.3	29.7	0.80	3.02	0.022	2.73	5.21	27.5	0.50	0.21	0.57	0.23	0.98	0.39		
13	18-Sep-07	16.5	30.8	1.16	1.58	-0.189	1.89	3.37	41.7	0.56	0.23	0.42	0.17	0.67	0.27		
14	19-Sep-07	14.5	23.2	1.39	5.48	-0.120	3.63	8.75	303.3	0.04	0.02	0.18	0.07	0.38	0.15		
15	20-Sep-07	10.6	21.8	0.73	2.32	-0.070	2.45	4.01	344.1	0.20	0.08	0.18	0.07	0.28	0.11		
16	21-Sep-07	15.0	15.0	0.99	0.99	-0.504	1.49	2.13	49.2	0.03	0.01	0.00	0.00	0.00	0.00		
										Kg Lost:		158.6 kg		77.7kg		131.0kg	
										% of Applied:		23%		11%		19%	
										Maximum period flux:		26.2 ($\mu\text{g}/\text{m}^2 \text{ s}$)		11.7($\mu\text{g}/\text{m}^2 \text{ s}$)		29.9($\mu\text{g}/\text{m}^2 \text{ s}$)	
										Time of Maximum flux:		2.105 (d)		2.04(d)		2.35(d)	

28944m² Area
697kg Applied C-35

Table 4.3.1 also provides the total mass lost (kg) and total mass lost as a percent of applied chemical. The ADM and CalPuf methods provide similar total loss estimates (i.e., 23% and 19% of applied). The ISCST estimate is considerably lower (11%).

The back-calculation methods rely on a linear relationship between the simulated and measured concentrations. Often, this relationship is found not to be statistically significant, which may lead to questionable flux estimates. One approach to improve the statistical relationship between the simulation and the measurements is to perform an ordered ranking of the simulated and measured data (Johnson et al., 1999), followed by conducting a regression analysis on the sorted data. While this produces an improvement in the statistical characterization, there is no theoretical basis for adopting this transformation. However, for completeness, both the sorted and non-sorted analysis is shown in Table 4.3.2. Generally, sorting produces higher total flux values compared to the more theoretically valid non-sorting methodology. However, in either case, the difference is less than 3% total emissions. Furthermore, sorting doesn't increase the ISCST flux estimate to be comparable with the ADM and CalPuf methods.

Table 4.3.2 Summary of the total flux estimates for Telone C-35 and component fumigants from the Control Field plot.

Method	Percent contribution to total Telone C-35 emissions			Total Telone C-35 Emissions	
	1,3-D (cis)	1,3-D (trans)	chloropicrin		
Aerodynamic Method	58.7%	39.2%	2.1%	24.6%	
Integrated Horizontal Flux	-	-	-	-	
Theoretical Profile Shape	-	-	-	-	
ISCST3 -non sorted	57.9%	41.1%	1.0%	11.2%	
ISCST3 -sorted	58.0%	40.8%	1.2%	12.9%	
CalPuf -non sorted	57.5%	40.9%	1.6%	18.8%	
CalPuf -sorted	57.6%	40.3%	2.1%	21.7%	
Average =	57.9%	40.5%	1.6%	17.8%	Average total flux
Standard deviation =	0.5%	0.7%	0.5%	5.7%	Standard deviation
Contributions to Total Emissions				16.9%	Average total flux - high & low value removed
				6.1%	Standard deviation

Table 4.3.2 also contains a breakdown of the contribution of the cis isomer to the total Telone C-35 emissions. The total emissions were obtained by integrating the volatilization rate over time, multiplying by the total field area and dividing by the total Telone C-35 applied. As an example for the ADM method, 1,3-D (cis) contributed 58.7% of the total 24.6% Telone C-35 emissions. Likewise, the 1,3-D (trans) and chloropicrin contributed, respectively, 39.2 and 2.1%.

All of the methods to estimate emissions report similar values for each component fumigant's contribution to the total emissions. For 1,3-D (cis), 1,3-D (trans) and chloropicrin, respectively, the contribution averaged over all of the estimation methods were 57.9, 40.5 and 1.6% of the total emissions (i.e., 17.8%). The low variation between methods is apparent from the low standard deviation (i.e., < 0.7%).

Very low levels of chloropicrin were lost from this field. Two independent flux estimates both arrived at similar results. This indicates that some soil-based process was limiting chloropicrin movement to the soil surface and volatilization into the atmosphere.

Total Volatilization as Percent of Applied Telone® (cis+trans)

Reporting emissions as percent of applied fumigant mixture (i.e., Telone C-35) can lead to ambiguous emission percentages if different fractions of each component volatilize. For example, due to the very low chloropicrin emissions, one could be misled into thinking that the 1,3-D emission were also much lower than field and laboratory measurements conducted in similar soils and under similar environmental conditions. However, if the 1,3-D emissions are presented as a percentage of the applied 1,3-D (cis+trans); the total emission estimates from the ADM, ISCST and CalPuf methods, respectively, are 35.4%, 20.0%, and 27.2% of the applied 1,3-D (cis+trans). The average and standard deviation of the total emission from the 3 methods is, respectively, 27.5±7.7%. This is similar to the results from a laboratory study quantifying 1,3-D (cis) flux loss using soil collected from the irrigated field site described in Section 4.1, above (Ashworth and Yates, 2007). The study was conducted with temperatures cycles that closely matched field observations described in that experiment, and are similar to those observed in this experiment. This laboratory study reported that the total emissions of *cis*-1,3-D after 14 days were 33.1% for a control treatment. Since emissions of the *cis* and *trans* isomer are similar and the active ingredient for Telone is approximately a 50% by 50% mixture of isomers, the total emissions for 1,3-D (cis+trans) would be approximately the same value.

Emissions of 1,3-D in the range from 30%-40% have been reported in the literature. In a study conducted in a large field in the Salinas Valley of California, 1,3-D volatilization was reported to be approximately 25% of the applied material (Chen *et al.*, 1996, 1996; Cryer *et al.*, 2003) over a 14-day sampling period. Furthermore, Gao *et al.* (2008) conducted a field-plot experiment to investigate several methods to reduce emissions of 1,3-D after shank injection. The experiment was conducted in a Hanford sandy loam and included a 46 cm injection depth. Emissions were periodically measured using passive flux chambers and total emissions from a bare-soil, non-irrigated control were 36% of the applied 1,3-D; which is similar to the value obtained here and in the laboratory experiment of Ashworth and Yates (2007).

Soil Gas Phase Concentration

Shown in Figure 4.3.6 is the soil gas-phase concentration at various times after application of Telone C-35. After 24 hours, the soil gas phase concentration for 1,3-D (*cis*) at the injection depth exceeded 0.6 $\mu\text{g cm}^{-3}$, and the treated zone had extended from about 30 to 70 cm

depth. Each day, the concentrations in soil were reduced as diffusion moved 1,3-D throughout the soil. By day 4, a fairly constant concentration was observed from 20 cm to 100 cm depth. By day 11, soil concentrations were low along with the volatilization rate (see Figure 4.3.5).

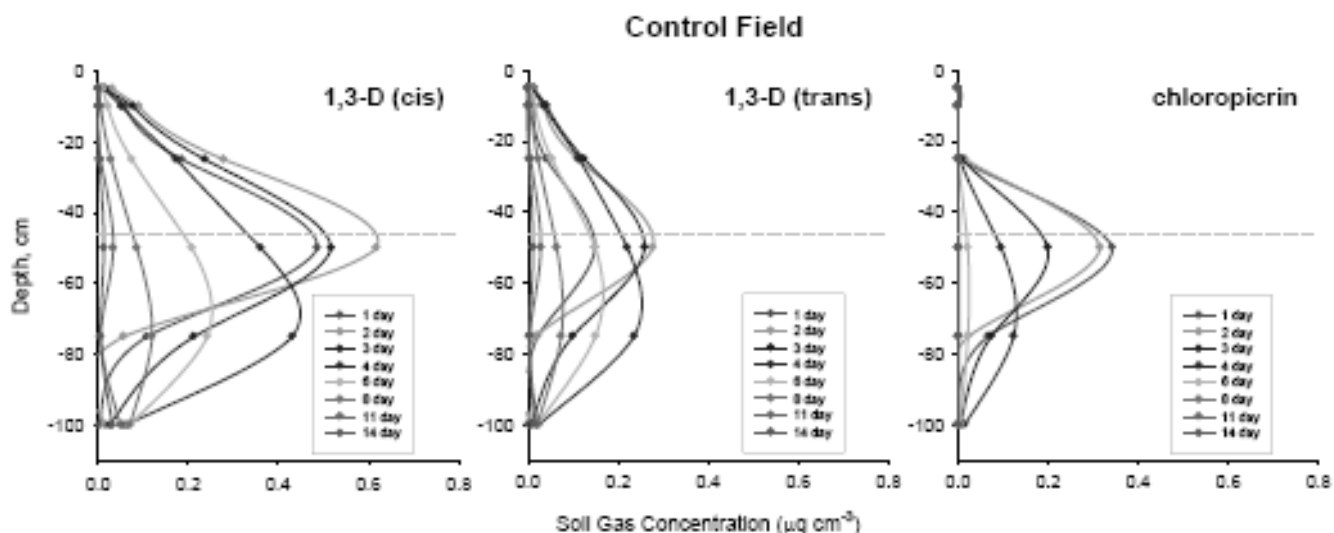


Figure 4.3.6. Soil gas concentration ($\mu\text{g cm}^{-3}$) of 1,3-D (cis), 1,3-D (trans), and chloropicrin as a function of depth in the soil and time after fumigation. The injection depth is marked by the dashed grey line at 46 cm depth.

These values are considerably lower than observed in previous experiments (Section 3.1 and 3.3) and observed at the ATS (North) and Deep Injection (South) field sites. Given the relatively large shank spacing, it is possible that the sampling site happened to be placed further from the shanks compared to the other fields. Sampling soils can be problematic due to spatial variability. For example, soil sampling for bromide ion (a degradation produce of methyl bromide) required 30 soil cores throughout the field location in order to obtain an accurate spatial representation of the methyl bromide degradation (Yates et al., 1996a). Due to limited equipment and cost constraints, only two locations in each field were sampled for soil gas concentration. Therefore, it would be expected that variability would be relatively high, especially at the beginning of the experiment. Another possibility is variability in the fumigation process may have led to reduced application rates in this area. However, the fumigation process was controlled by computer, so variations in the application rate are less likely than effects due to spatial variability. Furthermore, two replicates of the soil gas concentration were obtained. For the Control field, one of the replicates consistently had very low concentrations. Near zero values can occur when the sampling probes are plugged with soil or if the sample collection device has leaks. While this would be possible, it is rare that all depths at one location would experience plugging or leaking. A more likely explanation would be natural spatial variability or some soil structural feature that impeded fumigant diffusion in soil.

While the magnitude of the soil-gas concentration may be affected by spatial variability, the relative behavior between fumigant chemicals provides valuable information for interpretation of the results. For example, the total emission rate for chloropicrin is very low relative to 1,3-

D (see Table 4.3.2). From the soil concentration measurements, it is clear that chloropicrin movement to the surface was limited and very low soil-gas concentrations were measured above the 25 cm depth, and approximately zero levels at the soil surface. While it is not apparent what soil and/or environmental factor led to this effect, Figure 4.3.6 provides evidence that the flux estimates are correct and that chloropicrin emission levels were low during this experiment.

The soils in this region tend to have a relatively high soil degradation rate (Ashworth and Yates, 2007). This may have contributed to a reduction in chloropicrin levels as the soil consumed chloropicrin leading to low concentrations near the soil surface (Figure 4.3.6). In a laboratory study which simulates field conditions, and using soil that was collected during the experiment, Ashworth et al. (2009) measured half-lives for 1,-D and chloropicrin, respectively, as 90 and 2.9 h, at 25 °C. They also found that chloropicrin emissions ranged from 1.2% for a HDPE cover, 16% for deep injection, and 21% for a bare-soil control. This suggests that two factors that affect the chloropicrin emissions are the soil degradation rate and the properties of any barrier at the soil surface (i.e., HDPE).

While the 21% from the bare-soil control exceeds the value measured in this experiment, the 1.2% total emissions from the HDPE covered soil may suggest that the soil preparation and post-fumigation roller packing may have created a diffusion barrier that had a similar effect as using a HDPE film with a relatively high mass transfer coefficient (0.6 cm/h).

To investigate this further, a mathematical model was used that describes total emissions as a function of injection depth, presence of absence of a shank, porosity, bulk density, water/air contents, soil degradation, soil diffusion and surface resistance to volatilization (Yates, 2009).

From the model results, the most likely explanation for the low emissions is the very high chloropicrin soil degradation rate (i.e., $t_{1/2} = 2.9$ h). Simulating the soil and environmental conditions during the experiment, the predicted total emissions would be less than 1%. Even assuming the soil half-life is 10 times longer than the measured value (i.e., $t_{1/2} = 29$ h), emissions are less than 2.5% of applied even with very large surface mass transfer coefficients (i.e., low resistance to diffusion from soil to the atmosphere), as shown in Figure 4.3.7.

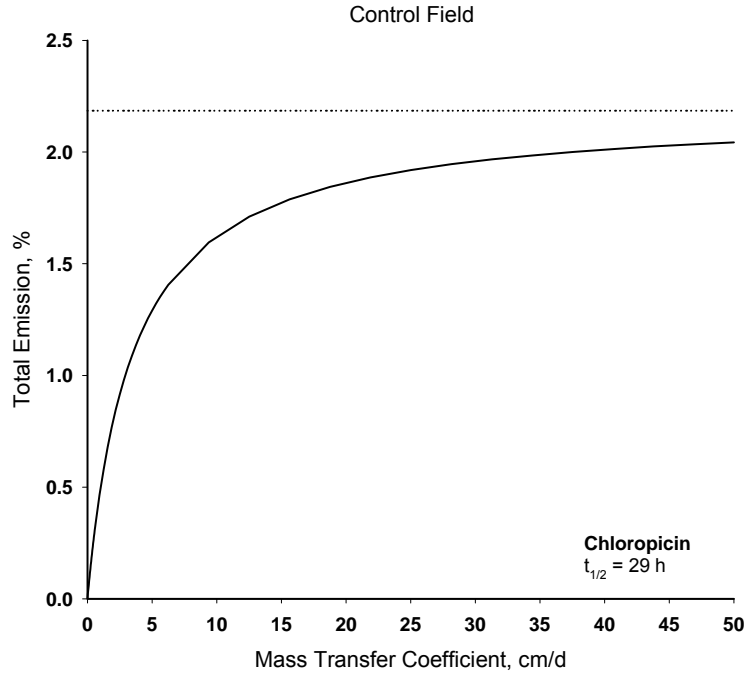


Figure 4.3.7. Effect of mass transfer coefficient on percent total emissions for chloropicrin $t_{1/2}$ of 29 h.

The total volatilization model is given in Equation 4.3.1 (see Yates, 2009) and the model parameters used in the simulation are shown in Table 4.3.3.

$$\text{Total Volatilization} = \frac{C_o H_E \sqrt{D_E} \left(e^{\frac{-z_d \sqrt{\mu}}{\sqrt{D_E}}} - e^{\frac{-z_o \sqrt{\mu}}{\sqrt{D_E}}} \right)}{(z_o - z_d) (H_E + \sqrt{D_E} \sqrt{\mu}) \sqrt{\mu}} \quad (4.3.1)$$

Table 4.3.3. Parameters used in volatilization model (Yates, 2009)

Injection depth, z_o	46	cm
Disking depth (i.e., top of shank-fracture depth), z_d	30	cm
Soil water content, θ	0.1	$\text{cm}^3 \text{cm}^{-3}$
Soil porosity, ϕ	0.4	$\text{cm}^3 \text{cm}^{-3}$
Soil bulk density, ρ_b	1.5	gm cm^{-3}
Mass transfer coefficient, h	0.0–50	cm/hr
Gas retardation coefficient, R_g	15	
Effective mass transfer coefficient, H_e	h/R_g	cm/hr
Effective soil diffusion coefficient, D_e	1284	$\text{cm}^2 \text{h}^{-1}$
Soil degradation half-life, $t_{1/2}$	$2.9^a - 29^b$	h

^a Ashworth *et al.*, 2009; ^b 29 is 10 times the measured value and is presented as a worst case scenario.

4.4 Field #4: Broadcast-Shank Telone C-35 Fumigation, Deep Injection Treatment (South Field Site).

4.4.1 Field Specific Information

The Deep Injection (South) Field site was located in southwest of the control site, and was positioned furthest south. The nearest distance to the Control Field site was 1340 m (i.e., 0.8 mi) and no other fumigated field was in the vicinity. The treated area was 2.80 ha (i.e., 6.93 ac). A total of 429.7 kg of (i.e., 947.2 lbs) of 1,3-D (cis + trans), and 241.9 kg chloropicrin (i.e., 533.3 lbs) was applied at a depth of 0.61 m (i.e., 24 in). The soil type for this field was Milham sandy loam. Figure 4.4.1 shows a picture taken during the experiment and gives a sense of the experimental conditions. Figure 4.4.2 shows a schematic of the field site and the positioning of instruments and sampling equipment.



Figure 4.4.1. Deep Injection (South) field site. Foreground shows the location of the soil temperature sensors. In the distance the micrometeorological sensors and gas sampling equipment is shown.

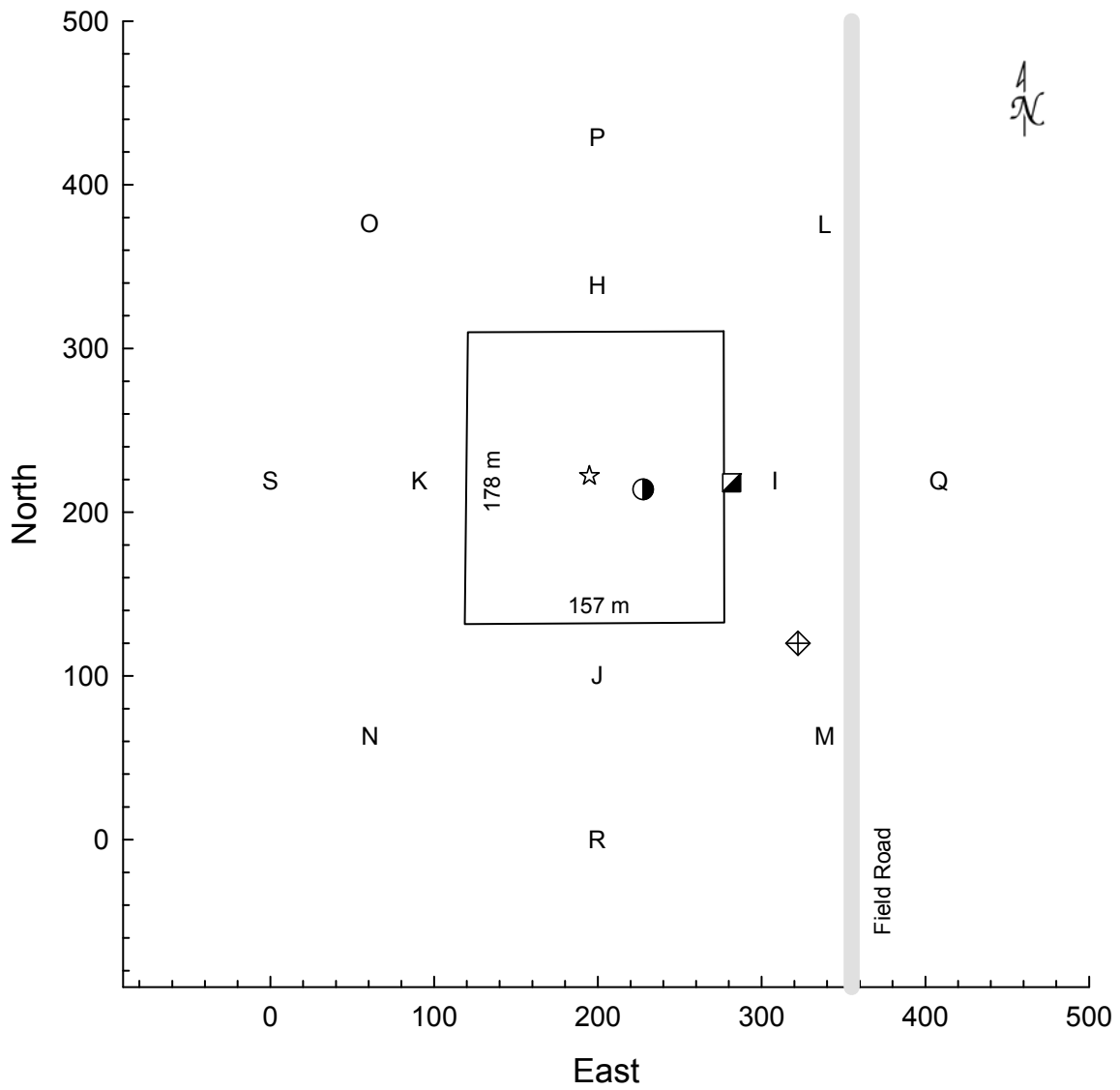


Figure 4.4.2. Field layout for the Deep Injection (South Field) site. The letters indicate the positions of the off-field sampling equipment used for the back-calculation (i.e., ISCST3) method. The star, half-filled circle and half-filled square, respectively, are the locations of the gas-sampling mast (i.e., micrometeorological flux methods), the position of the soil gas sampling equipment, and the position of the soil temperature and heat flux sensors.

4.4.2 Results and Discussion

Several methods were used to obtain estimates of the emission flux density, including micrometeorological methods: aerodynamic, integrated horizontal flux, theoretical profile shape and two back calculation methods: ISCST3 and CalPuf v6. The micrometeorological and back calculation methods provide independent flux estimates since the meteorological and atmospheric gas sampling was from different data sources.

Figure 4.4.3 shows the temperature gradient, wind speed gradient and the gradient Richardson's number for the first 12-days of the experiment as a bar graph. These values were obtained over the air concentration measurement period to yield a period-averaged estimate that coincides with the air concentration measurements.

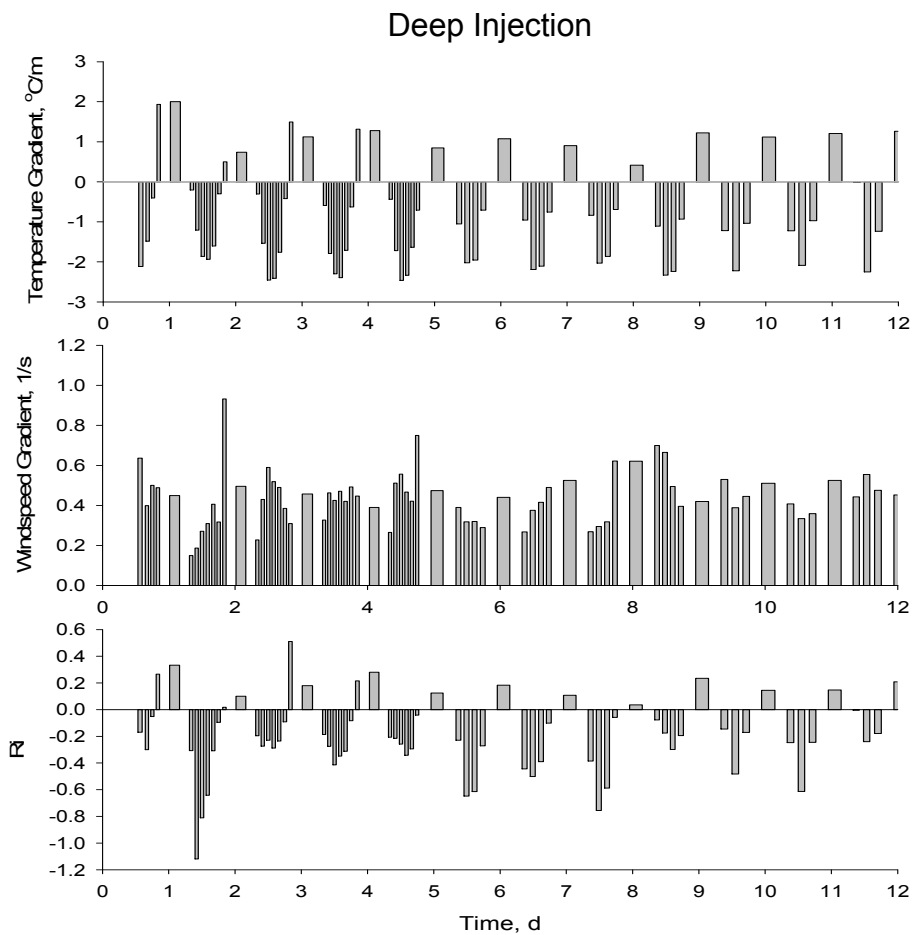


Figure 4.4.3 Temperature gradient, wind speed gradient and Richardson's Number at the Deep Injection (South) field site. The values shown are averages over the flux sampling periods (see Section 4.1).

This information provides the basis for obtaining flux estimates using the aerodynamic method. The aerodynamic methods require obtaining an estimate of the atmospheric stability, which is based on calculation of the Richardson's number, Ri (Figure 4.4.3c). Negative values for Ri indicate an unstable atmosphere, and enhances emissions; positive Ri

indicate stable conditions which often occur during nighttime. By definition, the sign of the Richardson number is determined by the temperature gradient.

Comparing the data presented in Figure 4.4.3 with 4.3.3, shows that both the Control field and South field (i.e., deep injection) experienced very similar temperature and wind speed gradient conditions.

The largest differences between fields were the relatively larger negative Ri values during the experiment, especially during the middle of Day 1. For the control field, the peak Ri was approximately -0.5 , where in the South (Deep Injection) field, the peak value was approximately -1.1 . During many other days, the mid-day peak value was somewhat larger in the South (Deep Injection) field, sometimes exceeding -0.5 .

In the South (Deep Injection) field, the Richardson number generally varied from $+0.3$ to -0.8 . Like the Control field, negative values generally occurred during the middle of the day and positive values at night. The maximum difference in Ri between fields during the nighttime was $.2$, with an average difference of 0.04 . During the daytime, the maximum difference was 0.63 , with an average difference of 0.10 . Using Equation 2.2, the effect of differences in Ri can be determined. For example, assuming a period where both field has identical flux rates, the maximum difference in Ri during unstable conditions would produce a 43% higher flux estimates in the South (Deep Injection) field ($Ri = -1.1$) compared to the Control field ($Ri = -0.49$). For stable conditions, the maximum difference in Ri, would produce a 88% reduction in the estimated flux South (Deep Injection) field ($Ri = 0.32$) and the Control fields ($Ri = 0.11$).

Fumigant Concentrations in the Air

Concentrations of 1,3-D and chloropicrin were collected at several heights in the center of the field. The concentrations at 40 above the surface are shown in Figure 4.4.4. The concentration of 1,3-D (cis+trans) was slightly lower at the Deep Injection (South) field site compared to the Control field. In general, the daily concentration of 1,3-D remained below $400 \mu\text{g m}^{-3}$, whereas in the Control field, levels reach $500 \mu\text{g m}^{-3}$.

The concentration of chloropicrin in the atmosphere has an erratic behavior throughout the experiment. The concentration levels remain below $4 \mu\text{g m}^{-3}$ but fluctuate between about $0.5 - 4 \mu\text{g m}^{-3}$ during the first 7 days. These daily concentration levels are considerably lower than the maximum $14 \mu\text{g m}^{-3}$ observed in the Control plot. Comparing chloropicrin to 1,3-D concentrations indicate that limited volatilization occurred from this site.

The maximum concentration levels in the middle of the field are comparable to the maximum concentrations measured at 12 locations surrounding the field. For example, the peak measured concentration located at the field center at a height of 150 cm was $143 \mu\text{g m}^{-3}$, and occurred at 3.35 days (morning sample). These levels are comparable to the maximum daily 1,3-D concentration measured at the 12 locations surrounding the field (i.e., $163 \mu\text{g m}^{-3}$) which occurred at 3.35 days 30 m outside the field boundary.

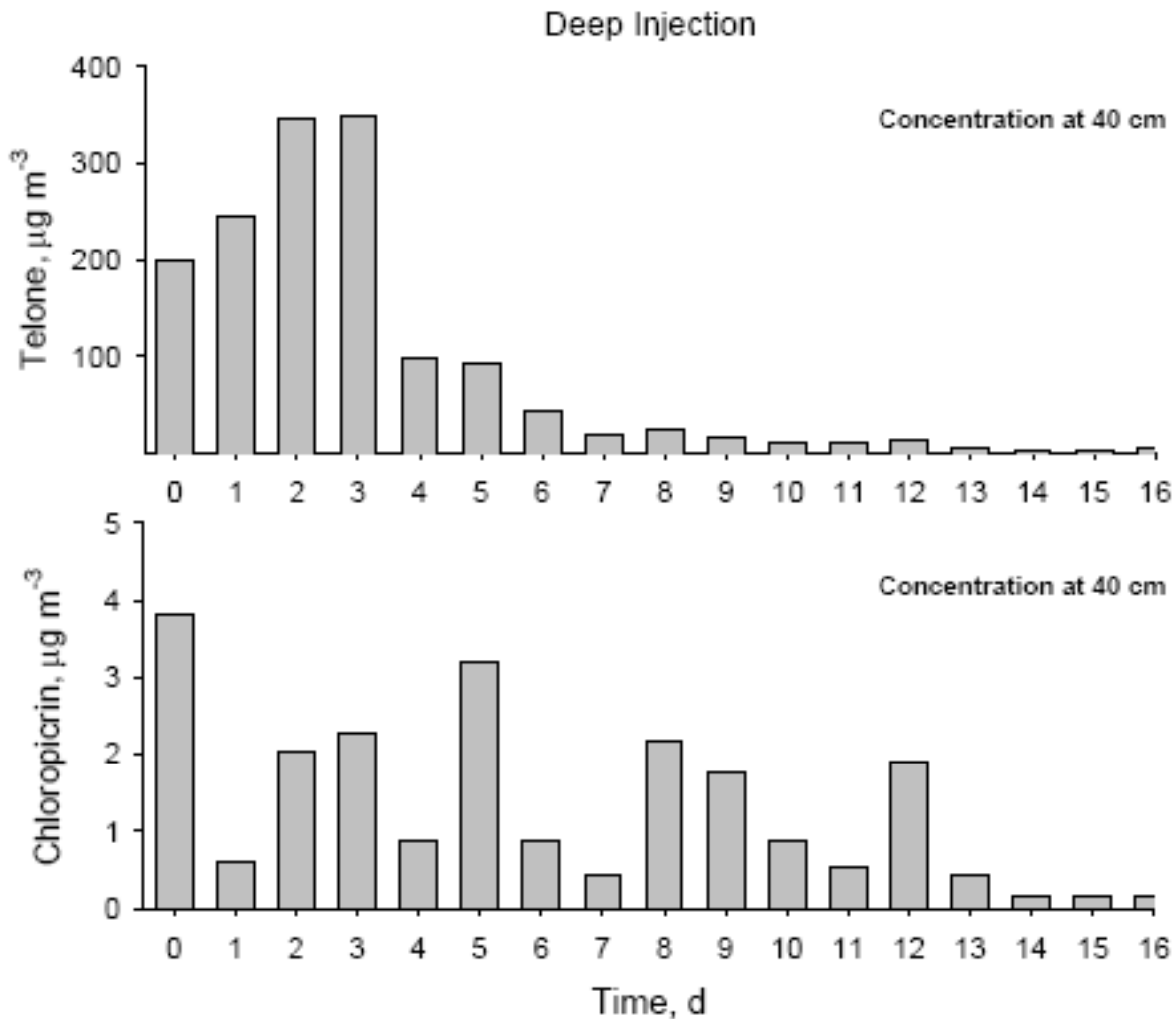


Figure 4.4.4 Concentration ($\mu\text{g m}^{-3}$) of Telone (cis + trans 1,3-D) and chloropicrin in the atmosphere during the experiment. The values shown are daily averages.

Telone C-35 Volatilization

The data presented in Table 4.4.1 are time series of the daily fumigant concentrations and volatilization rates using the three micrometeorological methods. Overall, each approach provides a similar temporal pattern throughout the experiment. Under these conditions, the peak fumigant flux occurred between 1.84 and 3.35 days, depending on the method. The maximum sampling-period flux values for the ADM, IHF and TPS methods, respectively,

were 32.4, 15.2, and 17.5 $\mu\text{g m}^{-2} \text{s}^{-1}$. The maximum daily-average flux values were considerably lower since they include lower nighttime flux rates (respectively, the values were 10.1, 7.2 and 5.9 $\mu\text{g m}^{-2} \text{s}^{-1}$). These represent, respectively, 17.2, 12.2, and 9.7% of applied Telone C-35 material.

Shown in Table 4.4.2 are the results for the back-calculation methods. For the ISCST3 approach, the peak fumigant flux occurred between 2.04 d and had a value of 7.5 $\mu\text{g m}^{-2} \text{s}^{-1}$ and the peak flux for the CalPuf approach occurred at 3.35 d and had a value of 10.85 $\mu\text{g m}^{-2} \text{s}^{-1}$. These methods, respectively, estimate that 10% or 17% of applied Telone C-35 would be lost to the atmosphere. The ISCST method closely matches the IHF and TPS approaches, whereas the Calpuf estimate more closely matches the ADM method.

Shown in Figure 4.4.5 is a graph of the daily-average flux density estimates for 1,3-D (cis+trans) and chloropicrin using the aerodynamic method.

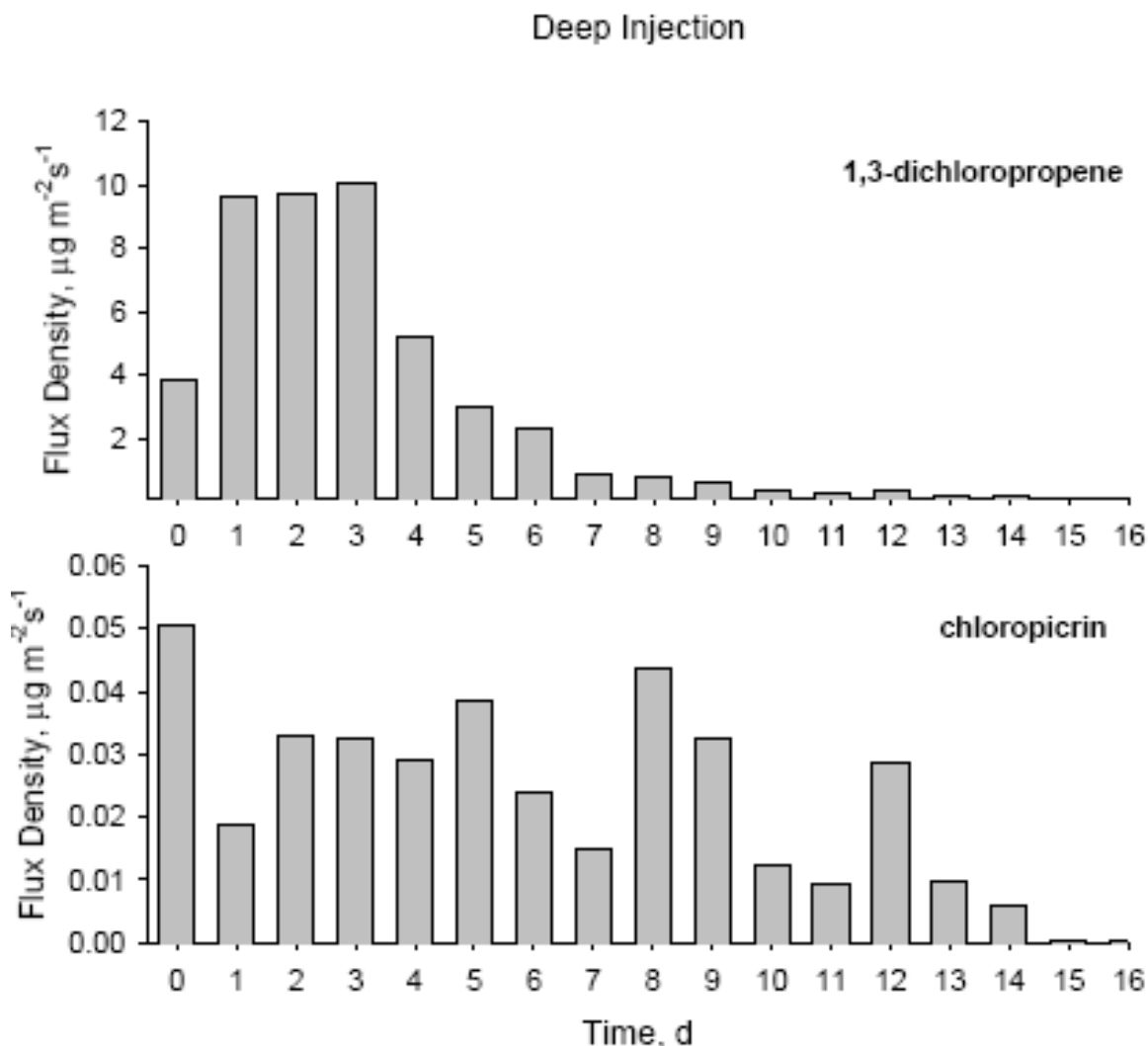


Figure 4.4.5. Emissions expressed as a flux density ($\mu\text{g m}^{-2} \text{s}^{-1}$) for Telone (cis + trans 1,3-D) and chloropicrin during the experiment for the Deep Injection (South) field site. The values shown are daily averages.

Table 4.4.1. Summary of Telone C-35 flux from the South Field Plot (Deep Injection Treatment) using micrometeorological methods.

Day Number	Calendar Date	Telone Air Conc ($\mu\text{g}/\text{m}^3$)	chloropicrin Air Conc ($\mu\text{g}/\text{m}^3$)	Aerodynamic Method		Integrated Horizontal Flux Method		Theoretical Profile Shape Method	
				Mass Lost (kg)	Flux Density Rate ($\mu\text{g}/\text{m}^2 \text{ s}$)	Mass Lost (kg)	Flux Density Rate ($\mu\text{g}/\text{m}^2 \text{ s}$)	Mass Lost (kg)	Flux Density Rate ($\mu\text{g}/\text{m}^2 \text{ s}$)
0	5-Sep-07	41.59	0.95	9.46	3.91	5.41	2.23	0.61	0.25
1	6-Sep-07	117.32	0.30	23.41	9.67	17.43	7.20	14.31	5.91
2	7-Sep-07	118.23	0.98	23.67	9.78	16.55	6.83	14.10	5.82
3	8-Sep-07	130.89	1.32	24.47	10.10	13.07	5.40	9.77	4.03
4	9-Sep-07	45.90	0.54	12.71	5.25	10.68	4.41	9.15	3.78
5	10-Sep-07	41.52	0.97	7.26	3.00	6.42	2.65	5.56	2.30
6	11-Sep-07	22.90	0.42	5.57	2.30	3.04	1.26	2.91	1.20
7	12-Sep-07	12.76	0.25	2.07	0.86	2.52	1.04	2.86	1.18
8	13-Sep-07	9.48	0.88	2.02	0.84	1.72	0.71	1.18	0.49
9	14-Sep-07	7.62	0.83	1.58	0.65	1.21	0.50	0.92	0.38
10	15-Sep-07	5.39	0.40	0.90	0.37	0.85	0.35	0.66	0.27
11	16-Sep-07	4.31	0.28	0.57	0.24	0.55	0.23	0.55	0.23
12	17-Sep-07	4.00	0.37	0.82	0.34	0.66	0.27	0.67	0.28
13	18-Sep-07	3.37	0.18	0.54	0.22	0.42	0.17	0.51	0.21
14	19-Sep-07	1.91	0.13	0.34	0.14	0.95	0.39	1.06	0.44
15	20-Sep-07	1.78	0.07	0.07	0.03	0.23	0.10	0.41	0.17
16	21-Sep-07	8.68	0.14	0.03	0.01	0.17	0.07	0.16	0.07
Kg Lost:				115.51 kg		81.90 kg		65.07 kg	
% of Applied:				17.2%		12.2%		9.7%	
Max period flux:				32.41 ($\mu\text{g}/\text{m}^2 \text{ s}$)		15.23 ($\mu\text{g}/\text{m}^2 \text{ s}$)		17.48 ($\mu\text{g}/\text{m}^2 \text{ s}$)	
Time of Maximum flux:				3.35 (d)		3.35 (d)		1.84 (d)	

Table 4.4.2. Summary of daily air temperature, wind speed, wind direction, atmospheric stability and Telone C-35 flux from the South Field Site (Deep Injection Treatment).

Day Number	Calendar Date	Min Air Temperature	Max Air Temperature	Min Wind Speed	Max Wind Speed	Richard-son's Number Ri	Average Wind Speed	Max Wind Speed	Average Wind Direction	ISCST3 Back-Calculation Method		CalPuf v6 Back-Calculation Method	
		@ 80 cm (°C)	@ 80 cm (°C)	@ 80 cm (m/s)	@ 80 cm (m/s)		@ 10 m (m/s)	@ 10 m (m/s)	@ 10 m (deg)	Mass Lost (kg)	Flux Density Rate (µg/m ² s)	Mass Lost (kg)	Flux Density Rate (µg/m ² s)
0	5-Sep-07	18.05	31.44	0.71	2.64	0.016	2.14	3.62	4.0	4.74	1.96	7.42	3.07
1	6-Sep-07	18.86	35.37	0.65	3.03	-0.395	2.10	5.20	335.3	18.15	7.50	26.28	10.85
2	7-Sep-07	19.01	32.06	0.52	2.69	-0.078	2.25	3.43	352.7	14.31	5.91	25.78	10.65
3	8-Sep-07	20.05	31.90	0.62	2.26	-0.140	2.09	3.53	333.5	12.43	5.13	21.42	8.84
4	9-Sep-07	21.11	33.86	1.15	2.60	-0.175	2.38	4.89	340.9	4.62	1.91	7.96	3.29
5	10-Sep-07	21.52	32.32	0.84	1.72	-0.315	1.80	2.68	311.2	4.93	2.04	8.92	3.68
6	11-Sep-07	22.22	34.04	1.13	2.09	-0.265	2.29	3.44	340.9	2.95	1.22	5.04	2.08
7	12-Sep-07	19.52	33.47	1.23	2.45	-0.349	2.62	5.62	328.3	1.70	0.70	3.66	1.51
8	13-Sep-07	16.72	25.80	0.75	2.86	-0.102	2.38	4.10	320.5	1.70	0.70	2.56	1.06
9	14-Sep-07	16.94	27.70	0.93	2.25	-0.163	2.25	3.51	313.5	1.56	0.65	2.28	0.94
10	15-Sep-07	17.17	28.52	1.02	1.83	-0.239	2.20	3.38	316.5	0.56	0.23	0.79	0.33
11	16-Sep-07	13.30	28.01	0.46	2.43	-0.053	2.68	3.41	318.5	0.44	0.18	0.75	0.31
12	17-Sep-07	16.25	29.68	0.80	3.02	0.022	2.73	5.21	27.5	0.38	0.16	0.85	0.35
13	18-Sep-07	16.50	30.85	1.16	1.58	-0.189	1.89	3.37	41.7	0.34	0.14	0.53	0.22
14	19-Sep-07	14.49	23.17	1.39	5.48	-0.120	3.63	8.75	303.3	0.17	0.07	0.35	0.14
15	20-Sep-07	10.64	21.76	0.73	2.32	-0.070	2.45	4.01	344.1	0.16	0.06	0.23	0.10
16	21-Sep-07	15.00	15.00	0.99	0.99	-0.504	1.49	2.13	49.2	0.00	0.00	0.00	0.00
Kg Lost:										69.2 kg		114.8 kg	
% of Applied:										10%		17%	
Max flux:										13.4 (µg/m ² s)		33.8 (µg/m ² s)	
Time of Maximum flux:										2.04 (d)		3.35 (d)	

The high flux rates early in the experiment are readily apparent. Furthermore, by day 16, the flux rates are essentially zero. The chloropicrin flux rate appears to fluctuate considerably. The emission of 1,3-D (cis+trans) follows the more typical pattern with increasing flux, reaching a maximum after a few days and then tailing off and approaching zero after a few weeks. The erratic nature of the chloropicrin flux is probably due, in part, to the low flux rates and the behavior of the atmospheric chloropicrin concentration, which was also very erratic.

Table 4.4.1 and 4.4.2 also provides the total mass lost (kg) and total mass lost as a percent of applied Telone C-35. The ADM and CalPuf methods provide similar total loss estimates (i.e., 17% of applied) and the IHF, TPS and ISCST estimates are also similar although considerably lower (10–12%).

Table 4.4.3 contains information on the contribution of the 1,3-D (cis), 1,3-D (trans) and chloropicrin to the total of the Telone C-35 emissions. This table shows that 1,3-D (cis) contributed approximately 57% of the total Telone C-35 emissions. Likewise, the 1,3-D (trans) and chloropicrin contributed, respectively, 41 and 2%. These results are similar to the observations from the Control plot.

For this field, very low levels of chloropicrin were lost. The two independent flux estimates both arrived at similar results, which indicate that some soil-based process was limiting chloropicrin movement to the soil surface and volatilization into the atmosphere.

Table 4.4.3. Summary of the total flux estimates for Telone C-35 and component fumigants from the Deep Injection (South) Field plot.

Method	Percent contribution to total Telone C-35 emissions			Total Telone C-35 Emissions	
	1,3-D (cis)	1,3-D (trans)	chloropicrin		
Aerodynamic Method	58.7%	40.6%	0.7%	17.2%	
Integrated Horizontal Flux	58.0%	40.6%	1.4%	12.2%	
Theoretical Profile Shape	56.1%	43.1%	0.8%	9.7%	
ISCST3 -non sorted	57.0%	41.6%	1.4%	10.3%	
ISCST3 -sorted	56.9%	41.5%	1.6%	11.7%	
CalPuf -non sorted	56.8%	41.1%	2.1%	17.1%	
CalPuf -sorted	56.5%	41.0%	2.6%	19.3%	
Average =	57.1%	41.4%	1.5%	13.9%	Average total flux
Standard deviation =	0.9%	0.9%	0.7%	3.8%	Standard deviation
Contributions to Total Emissions				13.7%	Average total flux - high & low value removed
				3.2%	Standard deviation

Total Volatilization as Percent of Applied Telone® (cis+trans)

The total emission estimates from the ADM, IHF, TPS, ISCST3 and CalPuf methods, respectively, are 26.7%, 18.8%, 15.1%, 15.8%, and 26.1% of the applied 1,3-D (cis+trans). The average and standard deviation of the total emission from the 5 methods is, respectively, $20.5 \pm 5.6\%$ and for the ADM, ISCST3, and CalPuf methods is, respectively, $22.9 \pm 6.1\%$.

Using the total emission estimates for the ADM, ISCST3 and CalPuf methods, deep injection reduces emissions of Telone (cis+trans) by approximately 17% compared to the standard fumigation methodology.

Soil Gas Phase Concentration

Shown in Figure 4.4.6 is the soil gas-phase concentration at various times after application of Telone C-35. During the first 24 hours, the soil gas phase concentration for 1,3-D (cis) at the injection depth exceeded $8 \mu\text{g cm}^{-3}$. It appears that the peak concentration occurred at 50 cm, but this is more a reflection of the sampling position (i.e., no sample at the injection depth). By day 3, the position of the injection depth can be determined by the shape of the curve. As was observed in the Control plot, the concentrations in soil were reduced each day as diffusion moved 1,3-D throughout the soil. By day 6, a fairly constant concentration was observed from 20 cm to 100 cm depth. By day 11, soil concentrations were low along with the volatilization.

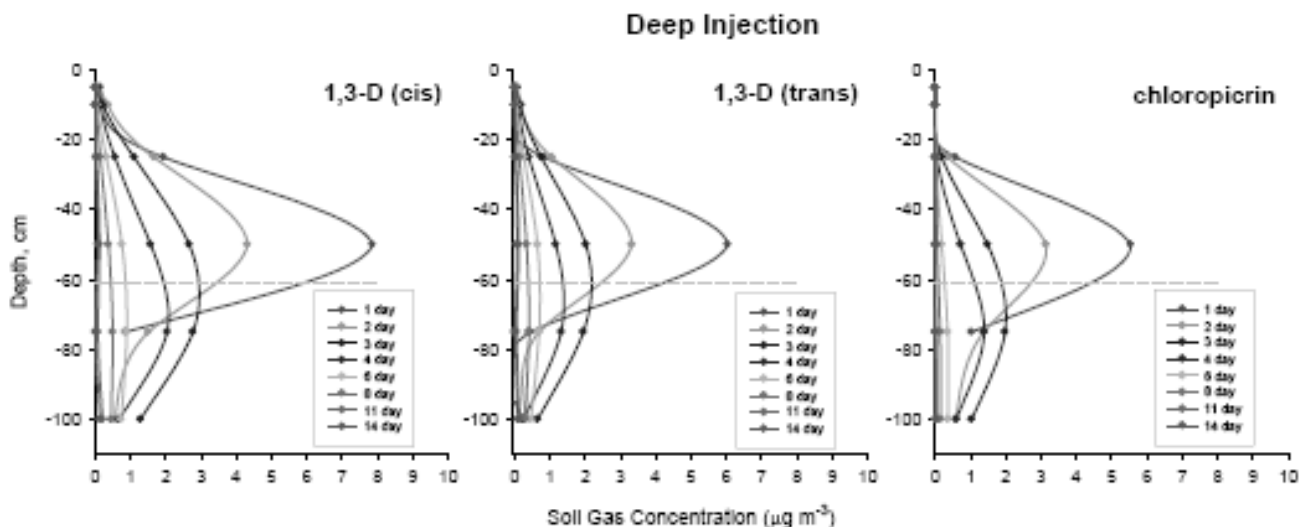


Figure 4.4.6. Soil gas concentration ($\mu\text{g cm}^{-3}$) of 1,3-D (cis), 1,3-D (trans), and chloropicrin as a function of depth in the soil and time after fumigation. The injection depth is marked by the dashed grey line at 61 cm depth.

Based on the analysis described above, it appears that the soil degradation in the surface soil depleted chloropicrin before sufficient time was available to transport the material to the soil surface, with very low soil-gas concentrations measured at the 25 cm depth, and approximately zero levels at the soil surface. Given the similarity in the 1,3-D and chloropicrin concentration curves between 1 and 4 days after fumigation, it appears that the low emission rates were due to high soil degradation above the 25 cm depth. Below this depth, the concentrations, and hence, soil degradation rates, appear similar.

Characterizing Shanks in Deep Injection Field

During soil fumigation, shanks are used to deliver the fumigant. After fumigation, the disking operation mixes soil above injection site (~30 cm) but leaves large openings (~20 cm) down to the injection depth. The extent of these openings depends on many factors, including size of shanks, soil type, etc. These openings can be clearly seen in Figure 4.4.7. Fracture openings were not observed in the other fields.



Figure 4.4.7 Trench showing position of shank fractures.

Digging the trench obscured the fractures. Here the soil was removed so that the fractures were completely opened. The arrows show the fracture locations.

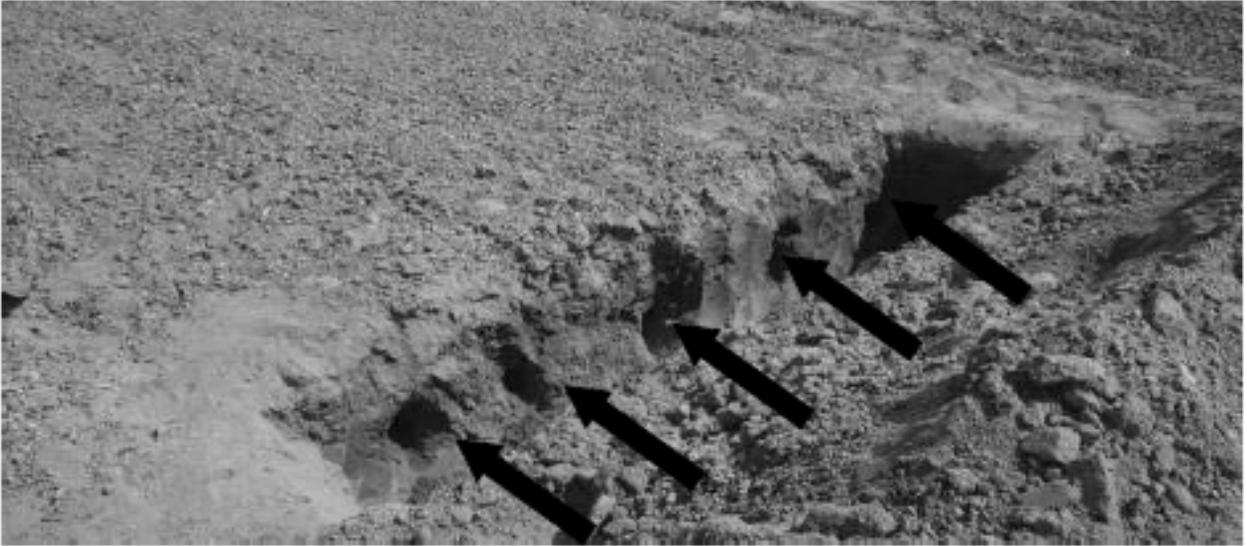


Figure 4.4.8 Trench showing position of shank fractures.

The fracture openings extended 9 ft at this location (Figure 4.4.9). The fumigant injected into the soil would quickly spread out creating a relatively uniform concentration throughout the opening. The effective injection depth would be reduced compared to an injection that did not produce a fracture opening.



Figure 4.4.9. Pictures of the fracture openings.



Using a mathematical model (Yates, 2009) shows that concentration profile for a shank source injection can be similar to a point source injection (Figure 4.4.10). This figure illustrates the effect of the shank in spreading the chemical in the soil and also provides an explanation for observations that peak emissions often occur sooner than predicted with point-source simulations. By 1 day, the depth of peak concentration and overall distribution in soil appears to be very similar. The shank distribution is slightly more oval in shape compared to the point source scenario. The shank fracture would improve fumigant efficacy by providing a more uniform concentration distribution in the soil profile.

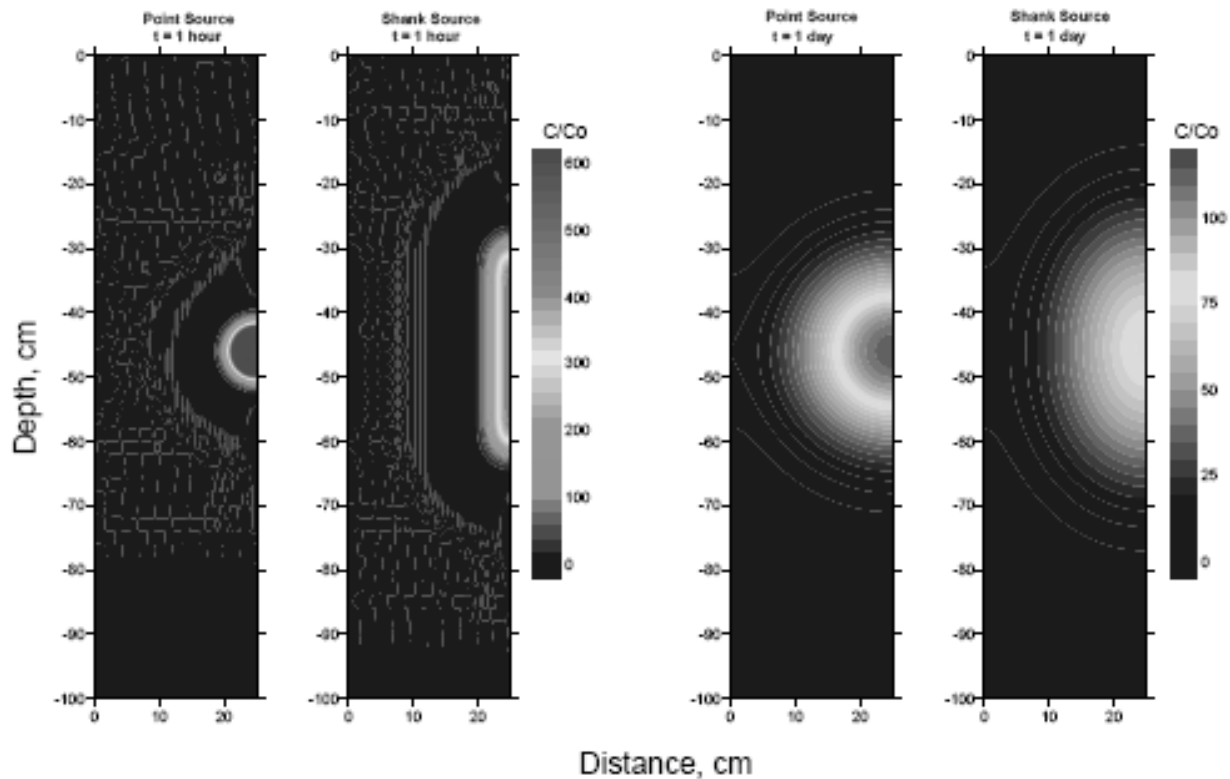


Figure 4.4.10. Simulation of point and shank sources at 1 hour and 1 day after fumigation. The depth of injection for a point source was 46 cm and 61 cm for a shank source. The shank extended from 30–61 cm depth.

The soil concentration values are considerably higher than observed in the Control plot. Given the relatively large shank spacing and the large fracture openings that were observed in this field, it is likely that (for this field) the position of the sampling site would be relatively insensitive to the position of shanks, compared to the other fields. The large fracture openings would disperse the fumigant over a wider extent compared to soils where fracture openings are not produced during fumigation.

Another factor that can lead to higher concentration would be favorable position of the sampling sites to the shanks and positioning of the sampling site in an area of the field where the fumigation equipment was operating in a stable and consistent manner. However, the fumigation process was controlled by computer; one would expect variations in the application rate to be minimal. Two replicates of the soil gas concentration were obtained and both replicate produces similar concentration levels. For the Control field, however, one of the replicates consistently had very low concentrations, which may be an indication of a sampling problem. A possible explanation for the low values in the Control plot would be natural spatial variability or some soil structural feature that impeded fumigant diffusion in soil to the sampling location.

4.5 Field #5: Broadcast-Shank Telone C-35 Fumigation, Ammonium Thiosulfate Treatment (i.e., North Field Site).

4.5.1 Field Specific Information

The ATS (North) Field site was located 1000 m (i.e., 0.6 mi) northeast of the Control site (see Figure 4.1.1). There were no other fumigated field was in the vicinity. The treated area was 2.87 ha (i.e., 7.09 ac). A total of 469.6 kg of (i.e., 1035.2 lbs) of 1,3-D (cis + trans), and 249.0 kg chloropicrin (i.e., 549.0 lbs) was applied at a depth of 0.46 m (i.e., 18 in). The soil in the fumigated portion of this field is classified as a Kimberlina fine sandy loam.

Figure 4.5.1 shows a picture taken during the experiment and gives a sense of the experimental conditions. To the north of the field road, an actively growing crop was present, but the vegetative material was short (i.e., < 1 m and periodically cut). Figure 4.5.2 shows a schematic of the field site and the positioning of instruments and sampling equipment.



Figure 4.5.1. ATS (North) Field site. Shown are the anemometer mast, the in-field weather station, the gas sampling mast and the temperature gradient mast. In the distance the soil temperature and heat flux sensors are shown.

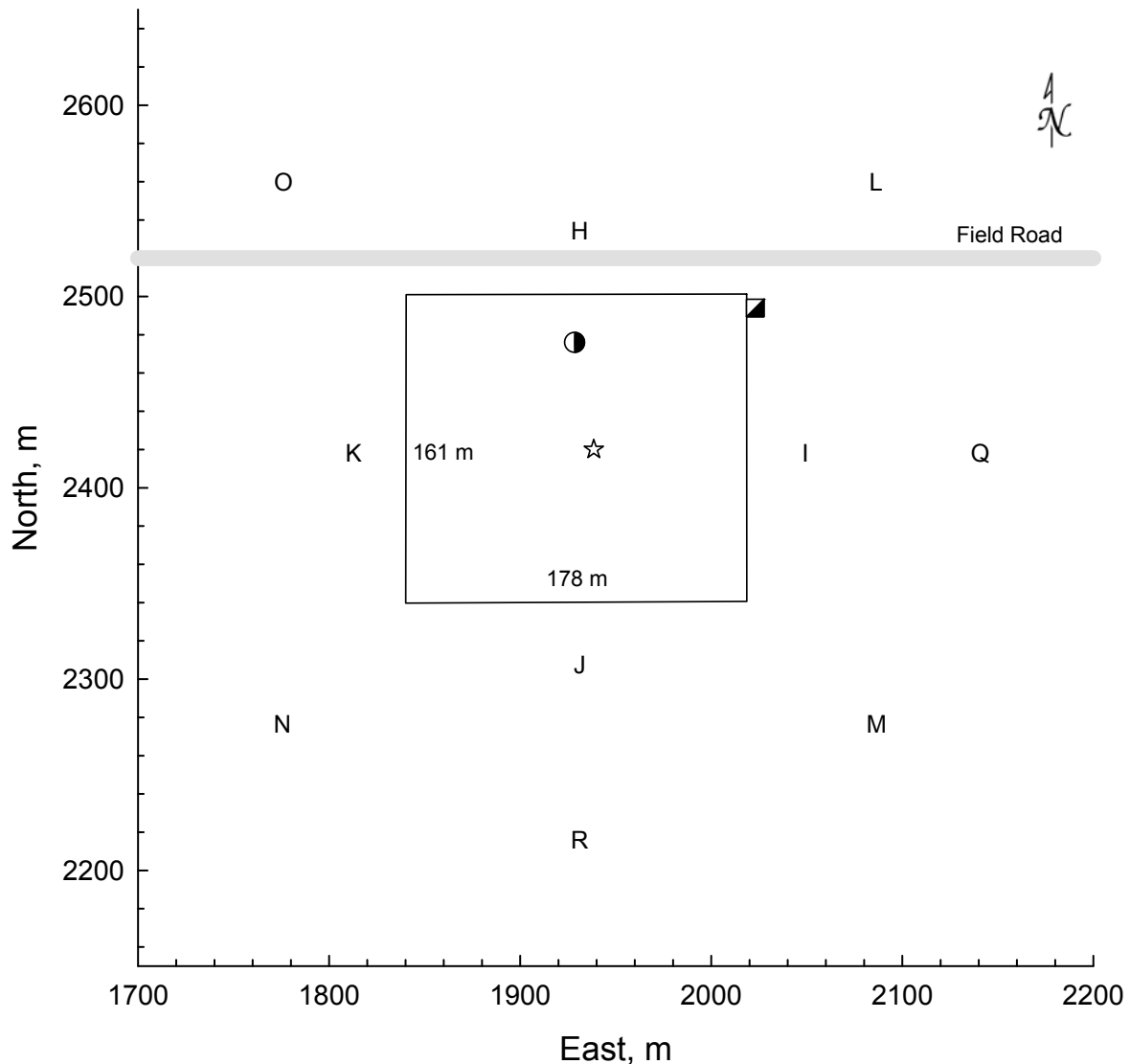


Figure 4.5.2. Field layout for the ATS application (North Field) site. The letters indicate the positions of the off-field sampling equipment used for the back-calculation (i.e., ISCST3) method. The star, half-filled circle and half-filled square, respectively, are the locations of the gas-sampling mast (i.e., micrometeorological flux methods), the position of the soil gas sampling equipment, and the position of the soil temperature and heat flux sensors.

Due to equipment limitations, this field had only 10 off-site sampling stations surrounding the field site. This was necessary to allow for the sampling of the fumigant concentration in the atmosphere between the fields (see Figure 4.1.1, Between Field Samplers). Since the winds are predominately from the northwest, the north-most and west-most samplers (i.e., samplers P and S) were not installed and this equipment used for air sampling between fields.

4.5.2 Results and Discussion

Comparing the data presented in Figure 4.5.3 with the Control Plot (i.e., Figure 4.3.3) shows that both the Control field and North field (i.e., ATS treatment) experienced very similar temperature and wind speed gradient conditions. All three fields have very similar patterns for wind speed and temperature.

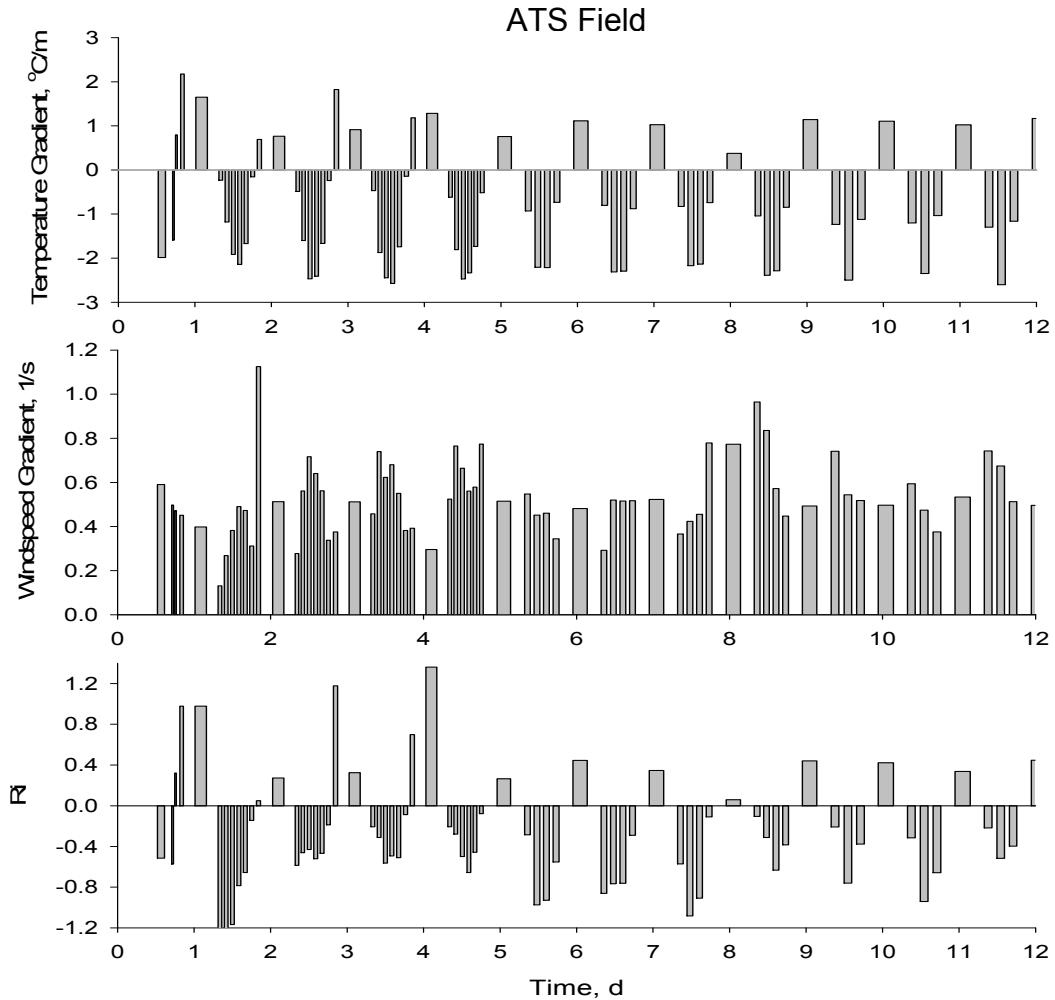


Figure 4.5.3 Temperature gradient, wind speed gradient and Richardson's Number at the ATS (North) Field site. The values shown are averages over the flux sampling periods.

The largest differences between fields were the relatively larger negative Ri values during the experiment, especially during the middle of Day 1. The control field experienced the smallest values for daily Ri for both stable and unstable conditions. The ATS (North) field had similar Ri as the Control field for stable conditions, but had more negative Ri during many unstable periods. The ATS (North) field had the widest range in Ri for both stable and unstable conditions. Under stable conditions, this would lead to a suppression of the fumigant flux, and for unstable conditions, would lead to flux increases.

This effect may be a reflection of the different soil type in the North field. Although the soil properties, soil preparation and soil appearance were very similar, it is possible that some combination of these factors may have led to differences in the Richardson number. Another potential factor maybe that a garlic crop was recently harvested in this field and there was some plant residue on the soil surface. Furthermore, this was the only field that had a crop growing in an adjacent field. While the plant height was short, and the crop was periodically cut, this may have some effect on the wind patterns.

While the Richardson's numbers were somewhat different between the fields, this difference would only affect the flux estimated using the aerodynamic method. The integrated horizontal flux method does not depend on atmospheric stability considerations and the theoretical profile shape method obtains information at a height above the soil where the effect of atmospheric stability is minimized.

Fumigant Concentrations in Air

Concentrations of 1,3-D (cis+trans) and chloropicrin were collected at several heights in the center of the field. The concentrations at 40 cm above the surface are shown in Figure 4.5.4.

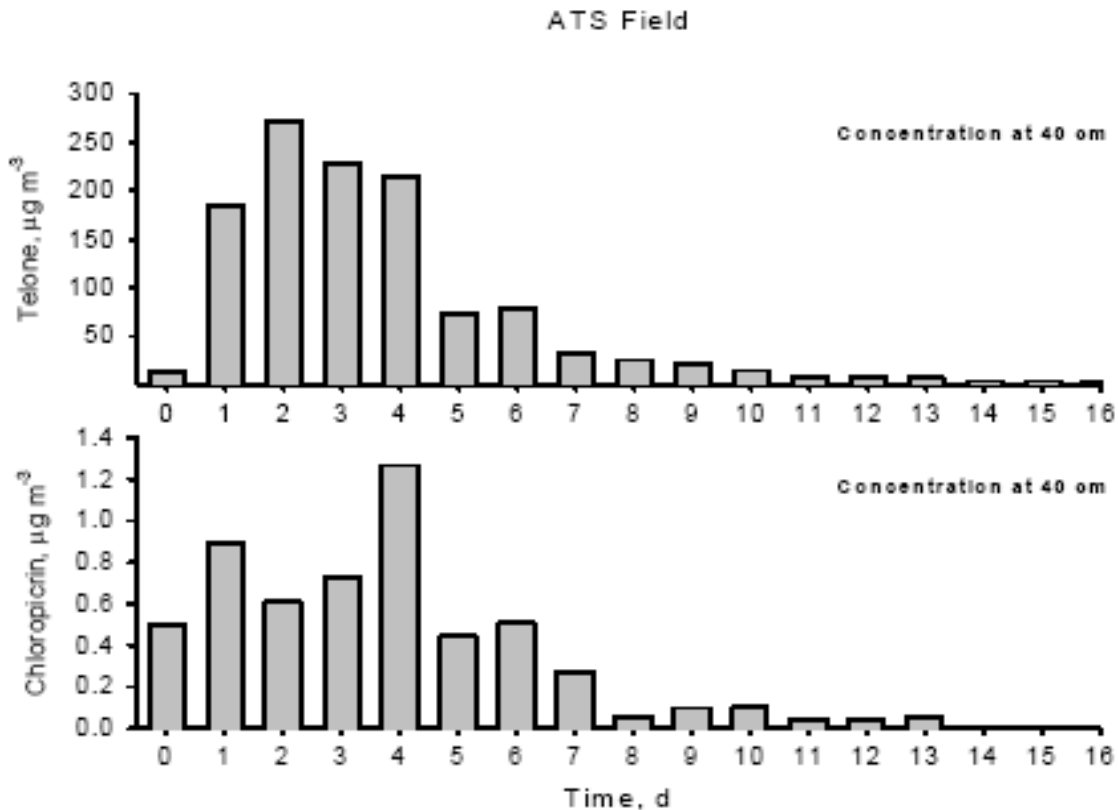


Figure 4.5.4 Concentration (µg m⁻³) of Telone (cis + trans 1,3-D) and chloropicrin in the atmosphere during the experiment. The values shown are daily averages.

For both 1,3-D and chloropicrin, the levels are initially low, then increase to a maximum during the first 2–4 days of the experiment and then become very low by the 16 day. The concentrations were somewhat lower at this field site (maximum 272 $\mu\text{g m}^{-3}$) compared to the Control (maximum 488 $\mu\text{g m}^{-3}$) and Deep Injection (South) fields (maximum 349 $\mu\text{g m}^{-3}$). This may be a reflection of differences in atmospheric stability observed at this field site. The maximum chloropicrin concentration was 1.27 $\mu\text{g m}^{-3}$ which is considerably lower than the concentrations for 1,3-D and observations at the other field sites.

The maximum concentration in the middle of the field is comparable to the maximum concentration measured at 10 locations surrounding the field. For example, the peak measured concentration located at the field center at a height of 150 cm was 116.4 $\mu\text{g m}^{-3}$, and occurred at 1.09 days (nighttime sample). The next highest concentration was 103 $\mu\text{g m}^{-3}$ and occurred at 3.09 d. The peak measured concentration at a height of 150 cm 30 m outside the field boundary was 139.2 $\mu\text{g m}^{-3}$ and occurred at 3.04 d (nighttime sample).

Telone C-35 Volatilization

Shown in Table 4.5.1 are time series of the daily fumigant concentration and volatilization rates using the three micrometeorological methods. Shown in Table 4.5.2 are the results for the back-calculation methods.

Overall, the aerodynamic approach and the CalPuf back calculation methodology provide similar total emission estimates (i.e., 17.6% and 18.0%). The other flux estimation methods provide total emission estimates in the range from 8.5–10%.

The temporal pattern for the flux density is similar to the other field sites (Figure 4.5.5). Under these field and treatment conditions, the peak period averaged flux occurred between 1.84 and 4.34 days, depending on the method. The maximum sampling-period flux values for the ADM, IHF and TPS methods, respectively, were 19.4, 6.75, and 7.65 $\mu\text{g m}^{-2} \text{s}^{-1}$. The maximum daily-average flux values were lower. The values, respectively, were 8.9, 4.7 and 5.1 $\mu\text{g m}^{-2} \text{s}^{-1}$. Total emissions were, respectively, 16.6, 8.6, and 8.5% of applied Telone C-35 material.

ATS Field

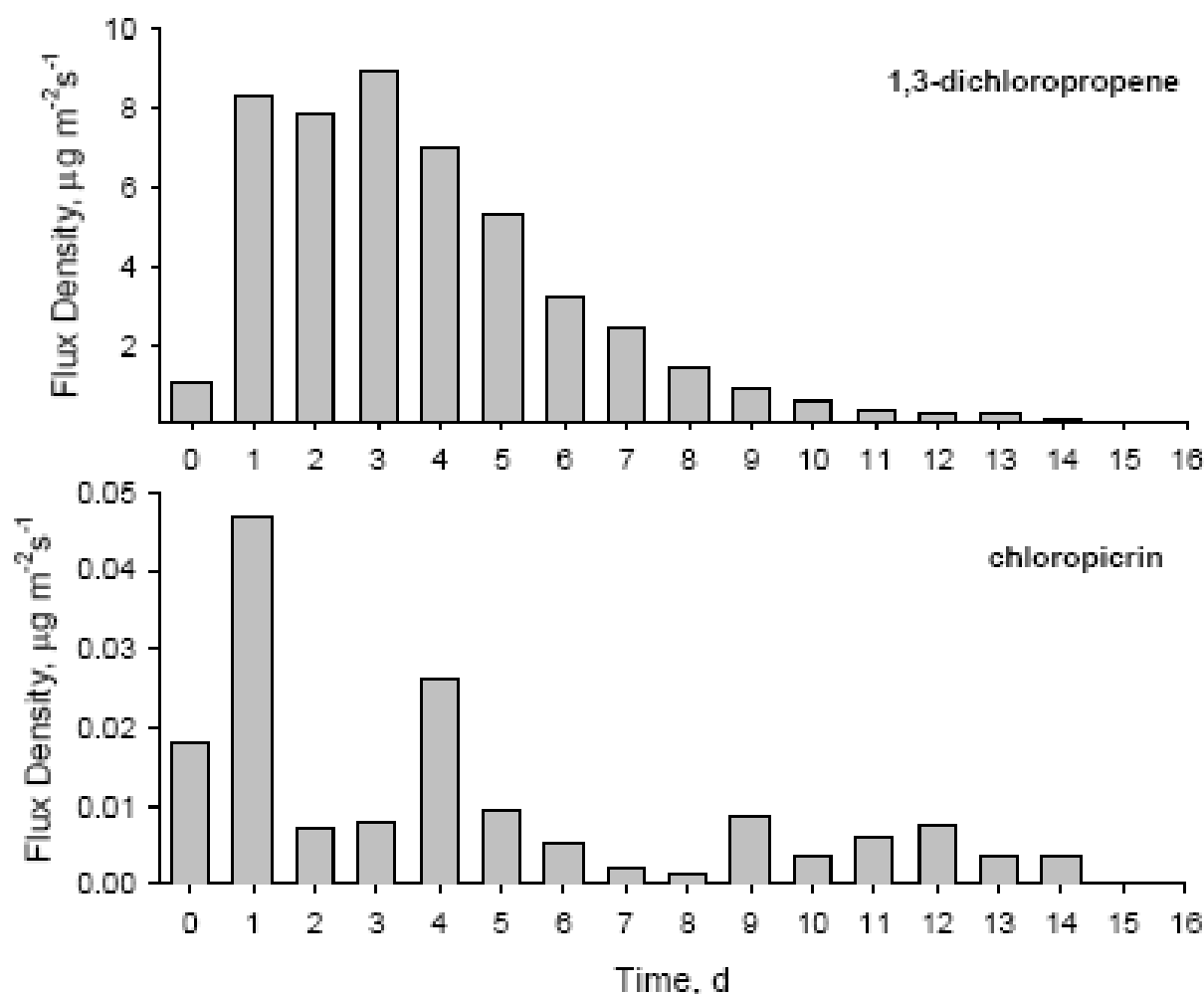


Figure 4.5.5. Emissions expressed as a flux density ($\mu\text{g m}^{-2} \text{s}^{-1}$) for Telone (cis + trans 1,3-D) and chloropicrin during the experiment for the ATS (North) field site. The values shown are daily averages.

For this field, the chloropicrin flux rates were very low with maximum daily flux rates of less than $0.05 \mu\text{g m}^{-2} \text{s}^{-1}$. The two independent flux estimates both arrived at similar results, which indicate that some soil-based process was limiting chloropicrin movement to the soil surface and volatilization into the atmosphere.

Table 4.5.3 contains information on the contribution of the 1,3-D (cis), 1,3-D (trans) and chloropicrin to the total of the Telone C-35 emissions. This table shows that 1,3-D (cis) contributed approximately 58% of the total Telone C-35 emissions. Likewise, the 1,3-D (trans) and chloropicrin contributed, respectively, 41 and 1%. These results are similar to the observations from the other field plots.

Table 4.5.1. Summary of Telone C-35 flux from the ATS (North) Field Plot using micrometeorological methods.

Day Number	Calendar Date	Telone Air Conc at 80 cm ($\mu\text{g}/\text{m}^3$)	chloropicrin Air Conc at 80 cm ($\mu\text{g}/\text{m}^3$)	Aerodynamic Method		Integrated Horizontal Flux Method		Theoretical Profile Shape Method	
				Mass Lost (kg)	Flux Density Rate ($\mu\text{g}/\text{m}^2 \text{ s}$)	Mass Lost (kg)	Flux Density Rate ($\mu\text{g}/\text{m}^2 \text{ s}$)	Mass Lost (kg)	Flux Density Rate ($\mu\text{g}/\text{m}^2 \text{ s}$)
0	5-Sep-07	41.6	0.95	2.64	1.06	6.62	2.65	3.99	1.60
1	6-Sep-07	117.3	0.30	20.58	8.30	10.53	4.21	11.26	4.50
2	7-Sep-07	118.2	0.98	19.43	7.84	11.75	4.70	12.80	5.12
3	8-Sep-07	130.9	1.32	22.05	8.90	8.95	3.58	7.09	2.84
4	9-Sep-07	45.9	0.54	17.27	6.97	7.26	2.90	7.31	2.92
5	10-Sep-07	41.5	0.97	13.13	5.30	4.67	1.87	5.43	2.17
6	11-Sep-07	22.9	0.42	8.01	3.23	2.78	1.11	3.12	1.25
7	12-Sep-07	12.8	0.25	6.04	2.44	1.76	0.70	1.95	0.78
8	13-Sep-07	9.5	0.88	3.51	1.41	1.73	0.69	1.68	0.67
9	14-Sep-07	7.6	0.83	2.19	0.88	1.01	0.41	0.99	0.40
10	15-Sep-07	5.4	0.40	1.40	0.57	0.67	0.27	0.90	0.36
11	16-Sep-07	4.3	0.28	0.88	0.35	0.56	0.23	0.70	0.28
12	17-Sep-07	4.0	0.37	0.70	0.28	0.34	0.14	0.48	0.19
13	18-Sep-07	3.4	0.18	0.64	0.26	0.30	0.12	0.42	0.17
14	19-Sep-07	1.9	0.13	0.41	0.17	0.34	0.14	0.65	0.26
15	20-Sep-07	1.8	0.07	0.29	0.12	0.26	0.10	0.38	0.15
16	21-Sep-07	8.7	0.14	0.07	0.03	0.07	0.03	0.05	0.02
Kg Lost:				119.2 kg		59.6 kg		59.2 kg	
% of Applied:				16.6%		8.6%		8.5%	
Max period flux:				19.44 ($\mu\text{g}/\text{m}^2 \text{ s}$)		6.75 ($\mu\text{g}/\text{m}^2 \text{ s}$)		7.65 ($\mu\text{g}/\text{m}^2 \text{ s}$)	
Time of Maximum flux:				4.34 (d)		3.10 (d)		1.84 (d)	

Table 4.5.2 Summary of daily air temperature, wind speed, wind direction, atmospheric stability and Telone C-35 flux from the ATS (North) Field Plot.

Day Number	Calendar Date	Min Air Temperature @ 80 cm (°C)	Max Air Temperature @ 80 cm (°C)	Min Wind Speed @ 80 cm (m/s)	Max Wind Speed @ 80 cm (m/s)	Richard-son's Number Ri	Average Wind Speed @ 10 m (m/s)	Max Wind Speed @ 10 m (m/s)	Average Wind Direction @ 10 m (deg)	ISCST3 Back-Calculation Method		CalPuf v6 Back-Calculation Method		
										Mass Lost (kg)	Flux Density Rate (µg/m ² s)	Mass Lost (kg)	Flux Density Rate (µg/m ² s)	
0	5-Sep-07	18.05	31.44	0.71	2.64	0.016	2.14	3.62	4.0	4.61	1.86	7.75	3.10	
1	6-Sep-07	18.86	35.37	0.65	3.03	-0.395	2.10	5.20	335.3	19.97	8.05	31.82	12.72	
2	7-Sep-07	19.01	32.06	0.52	2.69	-0.078	2.25	3.43	352.7	12.66	5.11	23.81	9.52	
3	8-Sep-07	20.05	31.90	0.62	2.26	-0.140	2.09	3.53	333.5	12.25	4.94	19.44	7.77	
4	9-Sep-07	21.11	33.86	1.15	2.60	-0.175	2.38	4.89	340.9	5.02	2.02	13.72	5.49	
5	10-Sep-07	21.52	32.32	0.84	1.72	-0.315	1.80	2.68	311.2	5.44	2.19	10.37	4.15	
6	11-Sep-07	22.22	34.04	1.13	2.09	-0.265	2.29	3.44	340.9	2.99	1.21	7.08	2.83	
7	12-Sep-07	19.52	33.47	1.23	2.45	-0.349	2.62	5.62	328.3	1.75	0.70	3.84	1.54	
8	13-Sep-07	16.72	25.80	0.75	2.86	-0.102	2.38	4.10	320.5	1.37	0.55	2.50	1.00	
9	14-Sep-07	16.94	27.70	0.93	2.25	-0.163	2.25	3.51	313.5	1.19	0.48	1.98	0.79	
10	15-Sep-07	17.17	28.52	1.02	1.83	-0.239	2.20	3.38	316.5	0.56	0.22	0.90	0.36	
11	16-Sep-07	13.30	28.01	0.46	2.43	-0.053	2.68	3.41	318.5	0.44	0.18	0.81	0.33	
12	17-Sep-07	16.25	29.68	0.80	3.02	0.022	2.73	5.21	27.5	0.34	0.14	0.77	0.31	
13	18-Sep-07	16.50	30.85	1.16	1.58	-0.189	1.89	3.37	41.7	0.31	0.13	0.47	0.19	
14	19-Sep-07	14.49	23.17	1.39	5.48	-0.120	3.63	8.75	303.3	0.14	0.06	0.31	0.12	
15	20-Sep-07	10.64	21.76	0.73	2.32	-0.070	2.45	4.01	344.1	0.14	0.06	0.24	0.09	
16	21-Sep-07	15.00	15.00	0.99	0.99	-0.504	1.49	2.13	49.2	0.00	0.00	0.00	0.00	
										Kg Lost:	69.17 kg		125.81 kg	
										% of Applied:	10%		18%	
										Max flux:	14.18 (µg/m ² s)		19.72 (µg/m ² s)	
										Time of Maximum flux:	2.04 (d)		3.35 (d)	

Table 4.5.3. Summary of the total flux estimates for Telone C-35 and component fumigants from the ATS (North) Field plot.

Method	Percent contribution to total Telone C-35 emissions			Total Telone C-35 Emissions	
	1,3-D (cis)	1,3-D (trans)	chloropicrin		
Aerodynamic Method	56.1%	42.4%	1.5%	16.6%	
Integrated Horizontal Flux	57.5%	41.5%	1.0%	8.3%	
Theoretical Profile Shape	55.1%	44.5%	0.5%	8.2%	
ISCST3 -non sorted	60.0%	38.6%	1.4%	9.6%	
ISCST3 -sorted	61.7%	36.8%	1.6%	12.1%	
CalPuf -non sorted	55.0%	44.5%	0.5%	17.5%	
CalPuf -sorted	56.9%	42.6%	0.5%	22.9%	
Average =	57.5%	41.6%	1.0%	13.6%	Average total flux
Standard deviation =	2.4%	2.9%	0.5%	5.6%	Standard deviation
Contributions to Total Emissions				12.8%	Average total flux - high & low value removed
				4.1%	Standard deviation

Total Volatilization as Percent of Applied Telone® (cis+trans)

The total emission estimates from the ADM, IHF, TPS, ISCST3 and CalPuf methods, respectively, are 25.0%, 12.5%, 12.5%, 14.5%, and 26.7% of the applied 1,3-D (cis+trans). The average and standard deviation of the total emission from the 5 methods is, respectively, 18.2±7.0% and for the ADM, ISCST3, and CalPuf methods is, respectively, 22.1±6.6%.

Using the total emission estimates for the ADM, ISCST3 and CalPuf methods, spraying the field with ATS reduces emissions of Telone (cis+trans) by approximately 19.9% compared to the standard fumigation methodology.

Soil Gas Phase Concentration

Shown in Figure 4.5.6 is the soil gas-phase concentration at various times after application of Telone C-35. During the first 24 hours, the soil gas phase concentration for 1,3-D (cis) at the injection depth exceeded 5 µg cm⁻³. As was observed in the other plots, the concentrations in soil were reduced each day as diffusion moved 1,3-D throughout the soil. By day 6, a fairly constant concentration was observed from 20 cm to 100 cm depth. By day 11, soil concentrations were low along with the volatilization.

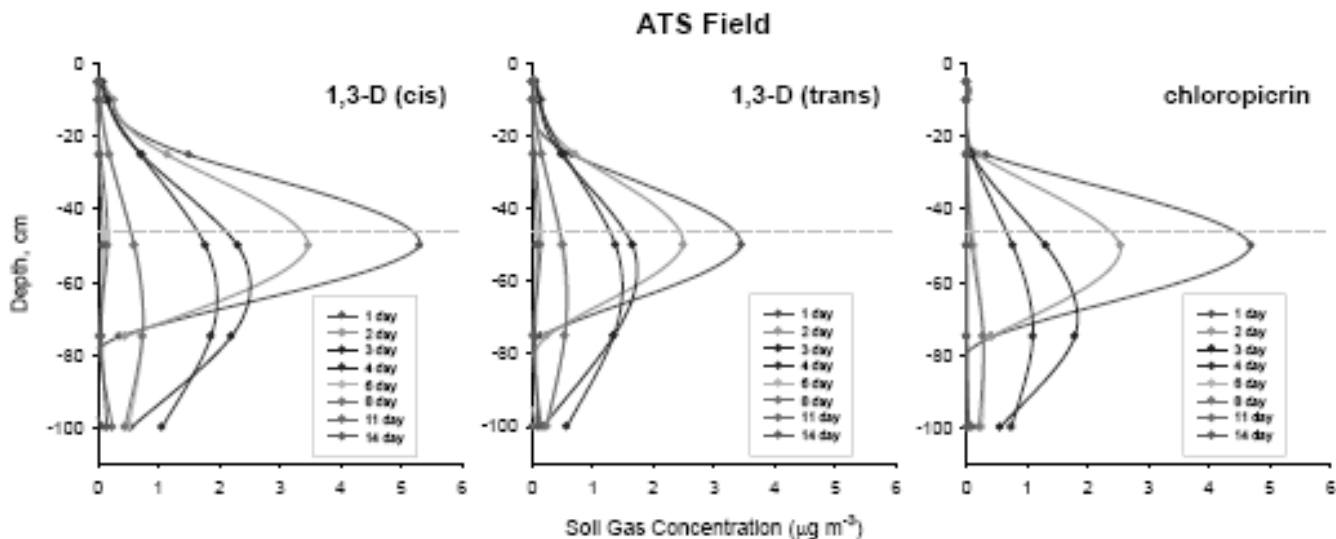


Figure 4.5.6. Soil gas concentration ($\mu\text{g cm}^{-3}$) of 1,3-D (cis), 1,3-D (trans), and chloropicrin as a function of depth in the soil and time after fumigation. The injection depth is marked by the dashed grey line at 61 cm depth.

After 24 hours, the concentration of each component was approximately the same near the injection depth. However, as observed for the other fields, it appears that the soil degradation in the surface soil layer depleted chloropicrin before sufficient time was available to transport the material to the soil surface. Therefore, very low soil-gas concentrations were measured at the 25 cm depth, and approximately zero levels at the soil surface. Given the similarity in the 1,3-D and chloropicrin concentration curves between 1 and 4 days after fumigation, it appears that the low emission rates were due to high soil degradation above the 25 cm depth. Below this depth, the concentrations, and hence, soil degradation rates, appear similar.

The soil concentration values are considerably higher than observed in the Control plot but lower than the Deep Injection plot. Two replicates of the soil gas concentration were obtained and both replicates produced similar concentration levels. For the Control field, however, one of the replicates consistently had very low concentrations, which may be an indication of a sampling problem. Another possible explanation for the low values in the Control plot would be natural spatial variability or some soil structural feature that impeded fumigant diffusion in soil to the sampling location.

5 Summary

A variety of approaches to reduce fumigant emissions were tested during the course of this project. They include: surface sealing by applying sprinkler irrigation, deep injection, and soil amendment with organic material or with a fertilizer amendment. Two independent sets of data were collected to compute fumigant emissions. From the 3–5 different methods used to estimate total emissions, the following summary is provided.

Intermittent Sprinkler Irrigation. The results of the 2005 study indicate that applying sprinkler irrigation water to the soil surface following soil fumigation leads to total 1,3-D (cis+trans) emissions between 10 to 15% of the applied material. Based on recent laboratory and field experiments conducted under similar soil and environmental conditions, it appears that atmospheric emissions of 1,3-D can be reduced by approximately 45–70% compared to conventional application methods.

Application of Composted Municipal Green Waste. The addition of composted municipal green waste material provides a means to reduce emissions of 1,3-D (cis+trans) after preplant soil fumigation. Application of green waste at a rate of 300 tons per acre the previous year and incorporated in the field soil reduced total of 1,3-D from approximately 30% to approximately 5% of the applied fumigant. Based on recent laboratory and field experiments conducted under similar soil and environmental conditions, it appears that atmospheric emissions of 1,3-D can be reduced by approximately 80–85% compared to conventional application methods. This approach provides a simple, environmentally beneficial, effective and relatively low cost method to protect the environment from agricultural chemicals and to reduce VOC emissions to the atmosphere.

Chloropicrin Emissions. During the 2007 Field Experiment, very low levels of chloropicrin were lost from the three fields (i.e., < 2% total emissions). Two independent flux estimates both arrived at similar results and supported by soil gas measurements. It appears that soil-based processes were limiting chloropicrin movement to the soil surface and volatilization into the atmosphere. The most likely explanation is enhanced soil degradation in the near surface soil that rapidly degraded chloropicrin.

Due to the very low emission of chloropicrin, total emissions of Telone ® C-35 appear lower than expected. This is due to 1/3 of the Telone ® C-35 mass remaining in soil (i.e., the chloropicrin component).

Standard Fumigation Methodology. Total emission estimates of applied 1,3-D (cis+trans) for the ADM, ISCST and CalPuf methods, respectively, are 35.4%, 20.0%, and 27.2%. The average and standard deviation of the total emission from the 3 methods is, respectively, $27.5 \pm 7.7\%$.

Deep Injection Fumigation. The total emission estimates from the ADM, IHF, TPS, ISCST3 and CalPuf methods, respectively, are 26.7%, 18.8%, 15.1%, 15.8%, and 26.1% of the applied 1,3-D (cis+trans). The average and standard deviation of the total emission from the 5 methods is, respectively, $20.5 \pm 5.6\%$ and for the ADM, ISCST3, and CalPuf methods is, respectively, $22.9 \pm 6.1\%$.

By comparing the total emission estimates for the ADM, ISCST3 and CalPuf methods, deep injection reduces emissions of Telone (cis+trans) by approximately 16.9% compared to the standard fumigation methodology.

Numerical experiments using a model developed by Yates (2009) suggests that deep-injection may not lead to significant emission reduction unless the shank fracture is completely closed. For the Deep Injection treatment, measurement of the shank fracture indicates a large opening extending from the injection depth to the bottom of the plow/disk layer. These would facilitate transport in the soil profile and lead to soil concentrations that would be more similar to the shallow injection method compared to injection that leave no fracture opening.

Soil Amendment with Ammonium Thiosulfate (ATS) as a Surface Spray. The total emission estimates from the ADM, IHF, TPS, ISCST3 and CalPuf methods, respectively, are 25.0%, 12.5%, 12.5%, 14.5%, and 26.7% of the applied 1,3-D (cis+trans). The average and standard deviation of the total emission from the 5 methods is, respectively, $18.2 \pm 7.0\%$ and for the ADM, ISCST3, and CalPuf methods is, respectively, $22.1 \pm 6.6\%$.

Using the total emission estimates for the ADM, ISCST3 and CalPuf methods, spraying the field with ATS reduces emissions of Telone (cis+trans) by approximately 19.9% compared to the standard fumigation methodology.

Further experimentation using ATS sprays with minimal water addition have shown that best performance occurs when ATS is applied with significant water, obtaining a benefit from both ATS and the plugging of soil pores (i.e., combined effect of surface water seal and amendment with ATS).

References

- Ashworth, D.J.; Yates, S.R. 2007. Surface irrigation reduces the emission of volatile 1,3-D from agricultural soils, *Environ. Sci. Technol.* 2007, 41, 2231-2236.
- Ashworth, D.J.; Yates, S.R. (2009) Assessing emission reduction strategies for the agricultural fumigant 1,3-D and chloropicrin, *Environ. Sci. Technol.* (In Press).
- Brutsaert W (1982) *Evaporation into the atmosphere*. Reidel, Dordrecht. 299 pp.
- Chen, C; Green R.E.; Thomas, D.M; Knuteson, J.A. Modeling 1,3-dichloropropene vapor-phase advection in the soil profile. *Environ. Sci. Technol.* 1995, 29, 1816-1821.
- Chen, C; Green R.E.; Thomas, D.M; Knuteson, J.A. 1996. Correction: Modeling 1,3-dichloropropene vapor-phase advection in the soil profile. *Environ. Sci. Technol.*, 30:359.
- Chen D, Rolston DE, Yamaguchi T (2000) Calculating partition coefficients of organic vapors in unsaturated soil and clays. *SOIL SCIENCE* 165: 217-225
- Cryer, S.A.; Van Wesenbeeck, I.J.; Knuteson, J.A. Predicting regional emissions and near-field air concentrations of soil fumigants using modest numerical algorithms: a case study using 1,3-dichloropropene. *J. Agr. Food Chem.* 2003, 51, 3401-3409.
- Denmead OT, Simpson JR, Freney JR (1977) A direct field measurement of ammonia emission after injection of anhydrous ammonia. *Soil Sci Soc Am J* 41:1001-1004.
- Dungan, R.; Gan, J.; Yates, S.R. Effect of temperature, organic amendment rate, and moisture content on the degradation of 1,3-dichloropropene in soil. *Pest Manag. Sci.* 2001, 57, 1-7
- Dungan, R.S., Papiernik, S., Yates, S.R. 2005. Use of composted animal manures to reduce 1,3-dichloropropene emissions *Journal of Environmental Science & Health Part B-Pesticides Food Contaminants and Agricultural Wastes.* 40:355-362.
- Fleagle RG, Businger JA (1980) *An introduction to atmospheric physics*, 2nd Ed. International Geophysics Series, Vol 25. Academic Press, New York.
- Gan, J., S.R. Yates, D. Crowley, and J.O. Becker. 1998. Acceleration of 1,3-dichloropropene degradation by organic amendments and potential application for emissions reduction. *J. Environ. Qual.* 27: 408–414.
- Gan, J.Y., Becker, J.O., Ernst, F.F., Hutchinson, C. and Yates, S.R. 2000a. Surface application of ammonium thiosulfate fertilizer to reduce volatilization of 1,3-dichloropropene from soil. *Pest Manag. Sci.* 56:264-270.
- Gan, J., Yates, S.R., Becker, J.O. and Knuteson, J. 2000b. Transformation of 1,3-dichloropropene by thiosulfate fertilizers. *J. Environ. Qual.* 29:1476-1481.
- Gao, S.; Trout, T.J.; Schneider, S. 2008. Evaluation of fumigation and surface seal methods on fumigant emissions in an orchard replant field. *J. Environ. Qual.*, 37, 369–377.
- Jin, Y.; Jury, W.A. Methyl bromide diffusion and emission through soil under various management techniques. *J. Environ. Qual.* 1995, 24, 1002-1009.
- Johnson, B., T. Barry, and P. Wofford. 1999. *Workbook for Gaussian modeling analysis of air concentration measurements*. California Environmental Protection Agency, Sacramento, CA. Report EH99-03, September 1999. 61 pp.
- Karris, G. C., and Downey, J. R. (1987a). Vapor pressure of cis-1,3-dichloropropene. Unpublished report of The Dow Chemical Company. ML-AL 87-40207.

- Karris, G. C., and Downey, J. R. (1987b). Vapor pressure of trans-1,3-dichloropropene. Unpublished report of The Dow Chemical Company. ML-AL 87-40208.
- Leistra, M. Distribution of 1,3-Dichloropropene over the phases in soil. *J. Agr. Food Chem.* 1970, 18, 1124-1126.
- Majewski MS (1997) Error evaluation of methyl bromide aerodynamic flux measurements. In: Seiber JN, Knuteson JA, Woodrow JE, Wolfe NL, Yates MV, Yates SR (eds) *Fumigants: Environmental Fate, Exposure, and Analysis*. ACS Symposium Series 652, American Chemical Society, Washington, DC., pp 135-153.
- Majewski MS, Glotfelty DE, Paw KT, Seiber JN (1990) A field comparison of several methods for measuring pesticide evaporation rates from soil. *Environ Sci Technol* 24: 1490-1497.
- Majewski MS, Glotfelty DE, Seiber JN (1989) A comparison of the aerodynamic and the theoretical-profile-shape methods for measuring pesticide evaporation from soil. *Atmos Environ* 23:929-938.
- Majewski MS, McChesney MM, Woodrow JE, Prueger JH, Seiber JN (1995) Aerodynamic measurements of methyl bromide volatilization from tarped and nontarped fields. *J Environ Qual* 24:742-751.
- McDonald, J.A., S.Gao, R.Qin, and J. Thomas. 2008. Thiosulfate and manure amendment with water application and tarp on 1,3-dichloropropene emission reductions. *Environ. Sci. Technol.* 42:398–402.
- Parmele LH, Lemon ER, Taylor AW (1972) Micrometeorological measurement of pesticide vapor flux from bare soil and corn under field conditions. *Water, Air, Soil Pollut* 1:433-451.
- Rosenberg NJ, Blad BL, Verma SB (1983) *Microclimate, The biological environment*. John Wiley & Sons, New York.
- Walbroehl, Y. (1987a). Determination of water solubility of cis-1,3-dichloropropene. Unpublished report of The Dow Chemical Company. ML-AL 87-70907.
- Walbroehl, Y. (1987b). Determination of water solubility of trans-1,3-dichloropropene. Unpublished report of The Dow Chemical Company. ML-AL 87-70907.
- Wauchope, R.D.; Buttler, T.M.; Hornsby, A.G.; Augustijn-Beckers, P.W.M.; Burt, J.P. *The SCS/ARS/CES Pesticide properties database for environmental decision-making*. *Rev. Environ. Contamin. Toxic.* Springer-Verlag. 1992, 123, 1-155.
- Wilson, J. D.; Shum, W.K.N A re-examination of the integrated horizontal flux method for estimating volatilisation from circular plots. *Agric. and Forest Meteorology*. 1992, 57, 281-295.
- Wilson JD, Thurtell GW, Kidd GE (1981a) Numerical simulation of particle trajectories in inhomogeneous turbulence, I: Systems with constant turbulent velocity scale. *Boundary Layer Meteor* 21:295-313.
- Wilson JD, Thurtell GW, Kidd GE (1981b) Numerical simulation of particle trajectories in inhomogeneous turbulence, II: Systems with variable turbulent velocity scale. *Boundary Layer Meteor* 21:443-463.
- Wilson JD, Thurtell GW, Kidd GE (1981c) Numerical simulation of particle trajectories in inhomogeneous turbulence, III: Comparison of predictions with experimental data for the atmospheric surface layer. *Boundary Layer Meteor* 21:443-463.

- Wilson JD, Thurtell GW, Kidd GE, Beauchamp EG (1982) Estimation of the rate of gaseous mass transfer from a surface source plot to the atmosphere. *Atmos Environ* 16:1861-1867.
- Wilson JD, Catchpoole VR, Denmead OT, Thurtell GW (1983) Verification of a simple micrometeorological method for estimating the rate of gaseous mass transfer from the ground to the atmosphere. *Agric Meteor* 29:183-189.
- Yates SR, Gan JY, Ernst FF, Mutziger A, Yates MV (1996a) Methyl bromide emissions from a covered field I. Experimental conditions and degradation in soil. *J Environ Qual* 25:184-192.
- Yates SR, Ernst FF, Gan JY, Gao F, Yates MV (1996b) Methyl bromide emissions from a covered field II. Volatilization. *J Environ Qual* 25:192-202.
- Yates SR, Gan JY, Ernst FF (1996c) Methyl bromide emissions from a covered field. III. Correcting Chamber Flux for Temperature. *J Environ Qual* 25:892-898.
- Yates SR, Gan JY, Wang D, Ernst FF (1997) Methyl bromide emissions from agricultural fields. Bare-soil, deep injection. *Environ Sci Technol* 31:1136-1143.
- Yates, S.R. Analytical Solution Describing Pesticide Volatilization From Soil Affected by a Change in Surface Condition. *Journal Environmental Quality*. 38: 259-267. 2009.
- Yates, S.R., Knuteson, J. Ernst, F.F., Zheng, W. and Wang, Q. The Effect of Sequential Surface Irrigations on Field-scale Emissions of 1,3-dichloropropene. *Environmental Science & Technology*. 42:8753-8758. 2008.
- Zheng, W., Papiernik, S.K., Guo, M. and Yates, S.R. Competitive degradation between fumigants chloropicrin and 1,3-dichloropropene in unamended and amended soils, *Journal Environmental Quality*. 32:1735-1742. 2003.
- Zheng, W., Yates, S.R., Guo, M., Papiernik, S.K., and Kim, J.H. Transformation of chloropicrin and 1,3-dichloropropene by metam sodium in a combined application of fumigants. *Journal of Agricultural & Food Chemistry*. 52:3002-3009. 2004